Timo Veldt

The effect of wave directional spread on coastal hazards at coastlines fronted by a coral reef

TU Delft

Deltares
Enabling Delta Life

The effect of wave directional spread on coastal hazards at coastlines fronted by a coral reef

by

T. (Timo) Veldt

to obtain the degree of Master of Science
at the Delft University of Technology,
to be defended publicly on Friday June 28, 2019 at 10:00 AM.

Student number:	4240588	
Project duration:	July 1, 2018 – June 28, 2019	
Thesis committee:	Dr. ir. M. S. F. Tissier,	Delft University of Technology, chair
	Prof. dr. ir. A. J. H. M. Reniers,	Delft University of Technology
	Dr. ir. J. D. Bricker,	Delft University of Technology
	Dr. ir. A. R. Van Dongeren,	Deltares
	Ir. S. G. Pearson,	Delft University of Technology & Deltares

An electronic version of this thesis is available at `http://repository.tudelft.nl/`.

Cover: Aerial photo of Waimanalo coastline, Oahu. Source:
http://bigislandnow.com/wp-content/uploads/2019/05/Waimanalo_coastline_Oahu.jpg

TU Delft

Acknowledgments

This master thesis is the final part of my masters degree in Hydraulic engineering at Delft University of Technology. The project has been executed in collaboration with Delft University of Technology and Deltares.

Firstly, I want to thank my supervisors Marion Tissier, Ad Reniers and Jeremy Bricker from the TU Delft. They provided me with great guidance throughout the project. It was really nice to work together with people who have great knowledge in this topic, I learned a lot from you.

I also want to thank Deltares for providing me the tools needed for this project. Furthermore, I would like to thank my supervisors from Deltares; Ap van Dongeren and Stuart Pearson. I am very grateful for the challenging discussions with Ap during our meetings. Thank you Stuart for your eternal enthusiasm about the work I did, it really kept me motivated throughout the project.

In general, I would like to thank my friends an family for supporting me in this final stage of my masters degree. With special thanks to my girlfriend Emma Eltringham.

Abstract

Currently, low lying islands fronted by a coral reef are experiencing flooding due to extreme water levels driven by waves. Multiple studies have reported flooding in coral reef environments due to locally generated storm waves and distant generated waves. This wave driven flooding in a coral reef environment could lead to multiple coastal hazards, for instance; the reduction of the fresh water availability, coastal erosion and damage to existing infrastructure. Moreover, it is expected that due to direct (i.e. overfishing, coastal development and pollution) and indirect (i.e. climate change) impact of human activity on the coral reef environments the quantity and severity of wave driven flooding will increase in the near future. Various studies have been investigating the reef-hydrodynamics in order to predict the wave runup, which is used as proxy for wave driven flooding. However, most are focused on a 1D simplification of the coral reef environment and thus hydrodynamics. These studies neglect the impact of 2D processes, for example wave directional spread. In this study an attempt is made to understand and investigate the influence of wave directional spread on wave runup.

XBeach Non-Hydrostatic with an additional vertical layer is used to perform a great amount of digital experiments. A synthetic database is created consisting of 540 different model runs. Subsequently, the model output is post processed and analyzed.

The analyses of the synthetic database lead to multiple findings. Firstly, the evolution of directional spreading within the model domain is analyzed with a routine time series analysis. This showed that the directional spectrum narrows on the fore reef slope and broadens inside the surf zone. This is due to wave-current interaction inside surf zone. Furthermore, it was shown that the amount of vorticity and the size of the vorticity fields controls the directional broadening. Secondly, the influence of directional spreading on the runup components is investigated. This analysis showed that wave directional spread mainly influences the setup and Low Frequency runup, and has a limited impact on the High Frequency runup. Thirdly, the complete dataset is analyzed by performing a regression analysis, this showed that incorporating directional spreading in a runup model will improve the runup predictions. Furthermore, the influence of directional spreading on the setup and LF runup is the lowest compared to the influence of the wave height, wave steepness, reef flat width, reef flat submergence level, and fore reef slope. Lastly, a comparison of runup data from a XBeach Non-Hydrostatic model with and without directional spreading (i.e. 2DH compared with a 1D model) showed that the addition of directional spreading leads to a reduction wave runup. Hence, a 1D model makes a conservative prediction of the runup.

Based on the results presented in this study it is suggested that incorporation of directional spreading will improve the prediction of wave setup and Low Frequency runup in coral reef environment. However, neglecting directional spreading will lead to a conservative calculation of the wave runup, hence previous 1D modeling studies on coastal hazards are expected to be conservative. Furthermore, it was shown that wave directional spread has the least influence on wave runup. Therefore, it is suggested that it is less important to know the exact wave directional spread, but it is advised to account for directional spread, since it generally reduces the wave runup.

Contents

List of Figures

List of Tables

1

Introduction

1.1. Motivation

Coral reefs surround many small islands like atolls (low-lying islands), islands with an elevated topography (fringing reefs) and sometimes with some distance from the coastline (barrier reefs). In 2007 around 275 million people lived within 10 km from a coastline fronted by a coral reef and around 850 million people lived within 100 km of a coral reef coastline (WRI, 2011). The local inhabitants benefit from the coral reefs through its economic value. The reefs provide them with a fast source of food and attracts visitors form all over the world (WRI, 2011). Next to that, coral reefs have an important environmental value by providing shelter and nutritions for various ocean species. This makes them one of the world's most biodiverse ecosystems and that is why they are also called the "rain forests of the sea" (WRI, 2011). Furthermore, coral reefs function as great coastal protections against waves, wind and flooding. Research shows that a coral reef is capable of dissipating upto 97% of the incoming wave energy (Ferrario et al., 2014). So, reefs fulfill some important functions, however that it is capable of doing it for the coming century is uncertain. Climate change and population growth is stressing these systems of which the effect on its functions is still uncertain. For this reason research in coral reef environments is required. This study focus on the function of a coral reef as coastal protection.

1.1.1. Vulnerability of coral reef coastlines

At the moment coral reefs are stressed by multiple factors, which directly or indirectly relate to human activity. WRI (2011) found that over 60% of the coral reefs are threatened by human activities (e.g. overfishing, destructive fishing, coastal development, pollution and damage). The indirect effect of human activity is climate change. Climate change is a collective name for multiple processes and some of the processes affect coral reef coastlines such as; seawater temperature increase, sea level rise, ocean acidity and storm intensity (Woodroffe, 2008). WRI (2011) states that the combined impact of climate change and local human activities will threaten over 90% of the coral reefs by 2030.

Furthermore, waves could have a significant impact on coastlines fronted by a coral reef, since energetic wave fields could result in extreme water levels at the coastline. This could cause wave driven flooding, which could lead to multiple coastal hazards. Such as; damage the existing infrastructure, causing coastal erosion and reduction of the freshwater availability (Storlazzi et al., 2015; Woodroffe, 2008). That wave driven flooding is currently affecting coastlines is reported by; Hoeke et al. (2013a), who reported the inundation of low lying islands by remotely generated waves. Tajima et al. (2016a 2017) reported the inundation of coastlines fronted by a coral reef due to the effect of waves generated by typhoon Haiyan and Meranti.

The combination of local human activity and climate change is expected to increase the wave driven flooding at coastlines fronted by a coral reef in the near future. The following effects are expected; 1) Threatened coral reefs could result in coral degradation. The reduced presence of coral leads to a smoother bottom. This could enhance wave driven flooding (Quataert et al., 2015). 2) Recent research shows that vertical coral growth can not keep-up with the sea level rise predictions (under Representative Concentration Pathway 8.5) and that most of the reefs will experience a water level increase of a few decimeters above the reef flat (Perry et al., 2018). This affects coastal safety, since more wave driven flooding is expected (Quataert et al., 2015). 3) Climate change could increase the number and intensity of tropical storm which will increase incoming wave energy and this will increase the impact and quantity of wave driven flooding (Quataert et al., 2015). Storlazzi et al. (2015) modeled inundation levels and showed that low-lying islands will inundate more frequently due to the combined impact of SLR and wave driven processes. This also means that low-lying coral reef coastlines will experience wave driven flooding for lower levels of SLR, hence might become uninhabitable mid 21st century (Storlazzi et al., 2018).

So, at the moment coastlines fronted by a coral reef are affected by wave driven flooding of remotely generated waves (Hoeke et al., 2013b) and typhoon waves (Tajima et al., 2016b). Furthermore, it is expected that this pressure will increase due to the effects of climate change and human activity in the coral reef zone. Furthermore, we have shown that the this could lead to multiple hazards at these coastlines, hence increased knowledge about wave driven flooding leads to improved the assessment of coastal hazards. This improvement makes it possible to create strategies in order to preserve the coastal communities living at these coastlines. Furthermore, early waring systems for wave driven flooding could benefit from the obtained knowledge.

1.2. Significance of research

The previous Section showed the effect of wave driven flooding on multiple coastal hazards. Furthermore it indicated an increased wave driven flooding due to the effects of human activity in the coral reef zone and climate change. Therefore, an attempt is made to increase the knowledge on wave driven flooding in a reef environment.

1.2.1. Current state of knowledge

In the coming decades inhabitants of tropical islands fronted by a coral reef can experience an increasing risk of wave driven flooding. This leads to the need for models which are able to represent the hydrodynamics, since a poor evaluation of the hydrodynamics will give uncertain results. At the moment many types of hydrodynamic models are applied to coral reefs. Firstly, theory applicable on the dissipative beaches is applied in coral reef environments. For instance, Symonds et al. (1995) made an analytical model to describe circulations patterns driven by waves in coral reef environments. This model showed that the theory from dissipative beaches is applicable in reef environments.

Furthermore, field studies from Péquignet et al. (2009) and Pomeroy et al. (2012b) created insight in the wave transformation in a coral reef environment. Their research was of importance to the understanding of reef hydrodynamics. Later on numerical models were applied to coral reef environments e.g. Van Dongeren et al. (2013). Who used a process-based XBeach Surfbeat model (Roelvink et al., 2015) (i.e. solves the short-wave envelop on the scale of a wave group). The results were compared with a field study at Ningaloo reef, located on the northwest coast of Australia. The model captured most of the important reef hydrodynamics. The same type of model is used by Quataert et al. (2015), who performed a sensitivity analysis on wave driven flooding in a coral reef environment. Furthermore, a process-based phase resolving Xbeach model (i.e. Non-Hydrostatic mode (Smit et al., 2010)) is also calibrated and validated on data from Roi-Namur island and used to create a database for an Estimator for wave attack in Reef Environments (BEWARE) (Pearson et al., 2017). The tool was capable of predicting wave runup for different reef geometries and under multiple wave conditions. However, only 1D model output is used to construct the tool. Lashley et al. (2018) compared the runup predictions of XBeach Surfbeat and XBeach Non-Hydrostatic mode on two 1D fringing reef profiles. They found that both models were able the accurately predict wave runup. Shimozono et al. (2015) used a Bousinessq type model to analyse the extreme water levels at the coastline of Eastern Samar during passage of Typhoon Haiyan.

Thus, in order to understand the wave transformation a great amount of analytical models, field measurements and numerical models are applied to coral reef environments. Nevertheless, most of the models focus on a 1D simplification of the coral reef environment. The models that take a 2D coral reef environment into account lack the connection to wave driven flooding.

1.2.2. Knowledge gap

The importance of knowledge about waves and coastal safety is well established. However, the previous section showed that most studies have one limitation in common; they look at 1D transects. Which is convenient, since the computational time is significantly reduced at the cost of simplifying the problem. However, this means that 2D wave mechanisms are not taken into account.

Multiple processes become important or can be incorporated when going from 1D modeling to 2D modeling. For instance, in a 1D model is assumed that all waves/wave components are normally incident, this is a simplification of the wave field, hence could lead to erroneous results when assessing flooding by waves. This study will elaborate one process that might have an influence on wave driven flooding, namely wave directional spread.

Directional spreading

Wave directional spread is a measure to indicate the wave energy distribution over direction. In other words, it gives information about the amount of wave energy that is traveling in a certain direction. Guza and Feddersen (2012) investigated the influence of directional spreading on the wave runup on dissipative beaches. They found an effect of this parameter on the runup. However, the effect of directional spreading in a coral reef environment is unknown and therefore part of this thesis.

1.3. Scope & Research Questions

The previous section have shown that coastlines fronted by a coral reef are subjected to wave driven flooding. Next to that, it is expected that the negative effects of waves on the coastal hazards will continue to grow due the effects of climate change and human activity in coral reef environments. This gives a need for the to understand the wave transformation in a coral reef environment. Although, the knowledge has increased the last years, there is still lack of knowledge about the influence of 2D mechanisms on wave driven flooding in coral reef environments, and especially wave directional spreading. This research will focus on that knowledge gap, this leads tot the following main objective:

To investigate the influence of directional spreading on wave driven flooding in a coral reef environment.

In this research is focused on the effect of directional spreading on the wave driven flooding. As mentioned before, flooding due to waves causes coastal erosion, causing damage to existing infrastructure and reducing the fresh water availability. The influence of directional spreading on wave driven flooding is investigated by looking a the wave induced runup. since this is a practical measure and more often used as a proxy for wave driven flooding (Pearson et al., 2017). Wave runup is discussed in Section 2.2.1. This leads to the following research questions and sub research questions.

Main research question

What is the effect of wave directional spread on the wave runup at coastlines fronted by a coral reef?

Sub research questions

The general build-up of the sub-research questions:

- How does wave directional spread evolve in a coral reef environment?
- Does directional spreading influence wave runup in a coral reef environment and how does wave directional spread influence the wave runup?
- How important is it to include directional spreading in the prediction of wave runup?
- What is the difference between wave runup including wave directional spread and wave runup excluding wave directional spread?

1.3.1. Approach

The scarce availability of appropriate field data on wave driven flooding, offshore wave conditions and reef geometry makes research on existing datasets difficult. Additionally, the high temporal and spacial variability makes measurement campaigns useful for solving a particular problem at a local scale, but less useful to understand the influence of wave directional spread in various coral reef systems. This requires a more generic approach like physical or digital experiments where every parameter can be varied. Physical experiments will be to costly, therefore a digital environment is used to set up the experiments and create a database. The creation of this database is the core of this thesis. There will be build on the analysis of Pearson et al. (2017) to construct the database. Their research showed great potential in the construction and analysis of a database with XBeach Non-hydrostatic. In order to fulfill the objective of the project the following consecutive steps will be followed.

1) Background - Firstly, a literature review is executed in order to create a basis of knowledge about coral reef coastlines, waves, wave-wave interactions and wave transformation in a coral reef environment.

2) Creating synthetic database - Data is needed to analyze the influence of directional spreading and waves on wave runup. XBeach Non-Hydrostatic will be used to generate data for multiple reef geometries under different wave forcing. The number of models will depend on the computational time of an individual model and will be based on practical and scientific considerations.

3) Analyzing the dataset - Subsequently the dataset will be analyzed. As mentioned before, the shape of coral reefs differs in space and the boundary conditions differ in time. Therefore, the effect of directional spreading in different reef environments will be investigated.

4) Connection to literature - It is possible to critically review the results and connect certain findings to literature. This step can also be seen a verification of the model output, where any abnormalities require extra attention.

5) Post process results - The dataset will be used to perform a regression analysis. Subsequently, relations between wave runup and several other parameters can be found. And most important the importance of a parameter in a predictive model can be assessed.

1.4. Thesis Outline

In Chapter 2 background information on this topic is given. Chapter 3 will focus on the methodology and the purpose is to inform and clarify some decisions made in this study. In Chapter 4 is focused on the wave transformation in a reef environment, which is important for the study on the influence of wave directional spread on wave runup. Next, the wave runup is analyzed (Chapter 5). This Chapter will focus on the influence of directional spreading on wave runup. Subsequently, the XBeach Non-Hydrostatic dataset is analyzed an the importance of wave directional spread in wave runup assessments is investigated. Next, the results are discussed (Chapter 6) and conclusions (Chapter 7) are drawn. Lastly, based on the findings in this study recommendations are given and are presented in Chapter 8.

2
Background

In this chapter background information is given and is used as theoretical basis of this study. Firstly, the formation of reef islands and typical geometries are discussed. Subsequently, wave driven flooding is discussed. Lastly, the wind generated waves and the generation of low frequency waves is discussed.

2.1. Reef islands

The shape of the reef and the geometrical characteristics of a coral reef are important for the coastal safety of reef islands. In this section the formation and characteristics of coastlines fronted by a coral reef are derived from literature.

2.1.1. Coral reef islands formation

The shape of reef fronted coastlines can be explained by land subsidence and Charles Darwin explained this in 1842. According to Darwin's theory three main types of coral reef coastlines can be distinguished (see Figure 2.1). The first type is the formation of a reef on a volcanic island, these reefs are called fringing reefs and extend from the coastline offshore (Figure 2.1a). The second type are barrier reefs, these are formed due to the continuous growth of coral platforms towards the water surface while the sea level rises and the land subsides. As a consequence, a lagoon is formed between the coastline and reef (Figure 2.1b). The last stage is reached when the land subsides below the water surface. This forms a circular shaped coral reef with a lagoon in the middle and is called atolls (Figure 2.1c). Darwin states that this explains their circular shape. However, in nature these islands often have an irregular shape which can be explained by land slides (Terry and Goff, 2013). So to conclude the reefs on these coasts differ widely in their shape, size and physical characteristics; the wave and water level conditions affecting these coastlines also vary in space and time.

This study focuses on only two types of coral reef coastlines; 1) islands with an elevated topography with a coral reef connected to the coastline (Fringing reefs, see Figure 2.1a) and 2) small low-lying tropical islands (atolls, see Figure 2.1c). Many of the pacific low-lying island have an elevation lower than + 4 meter with respect to the mean sea level (MSL), which makes them vulnerable to sea level rise (SLR) and wave driven flooding (Storlazzi et al., 2015). Coral reef islands with a more elevated topography have most population living close to the coastline due to their economic value. Which implies that most important infrastructure is located close to the coastline and thus lies within a few meter above MSL, which also makes them vulnerable to SLR and wave driven flooding (Pearson et al., 2017; Storlazzi et al., 2018).

2.1.2. Characteristics of coral reef coastlines

The study focuses on coastlines directly fronted by a coral reef. The reef profile is schematized as per Pearson et al. (2017); Quataert et al. (2015) and is shown in Figure 2.2. The offshore hydrodynamic boundary conditions are given by the offshore significant wave height ($H_{s,0}$), the peak period (T_p), the directional spread (s_0) and the angle of incidence (ϕ_0). The incoming wave characteristics in combination with the reef flat water

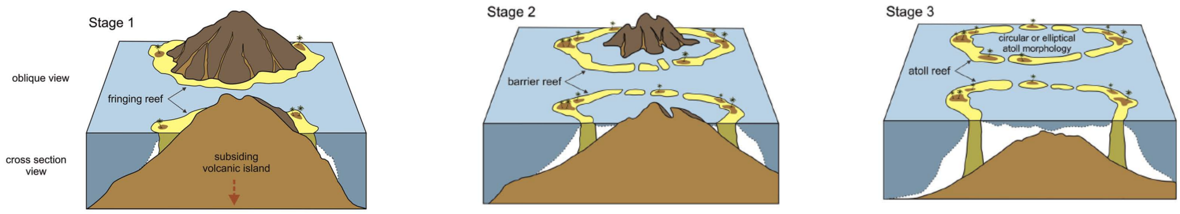

(a) Stage 1: Fringing reef (b) Stage 2: Barrier reef (c) Stage 3: Atoll reef

Figure 2.1: Darwin's three stages of Atoll island formation (From Terry and Goff (2013))

depth ($h_{0,RF}$) determine the location of the offshore boundary, hence the offshore water depth ($h_{0,off}$). The reef geometry is describe by the fore reef slope (β_{FR}), the reef flat width (W_{reef}) and the beach slope (β_b). The beach slope has an infinite length in this way only the wave runup is considered, which can be used as a measure of coastal safety. The reef geometry is discussed in this section and the hydrodynamics is discussed in section 2.5.

In general reef profiles could be more complex than presented in Figure 2.2. For instance, Gourlay (1996b) schematized a coral reef by defining a reef-face, reef-rim and lagoon. Where reef-face is defined as the relatively steep seaward facing underwater slope, this is in this study defined as the fore reef. The Reef-rim is defined as a flat seaward inclined surface between the reef face and the reef top and a Lagoon is defined as a body of water enclosed by a reef or land. These are disregarded in this study for model simplicity. Furthermore, the reef geometry simplification by Pearson et al. (2017); Quataert et al. (2015) show satisfying results for their case studies.

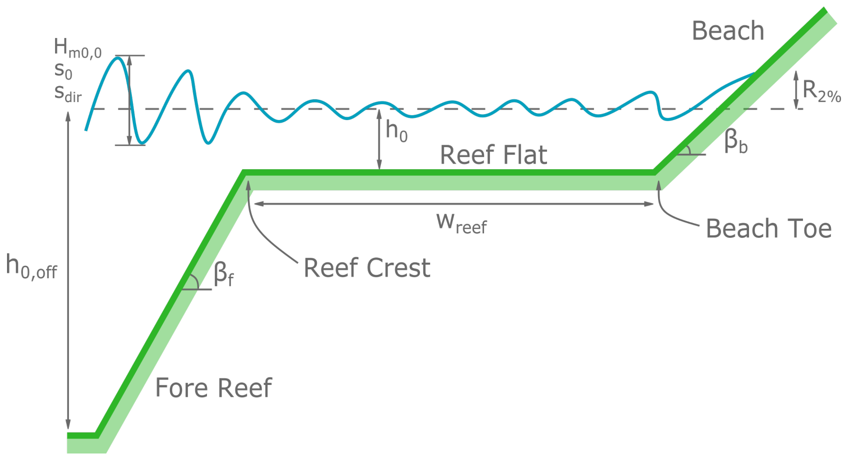

Figure 2.2: A schematization of a reef profile, adapted from Pearson (2016)

Fore reef slope

The fore reef slope is defined as the seaward facing slope, which is could be quite steep (i.e. 1/1 or a vertical wall (Gourlay, 1996b)), quite gentle with slopes up to 1/20 (Quataert et al., 2015). The fore reef slope is important for the reef hydrodynamics, since most wave transformation takes place until this point, i.e. wave breaking and refraction. Whereas wave breaking and refraction control the important reef hydrodynamics which will have implications for the runup at coral reef coastlines.

Reef flat width

The reef flat is defined as the surface between the fore reef and beach slope. The reef flat has generally a very mild slope or even a flat surface. The reef flat controls the wave attenuation towards the beach, due to the coral growth which enhances wave energy dissipation. A wide reef flat dissipates most of the incoming short wave energy which results in a wave runup that is dominated by long wave energy. On the other hand, a narrow reef flat shows little short wave energy dissipation and runup is dominated by short wave energy (Shimozono et al., 2015).

Beach slope

The beach slope is defined as the slope that begins at the beach toe and extents to the beach crest. The beach slope is partly submerged and is an important variable for wave runup calculations. The beach slope could influence the runup levels at coral reef coastlines with a narrow reef $W_{reef} < 400m$, in contrary wider reefs show little difference in runup levels for varying beach slopes. (Shimozono et al., 2015).

Roughness

The hydraulic roughness of coral reef is controls most wave transformation on the fore reef and reef flat due to frictional dissipation. The complex coral structure makes the coral reef beds relatively rough, which enhances the dissipation of wave energy on the reef flat when comparing it to sandy beaches. Quataert et al. (2015) show that an increase of the friction at the fore reef increases the wave setup, moreover it has a negligible effect on the wave runup. Furthermore, an increased reef flat friction increases the wave setup and decreases the short and infragravity wave height. Pearson et al. (2017) show that information about the bottom roughness is relatively less important for accurate runup predictions than information about H_0, h_0 and W_{reef}.

2.2. Wave driven flooding

This study is investigating the wave driven flooding of islands fronted by a coral reef. In order to do that wave runup is analysed, wave runup is more often used as a proxy for wave driven flooding, e.g (Pearson et al., 2017). The maximum water level elevation (i.e. runup) at the coastline due to incident waves can be decomposed into three components, namely runup due to short wave motions, runup due to long wave motions and wave setup (Stockdon et al., 2006), the latter is discussed in subsection 2.2.2. Merrifield et al. (2014) applied Stockdon's method on coastlines fronted by a coral reef. This model is validated on two case studies and is in good agreement with the observed data. The general shortcoming of these formulas is the use of offshore wave data, so nearshore wave transformation such as refraction is not included.

2.2.1. Wave runup

Wave runup is the vertical extent of the water level on a slope with respect to the mean water level. A simple runup model for a gently sloping beach is presented by Equation 2.1 (Hunt, 1959), it indicates that the wave runup depends on the breaker parameter or Iribarren number (Equation 2.2), which describes the ratio between the beach slope and the incoming wave steepness (a relation between wave height and wave length, Equation 2.3) and the incident wave height. The Iribarren number is given in Equation 2.2 this parameter gives information about the type of breaking occurring at the beach (Battjes, 1974).

$$\frac{R_u}{H} = \xi \tag{2.1}$$

Where:

R_u	Runup [m]
H	Wave height [m]
ξ	Iribarren number or similarity parameter [-]

$$\xi = \frac{tan(\alpha)}{\sqrt{s_0}} \tag{2.2}$$

Where:

α	Beach slope [-]
s_0	Offshore wave steepness [-]

$$s_0 = H/L_0 \tag{2.3}$$

Where:
L_0 Offshore wave length [m]

Many other simple runup formulations exist besides Hunt's empirical runup formulation. Most formulation do not take any alongshore variation into account, for example wave refraction. Vieira Da Silva et al. (2017) attempted to model runup by using nearshore wave characteristics, so at the breakpoint where is assumed that most wave transformation has occurred. The applicability of the method is limited since it is validated on one case study and the wave characteristics after refraction have to be known.

During energetic wave events the infragravity motions could dominate the runup on coasts fronted by coral reefs (Beetham et al., 2015; Nwogu and Demirbilek, 2010). Furthermore, Shimozono et al. (2015) showed that the infragravity wave motions were dominating the runup during a typhoon event, especially for wide reef flats. In contrary, the short wave energy was dominating the runup in the case of narrow reef flat.

2.2.2. Wave setup

Wave setup is defined as a difference of the water level compared to the mean water level which is a consequence of a balance between wave forces, hydrostatic pressure and bottom friction (Equation 2.4) (Buckley et al., 2016). The wave setup is stationary on short wave timescale, however it varies on the wave group timescale, which generates water level oscillations on a larger timescale. This is further discussed in **??**.

$$\frac{\delta(S_{xx}+R_{xx})}{\delta x}+\rho_w g h\frac{\delta\eta}{\delta x}+\tau_b=0 \tag{2.4}$$

Where:

First term	Cross shore change of radiation stress
Second term	Pressure gradient
Third term (τ_b)	Time averaged bottom stress [N/m^2]
S_{xx}	Cross shore component of wave radiation stress [N/m]
R_{xx}	Wave roller contribution to cross shore wave radiation stress [N/m]
η	Water level elevation from Mean Water Level (MWL) [m]

At coral reef coastlines most wave breaking takes place at the reef edge, this processes changes the wave height and thus the radiation stress. A change of these stresses can be interpreted as wave forces and in the case of a fringing reef, or a reef flat enclosed by land, result these forces in a setup over the reef flat. Becker et al. (2014) found that the wave setup is strongly influenced by the tidal modulation, or the reef flat water depth. Where largest wave setup is expected during energetic conditions and during low tide and is consistent with the findings of Beetham et al. (2015). Furthermore, Becker et al. (2014) states that an accurate wave setup prediction requires knowledge about the breaker parameter γ_b, which can be estimated from the theory applicable on sandy beaches (Raubenheimer et al., 1996) and is consistent with earlier findings by Vetter et al. (2010).

Additionally, (Quataert et al., 2015) found that wave setup on an idealized reef is influenced by the fore reef slope, the hydraulic roughness on the fore reef and the incident offshore wave height. The influence of the fore reef slope could be attributed to the change of γ_b, which depends on the slope Vetter et al. (2010). The effect of an increase in hydraulic roughness is two-folded; 1) due to a higher friction the waves tend to lose energy which has an effect on the gradient in radiation stresses and 2) it tends to increase the bottom friction which can reduce or enhance wave setup, and depends on the velocity field direction (Buckley et al., 2016). Quataert et al. (2015) showed that an offshore directed flow on the reef flat enhanced the wave setup and this is also found with experiments by Buckley et al. (2016). Furthermore, the experiments showed that the two mechanisms cancel each other when comparing setup for low and high bottom roughness. Whether this is an unique case study is unknown.

Gourlay (1996b) states that the reef crest could function as a submerged bar/breakwater, where as waves break water is pumped onto the reef flat. Considering a 2D schematization with a non-uniform coastline could this process lead to horizontal flow patterns, this is further discussed in subsection 2.5.1.

2.3. Wind generated waves

Waves are periodic water level elevations which can be described with a periodic function and are generated by surface shear between wind and the water surface. Typical frequency of wind generated waves, or short waves, is between 0.04 and 1 Hz (Bertin et al., 2018). Coral reef coastlines are threatened by two types of waves; 1) distant generated waves, and 2) waves generated by tropical storms like typhoons. Swell waves are a results of frequency and directional dispersion and are characterized by low amplitude, long wave length and a long crest. In coral reef environments the swell waves are generated by a distant tropical storm and could cause coastal flooding as shown by Hoeke et al. (2013a). Figure 2.3 shows that the significant wave height at coral reef coastlines do not reach higher than 3.0 meter, however this is a limit set by the author. Since typhoon waves could reach up to 17 meter and causes severe flooding of the coastal areas Shimozono et al. (2015). This happened during typhoon Haiyan in Eastern Samar and during typhoon Meranti at Batanes island.

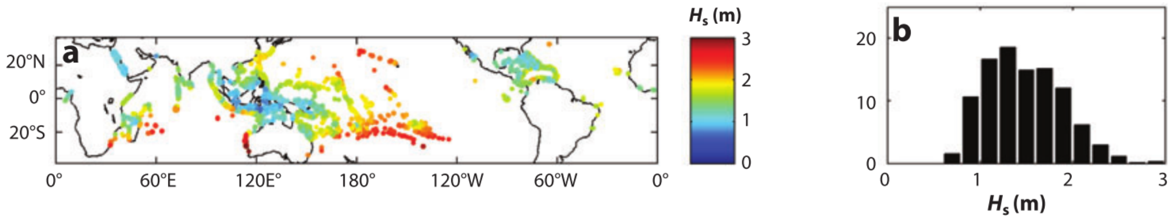

Figure 2.3: Global distribution of the significant wave height at coral reefs (From Lowe and Falter (2015)).

2.3.1. Spectral shape

Wave fields can be described with a energy density spectrum, which is a statical representation of the wave field in the frequency domain. The energy density spectrum or wave spectrum can have different shapes depending on the location. Pierson and Moskowitz (1964) proposed a spectral shape for fully developed seas, so long fetched wave fields. For short fetched wind seas is a JONSWAP spectrum proposed (Hasselmann et al., 1973), this introduces the peak enhancement function with the peak enhancement factor γ. For short fetched wind seas is $\gamma = 3.3$ a commonly used value. Nevertheless, the parameter is fitted on measured wave data and many different values are proposed in literature. Pearson (2016) performed a sensitivity analysis on the influence of γ on coral reef coastline's wave runup and found that the peak enhancement factor has relativity little influence on the runup.

2.3.2. Directional spreading

A wave field does not only consists of wave components traveling in the same direction. There is something that is called directional spreading, which is the description of the wave energy over multiple wave angles. The distribution of the wave angles can be described with a directional spectrum. Combined with a frequency spectrum a 2 dimensional spectrum can be obtained. A directional distribution can be described with the directional width of a wave field, which gives information about the short crestedness of the wave. The directional width can be described with a directional distribution (Equation 2.5) (Mitsuyasu et al., 1975). Parameter s gives the width of the directional distribution and depends on the frequency. Low value of s give a broad directional distribution, so a lot of directional spreading (short crested waves). A large value of s gives a narrow distribution (long crested waves, see Figure 2.4).

$$D(\theta) = \cos^{2s}(\theta/2) \tag{2.5}$$

Where:

$D(\theta)$	Directional energy distribution
θ	Wave angle [°]
$s(f)$	Parameter that controls the concentration of wave energy, depends on frequency

Another common description of the directional width is given by σ which represents the width of a Gaussian normal distribution and the are related via Equation 2.6. A comparison between the two models is made in

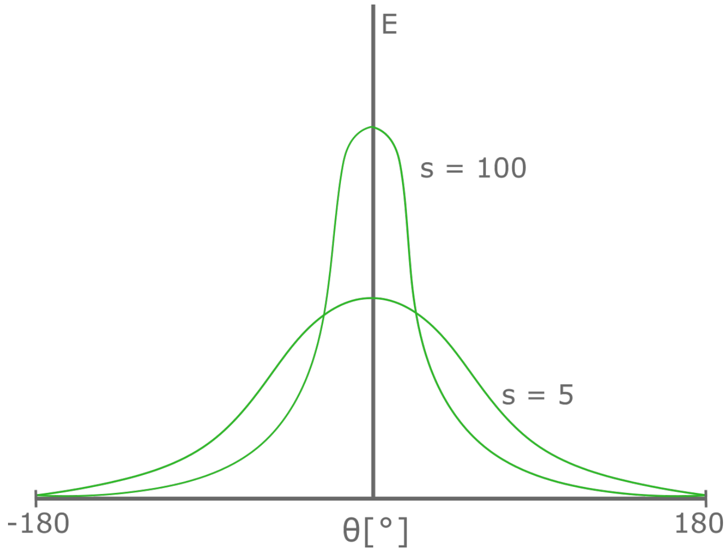

Figure 2.4: An idealized representation of the directional wave energy distribution for a certain frequency in order illustrate the influence of s parameter, adapted from Mitsuyasu et al. (1975)

Appendix A.

$$\sigma = \sqrt{\frac{2}{s+1}} \tag{2.6}$$

Directional spreading could affect the radiation stresses in cross-shore direction (x-direction) Feddersen (2004) compares field observations with the analytical expression of radiation stresses including directional spreading of a wave field (Equation 2.7). He shows that the radiation stress propagation in x-direction is reduced by incorporating the directional spreading in the analytical expression and is confirmed by the field observations. This indicates that the wave runup in coral reef environments can be influenced by a certain directional distribution. Guza and Feddersen (2012) confirms that a directionally spread wave field could affect the wave runup on a dissipative beach.

$$S_{xx} = E_0\left(n(1+S) - \frac{1}{2}\right) \tag{2.7}$$

Where:

S_{xx}	Radiation stresses $[kg/s^2]$
E_0	Wave energy $(1/8\rho g H_{rms})$
S	Correction for directional spreading $(\cos^2(\overline{\theta})(1-\sigma^{*2}) + \sin^2(\overline{\theta})\sigma^{*2})$
σ^*	Is the directional spreading and is given in Kuik et al. (1988)
$\overline{\theta}$	Mean wave direction

Directional spread is also important, since it affects wave refraction. The two dimensional spectral shape has an influence on the refraction of waves over elliptical depth contours (Vincent and Briggs, 1989). A directionally spread wave field propagating towards shore will become more narrow due to refraction. Snel's law shows that a decreasing depth will decrease the angle with coast, so wave crests tend to become parallel to the depth contours.

The directional spread of a wave field can be coupled to the age of a wave field, whereas the age of a wave field can be coupled to the wave steepness (Goda, 1985). Following this reasoning shows that there exists a relation between wave steepness and the directional spread. Typical values of directional spreading, taken from figure 2.13 in Goda (1985):

- Wind waves: $s_{max} = 10$

- Swell waves with short decay distance (relative large wave steepness) $s_{max} = 25$
- Swell waves with long decay distance (relative low wave steepness) $s_{max} = 75$

2.3.3. Shoaling

Waves propagating towards shore will significantly deform, due to the decreasing water depth will bottom friction become more important. Waves propagating into shallower water will reduce the wave celerity and thus the wavelength when following linear dispersion relationship. With a simple energy balance the wave height transformation can be described with the offshore wave height times a shoaling factor for the wave height growth, see Equation 2.9.

2.3.4. Refraction

Swell waves and sea waves travel from deep water towards shallow water. In shallow water various processes become important due to the influence of the bottom like shoaling, refraction and diffraction. In this section is focused on refraction of waves, which is the gradual direction change of the wave crest due to depth contours which are not parallel to the wave-crest. i.e. a depth difference along the wave crest causes phase speed difference along the crest, since the dispersion relation holds (Equation 2.8).

$$\omega^2 = gk \tanh kh \tag{2.8}$$

Where:

k	Wave number [1/m] ($k = 2\pi/L$)
ω	The angular frequency [1/s] ($\omega = 2\pi/T$)
h	Water depth [m]

So a certain bathymetry can change the wave crest angle which can lead to curved wave rays. The divergence or convergence of wave rays can alter the local wave height with a refraction factor (Equation 2.10). This can be shown by the derivation of for instance Johnson et al. (1948). Assumed is that wave rays are perpendicular to the wave crest and the energy is conserved between two successive wave rays. The energy balance gives two factors which can be used to determine the local wave height (i.e. $H_{local} = H_{offshore} K_{sh} K_r$).

$$K_{sh} = \sqrt{\frac{c_{g,0}}{c_{g,1}}} \tag{2.9}$$

Where:

K_{sh}	Shoaling factor
c_g	Wave group celerity

$$K_r = \sqrt{\frac{b_0}{b_1}} \tag{2.10}$$

Where:

K_r	Refraction factor
b	Distance between two successive wave rays

Determination of the local wave height thus requires knowledge about the wave ray paths. Snel's Law is an example of the wave ray tracing method and it is a simple method to determine the wave ray deflection (Equation 2.11). However, the applicability of the method is limited, i.e. only valid for straight parallel contour lines. López-Ruiz et al. (2015) proposed a new methodology by applying a correction factor to Snel's Law for curved depth contours at a dissipative beach, like beach undulations. This factor depends on coastline geometry (size of beach undulations) and the incident wave characteristics. The result of this method is the near shore wave angle.

$$\frac{\sin\theta_0}{c_0} = \frac{\sin\theta_1}{c_1} \tag{2.11}$$

Where:

c	Wave celerity ($c = \omega / k$)
θ	The angle between wave ray and normal to the depth contour

The interaction between the bottom and the waves also works the other way around. A normal incident wave field will refract over curved bottom contours. Wave refraction at circular islands is a typical example of refraction over curved depth contours and is treated in a lot of literature (e.g. (Arthur, 1946; Pocinki, 1950)). The hydrodynamics of refraction on circular depth contours is extended with work of Liu et al. (1995) who conducted experiments to study runup on such islands and an analytical model is proposed by Kanoglu and Synolakis (1998). Da Silva et al. (2018) show that alongshore variability of the coastline will lead to variations in the alongshore wave energy in the near shore.

2.3.5. Wave breaking

Wave breaking is important for many processes in coral reef environments, namely, it moves wave energy to lower frequencies, wave setup and dissipation of incident wave energy. As explained before, shoaling will affect the wave celerity hence the wave length. This results in wave steepening and eventually wave breaking. The crest becomes unstable when a particle velocity exceeds the crest velocity. A derivation of the maximum wave steepness shows that the theoretical maximum wave steepness equals 0.142, however this is not reached by wind waves or swell waves. From the maximum wave steepness a wave breaking parameter can be obtained, since breaking is expected when this value is exceeded. The parameter is the ratio between the maximum wave height and the water depth. This parameter increases for increasing beach slopes (Raubenheimer et al., 1996), however this relation is derived for sandy beaches. Vetter et al. (2010) show that in the case of coral reefs the parameter could reach 0.9-1.1 which also corresponds with the observations of Raubenheimer et al. (1996) for steep sandy beaches.

2.4. Infragravity waves

As mentioned in the previous section is short wave breaking important for the generation of setup and low frequency energy, which could results in low frequency waves or infragravity waves. Infragravity (IG) waves or long waves are surface waves with a frequency below wind generated wave. The frequency range of IG waves is defined as being between 0.004 and 0.04 Hz (Bertin et al., 2018). IG waves are a result of non-linear wave-wave interaction where energy is transfered to lower frequencies. In literature three types of IG wave generation are distinguished (Bertin et al., 2018):

- Bound wave
- Moving breakpoint mechanism
- Bore merging

In coral reef environments IG waves could dominate the hydrodynamics on the reef flat, due short wave energy dissipation by wave breaking and friction. They could generate reef flat resonance (Pomeroy et al., 2012b), dominate the wave runup (see subsection 2.2.1) and thus cause inundation (Hoeke et al., 2013a). So coastal safety of coral reef islands requires an adequate representation of the IG waves.

Battjes (2004) shows that for steep beach slopes it is expected that the breakpoint mechanism will dominate the bound long wave energy and for mild beach slopes the opposite is expected. The dominating IG wave generation mechanism is thus depended on the fore beach slope, and can be found with the normalized bed slope (Equation 2.12). Values of $\beta > 1.0$ indicate steep beaches and the moving breakpoint mechanism is dominating and for $\beta < 0.3$ (mild beach slope) dominates the bound long wave mechanism.

$$\beta = \frac{h_x}{\omega}\sqrt{\frac{g}{h}} \tag{2.12}$$

Where:

h_x	Bed slope [-]
ω	The angular frequency [1/s] ($\omega = 2\pi / T$)
h	Water depth [m]

Many coral reefs are characterized with relatively steep fore reef slopes (> 1/20) and it is expected that most IG waves at reefs are generated by breakpoint forcing, this is confirmed by observations of Péquignet et al. (2014); Pomeroy et al. (2012a).

2.4.1. Infragravity wave generation: Bound wave

Bound long waves are forced by the energy difference in a wave group, thus the energy of the IG wave is bound the wave group. This also means that the frequency of the bound wave equals the frequency of the wave group envelop, this is illustrated in Figure 2.5, where a bichromatic wave field is generated and the resulting bound long wave is shown. It also shows that the bound wave amplitude is 180 degrees out of phase with the group envelope. Furthermore the waves are generated in deep water and generally have a small amplitude which will transform in the near shore.

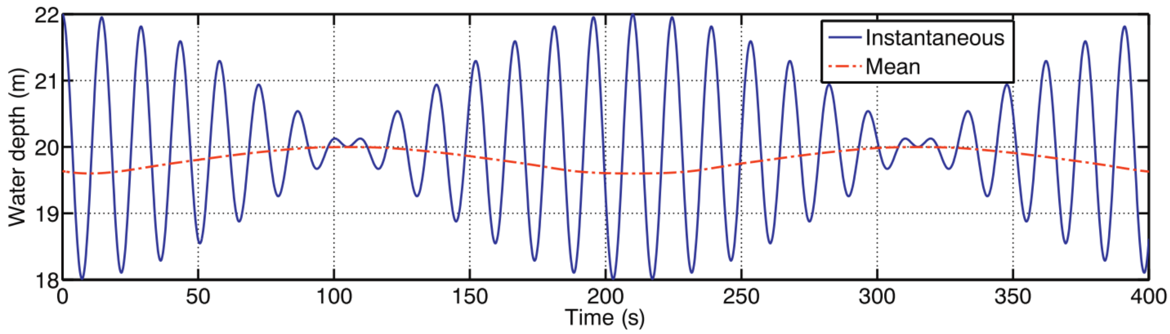

Figure 2.5: In blue is the water level elevation of a bichormatic wave field shown and in red the resulting bound long wave (From Bertin et al. (2018)).

2.4.2. Infragravity wave generation: Moving breakpoint

Moving breakpoint mechanism is generated within the surfzone and the main generation mechanism is wave breaking. Symonds et al. (1982) showed with a linear analytical model that a wave height difference (i.e. over a incoming wave group) generates a spatially and temporally varying breakpoint. Furthermore, this wave height difference generates a varying setup, due to the varying cross-shore change of radiation stresses, see subsection 2.2.2. The periodic change of the setup generates a water level oscillation with period larger than the incoming waves, see also Figure 2.6 for a visualization of the mechanism. The water level oscillation on the reef flat has the same period as and is in phase with the wave group envelope. The magnitude of the IG wave depends on the width of the surf zone, where a narrow surfzone enhances the breakpoint mechanism. The surf zone width depends on the mean breakpoint, frequency of incoming wave group envelope and bottom slope offshore and in the surf zone.

2.4.3. Infragravity wave generation: Bore merging

Bore merging is a mechanism that takes place within the surf zone. The bores travel on low frequency water level oscillations, where bores traveling on the crest catchup with the bores traveling on the through. The magnitude of the IG waves is lower than IG waves generated by moving breakpoint or bound long waves (Tissier et al., 2017). Furthermore, the process of bore merging is not fully understood yet and due to its magnitude relative to the other long wave generation mechanisms often neglected.

2.4.4. Infragravity wave propagation and deformation

In coral reef environments is bottom friction the main IG energy dissipation mechanism (Van Dongeren et al., 2013). On gentle slopes with low bottom friction (dissipative beaches) is the short wave energy low compared to the IG wave energy which is dominating (Bertin et al., 2018). This could also occur in coral reef environments with wide reef flats (Shimozono et al., 2015). For these beaches the IG wave components will interact with each other and generate higher IG harmonics. These harmonics give a sawtooth shape to the IG waves and thus lead to the steepening of IG waves close to coastline. Furthermore, it is shown that for beaches with a mild slope a relative large part of IG wave energy is dissipated at the coastline, which indicates IG wave break-

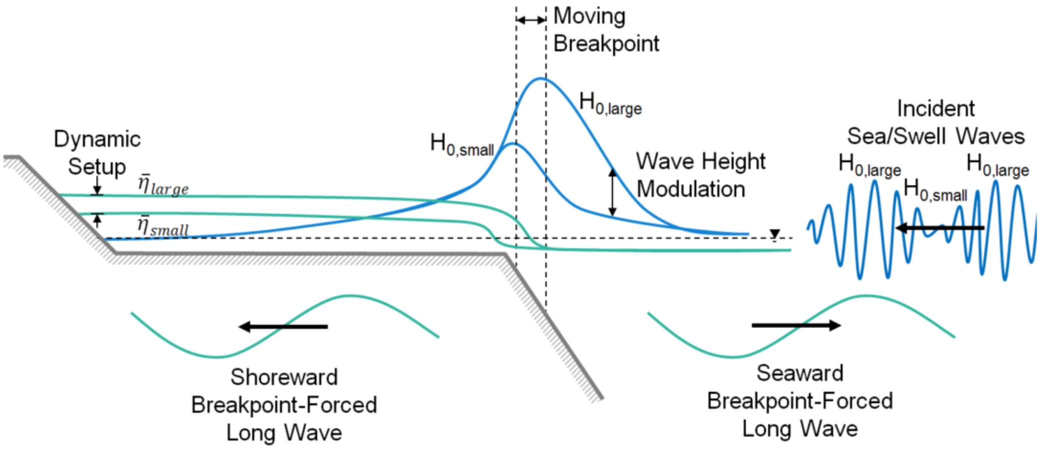

Figure 2.6: A visual explanation of the break point mechanisms. The dynamic setup varies with the incoming wave height, this generates a ocsilating water level with the period of the incoming wave group envelop (From Pearson (2016))

ing. van Dongeren et al. (2007) found bores from IG waves in a laboratory experiment. Roeber and Bricker (2015) showed that reef flat resonance and non-linear steepening of the IG water level elevations resulted in a bore propagating towards the coastline, which had a devastating effect.

The energy that is not dissipated by bottom friction, IG wave breaking or transfered away from the IG frequency band can be reflected on the beach slope. van Dongeren et al. (2007) found relation between the normalized bed slope (Equation 2.12) and the reflection coefficient. Almost full reflection is found for steep beach slopes and lower values for mild slopes. The period of the wave group envelop in combination with the reef flat submergence level and the IG wave reflection on the beach could lead to reef flat resonance. This is found in a field study of Péquignet et al. (2009) during tropical storm Man-Yi and confirmed by a XBeach model (Pomeroy et al., 2012b).

IG waves refract relatively more than short waves, due to their low wave numbers. So incident IG waves are more likely to approach the beach shore normal. However, in some cases offshore propagating reflected IG waves make an angle with the depth contours thus refraction is expected. On dissipative beaches it could occur that the reflected IG wave propagates offshore and escapes to deep water, these are called leaky waves. However, it is possible that the IG wave is deflected until it propagates back to the coastline, these are called trapped waves or edge waves (Bertin et al., 2018). Van Dongeren et al. (2013) modeled a 2D fringing reef in XB-SB and found mostly leaky waves, which could be explained by the very gentle slope of a reef flat where refraction is minimal until the reef edge. Including the steep fore reef slope results in little refraction before reaching deep water. However, Su and Ma (2018) modeled a concave shaped fringing reef with a Bousinessq type model and found besides leaky waves also edge waves.

2.4.5. Very low frequency waves

Very low frequency (VLF) waves are classified as having a frequency between 0.001 - 0.004 Hz (Cheriton et al., 2016; Pearson et al., 2017). In reef environments the VLF motions are generated by break-point mechanism and could become more pronounced due to reef flat resonance (Gawehn et al., 2016). Gawehn et al. (2016) divided VLF motions in coral reef environments into four classes; resonant, standing (non-resonant), progressive growing and progressive dissipating energy. By analyzing field data from Roi-Namur island (Republic of Marshall islands) they found that the resonant mode has the most impact on coastal safety and occurred 3.6% of the time (dataset of 5 months). Due to non-linear wave interactions the resonant VLF waves can develop into a bore-like wave form, which increases the impact. Such a thing could have occurred during typhoon Haiyan when a Tsunami-like bore struck the coast of Eastern Samar (Roeber and Bricker, 2015).

2.5. Other reef hydrodynamics

2.5.1. 2D flow patterns

As explained in subsection 2.2.2 will a change of the radiation stress lead to a water level elevation on the reef flat (setup). This process can be seen as waves pumping water onto the reef flat, which will generate a shoreward flux of water (Monismith, 2007). Continuity holds thus a circulation pattern has to develop, which could be in the vertical, but also in the horizontal. That the flow is generated by wave breaking is shown by Hearn (1999), with an analytical model he found relation between the incident wave height and the magnitude of the flow. This was earlier shown by Symonds et al. (1995), who also used a linear analytical model to analyse the processes. Gourlay (1996a) did laboratory model runs on an idealized 2D horizontal reef, these showed that the wave induced flow was large with wave breaking and decreased with a decreased wave breaking on the fore reef. These researches indicate that flow on coral reefs is mostly driven by incident wave energy.

Considering a 2D schematized reef as presented in Figure 2.2 and taking the reduced 1D cross-shore momentum balance (Equation 2.4) shows that a change in radiation stress is balanced by a pressure gradient. As mentioned before, circulation patterns are expected and these can be explained by a cross shore pressure balance (Figure 2.7). The depth integrated pressure balance, so a force balance, is equal when considering the a small body of water (dx). However, the magnitude of the radiation stress change differs over the depth where the pressure due to wave setup is constant over the depth. This generates a flow towards shore at the top of the water column and a offshore flow at the bottom, also called undertow.

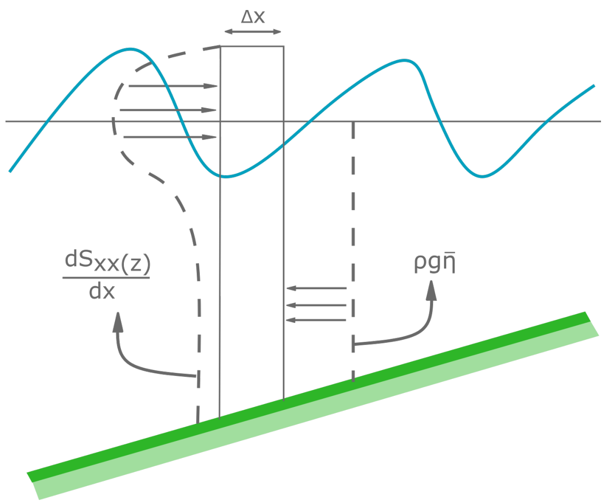

Figure 2.7: A pressure balance between radiation stresses and hydrostatic pressure. Bottom friction is excluded since it is expected to be an order of magnitude smaller than the pressure gradient, redrawn from Svendsen (2006)

Furthermore, circulation in the horizontal plane could occur. These can be quantified by calculating the horizontal vorticity (ω_z). This is rotation around the vertical axis, therefore the subscript z.

$$\omega_z = \frac{\delta v}{\delta x} - \frac{\delta u}{\delta y} \tag{2.13}$$

Where:

v, u	x,y velocities [m/s]
ω_z	Horizontal vorticity [1/s]

These 2D horizontal flow patterns can occur when an alongshore non-uniform coastline is considered. For instance a concave profile could refract waves which alters the wave setup and thus horizontal circulation cells can be expected. An other type of geometry induced flow, is circulation in a coral reef-lagoon channel system. Wave break on the reef crest which creates a setup over the reef crest, thus water is pumped into lagoon. Subsequently, the water flows back to deep water through channels in the reef crest (Lowe et al., 2009).

Furthermore, circulations could occur with the absence of alongshore variation of the bathymetry. For instance transient circulation cells, these are generated by the energy difference alongshore of incident wave groups (Dalrymple et al., 2011). Clark et al. (2012) hypothesized that the alongshore variation of wave forcing is leading to vorticity generation, and assumed that most vorticity is generated at the tip of short-crested wave rollers. However, they found that vorticity is generated along the whole wave crest, and argued that it could be due to spatial and temporal difference of the wave breaking.

Lastly, waves could generate alongshore current which lead to shear instabilities and thus circulations. These are a result of shear stresses between the alongshore flow inside the surf zone and stagnant water outside the surf zone (Dalrymple et al., 2011). Lippmann et al. (1999) investigated the dominance of shear waves over gravity waves and focused on the IG energy band. They defined a ratio which could be used to identify the variance that is contributing to IG shear waves (Equation 2.14). When $R = 1$ means that velocity to pressure variance is equal to g/h, which indicates gravity wave domination. $R \gg 1$ suggests shear wave domination.

$$R = \frac{\frac{\langle u^2+v^2\rangle}{\langle p^2\rangle}}{(g/h)} \tag{2.14}$$

Where:

$\langle v^2\rangle, \langle u^2\rangle, \langle p^2\rangle$	variance of u, v velocities and pressure
h	Water depth

2.5.2. Tide

Water level is modulated by the tide. Tide is a highly predictive water level oscillation on the timescale of approximately 12 hours (semi-diurnal) and approximately 24 hours (diurnal). The mean tidal range (MTR) is shown in Figure 2.8, most coral reefs have a MTR below 2 meter. However, the north of Australia and East coast of Africa show a MTR > 2.0. This figure only presents water level elevations until 3 meters, there exist cases where this level is larger.

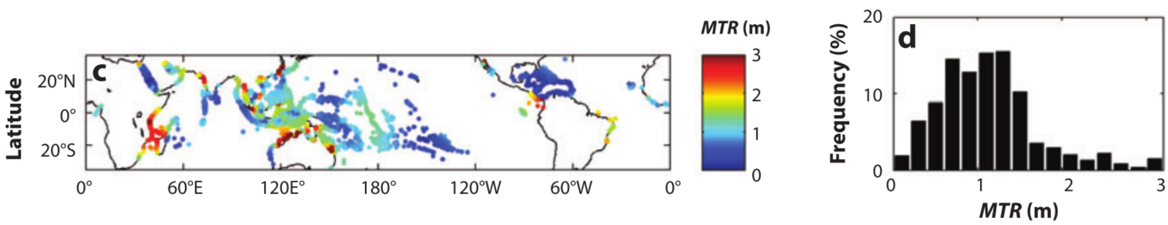

Figure 2.8: Global distribution of the mean tidal range (MTR) identified at coral reefs (from Lowe and Falter (2015)).

The tidal elevation is not an threat on itself, however the water level on the reef flat influences many processes and thus important for the assessment of coastal safety. Beetham et al. (2015) found that the runup mode is correlated to the reef flat water depth. The article shows that during low reef flat submergence, or low tide, the infragravity waves and wave setup are dominating the extreme water levels. High water levels on the reef flat show a runup dominated by infragravity wave and short wave energy. These findings are also confirmed by studies of Quataert et al. (2015) and Pearson et al. (2017). Costa et al. (2016) found a threshold of $h_{0,RF} = 2.0$ meter for which the transmitted wave height over the reef flat is controlled by the reef geometry. A larger depth shows a correlation between the incident wave height and the transmitted wave height.

3

Methods

This chapter elaborates on the various methods used in order to reach the research goal. At first the approach is discussed, subsequently every step is divided into multiple subsections, such that the approach is demonstrated in a structured manner. The goal of this chapter is to provide insight in the underlying framework, on which the results and conclusions are based.

3.1. Approach

In Figure 3.1 the structure of this chapter is shown. At first, artificial data is produced using a numerical model. Next, the methods of data processing are discussed, and all valuable data is cast into a database. At last, the methods of data analysis are discussed.

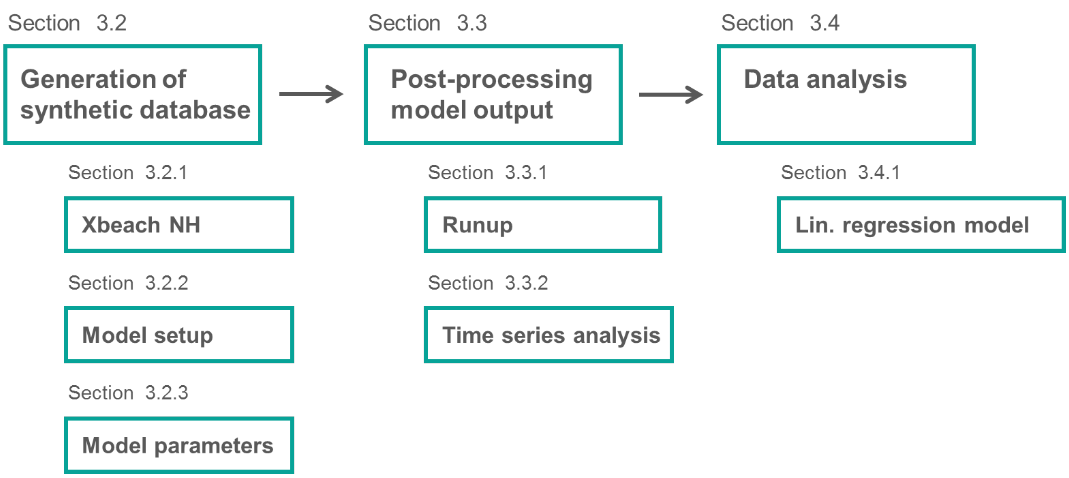

Figure 3.1: A visualization of the approach and outline of this chapter

3.2. Generation of a synthetic database

The lack of appropriate field data makes it difficult to investigate the influence of directional spreading and angle of incidence on the runup. For this reason, there is chosen to generate a synthetic database by using a numerical model.

The model has to resolve the wave field on the time scale of a single wave, also known as a full phase resolving model. This is important since such a model is able to model nonlinear waves, wave current interaction and wave breaking in the surf zone, and it captures nonlinear wave evolution. Two well-known types of full phase resolving models are: 1) Bousinessq models and Non-hydrostatic models. In this study the Non-Hydrostatic version of XBeach is used as numerical software (Roelvink et al., 2015; Smit et al., 2010) and is used to model wave transformation and coastline runup. There is chosen for XB NH since it has been used in coral reef environments multiple times and showed great potential. For example, Pearson et al. (2017) validated the model against data of Nwogu and Demirbilek (2010). Klaver (2018) used the model to investigate the effect of excavation pits on reef hydrodynamics. Lashley et al. (2018) validated the model against experimental datasets from Demirbilek et al. (2007) and Buckley et al. (2015). The XB NH model showed that it is capable of accurately predicting extreme runup at the coastline and wave transformation across a coral reef. In short, all studies were able to capture the important reef hydrodynamics, like wave runup and wave transformation.

The structure of this section is as follows, first of all XB NH is discussed, next the model parameters are discussed and at last a subsection is dedicated to the model setup.

3.2.1. XBeach Non-Hydrostatic XB NH

In this study XBeachX verion 1.23.5526 is used with the non-hydrostatic module. Furthermore, there is chosen to use an additional layer in the vertical (NH+). A brief explanation of the additional vertical layer is included below. In further reporting the + of NH+ is left out, since all models use the additional layer.

XB NH formulations are based on the single layer SWASH formulations, which are described by Zijlema et al. (2011). XB NH solves the non-linear shallow water (NLSW) equations, in order to describe the depth averaged, non-hydrostatic free surface motions (Smit et al., 2010). In other words, it uses the depth averaged continuity and momentum equations including the non-hydrostatic pressure term. Equation 3.1 gives the depth averaged continuity equation, which describes the relation between the velocity field and surface elevation. The depth integrated momentum equations are shown in Equation 3.2 & 3.3 & 3.4. A full derivation of these equations from the Navier-Stokes equations can be found in Smit et al. (2010). The equations are set up in a Cartesian coordinate system where x-direction is cross-shore, y-direction is alongshore and z-direction is vertical or depth (see subsection 3.2.2).

$$\frac{\partial \zeta}{\partial t} + \frac{\partial UH}{\partial x} + \frac{\partial VH}{\partial y} = 0 \tag{3.1}$$

Where:

ζ	Free surface
H	Total water depth $H = \zeta + h$, ζ is the surface elevation, h is the still water depth
U	Depth integrated velocity (x-direction), $U = \frac{1}{H}\int_{-h}^{\zeta} u dz$
V	Depth integrated velocity (y-direction), $V = \frac{1}{H}\int_{-h}^{\zeta} v dz$

$$\frac{\partial HU}{\partial t} + \frac{\partial}{\partial x}\left(HU^2 + \frac{1}{2}gH^2 + H\overline{p} - \frac{1}{\rho}H\overline{\tau}_{xx}\right) + \frac{\partial}{\partial y}\left(HUV - \frac{1}{\rho}H\overline{\tau}_{yx}\right) = gH\frac{\partial h}{\partial x} - p\frac{\partial h}{\partial x} + S_x \tag{3.2}$$

Where:

$\overline{p}$	Depth averaged dynamic pressure
$\overline{\tau}_{xx}, \overline{\tau}_{yx}$	Depth averaged turbulent or viscous stresses
S_x	The source and sink term, due to external stresses at bottom and free surface

$$\frac{\partial HV}{\partial t} + \frac{\partial}{\partial x}\left(HUV - \frac{1}{\rho}H\overline{\tau}_{xy}\right) + \frac{\partial}{\partial y}\left(HV^2 + \frac{1}{2}gH^2 + H\overline{p} - \frac{1}{\rho}H\overline{\tau}_{yy}\right) = gH\frac{\partial h}{\partial x} - p\frac{\partial h}{\partial x} + S_y \tag{3.3}$$

$$\frac{\partial HW}{\partial t} + \frac{\partial HUW}{\partial x} + \frac{\partial HVW}{\partial y} = -p_{surface} + p_{bottom} + \frac{1}{\rho}\frac{\partial H\overline{\tau}_{xz}}{\partial x} - + \frac{1}{\rho}\frac{\partial H\overline{\tau}_{yz}}{\partial y} \tag{3.4}$$

The depth-averaged non-hydrostatic pressure can be derived by following the same method as used for a single layer SWASH model. It is assumed that the dynamic pressure is zero at the surface and is linearly distributed over the depth (Zijlema et al., 2011). The capability of XB NH to solve the depth-averaged 2D non-linear shallow water equations makes it possible to investigate the influence of 2D mechanisms on wave runup. Furthermore, Zijlema and Stelling (2008) has shown that a non-hydrostatic model is able to accurately represent wave breaking and wave runup.

It is evident form Section 2.2.1 that an accurate representation of wave breaking is important to accurately model wave runup and therefore the wave breaking in XB NH is briefly discussed. In XB NH the wave breaking process is modeled by allowing the waves to steepen until the front face reaches a certain steepness, in XB NH defined as $maxbrsteep$. When this steepness is reached the wave steepness is reduced. This process of breaking is implicitly included in a non-hydrostatic model, i.e. the inclusion of non-linearities cause the waves to steepen, and in contrary frequency dispersion tends to counteract the steepening. Next to that, overturing and spilling breakers are not included in the model (Smit et al., 2010), this could lead to a slight underestimation of the wave setup, since the R_{xx} term in Equation 2.4 is not included in XB NH (Lashley et al., 2018). Furthermore, Zijlema and Stelling (2008) showed that a non-hydrostatic model is able to accurately represent the process and location of wave breaking.

Lastly, XB NH is based on the NLSW equations which are valid in shallow water. This means that model produces erroneous results when the waves are modeled in too deep water, or a too large kh, since frequency dispersion is not well captured. An accurate representation of frequency dispersion is important for wave transformation and wave-wave interaction. XB NH is able to correctly represent the dispersive behavior until a certain relative depth, generally $kh \leq 1.0$. This means that XB NH is not applicable when the offshore boundary is located in deep water. The model's ability to resolve frequency dispersion can be improved with the addition of vertical layers (Zijlema et al., 2011). However, this will be at the expense of computational time, therefore a reduced two-layer model was derived by Cui et al. (2014) and implemented into XB NH. This formulation accurately resolves frequency dispersion up to a relative depth of $kh = 5.0$ (de Ridder, 2018). The result is an increased flexibility of the offshore water depth, which makes it possible to model energetic wind-sea waves.

To summarize, XB NH is able to solve the 2DH non-linear shallow water equations. Next to that is has multiple times been used for wave modeling in coral reef environments, hence an appropriate choice for the present application.

3.2.2. Model setup

The aim of this subsection is to get insight into the model setup. At first, the domain and discretization of the domain is discussed, subsequently, the boundary conditions, and at last, there is elaborated on the model output.

Computational Domain

The computational domain is defined in a Cartesian coordinate system, where every point is defined relative to the coordinate (0;0), see Figure 3.2. Note that y is the alongshore direction and x is the cross-shore direction. Furthermore, the domain is enclosed with four boundaries; front, back, left and right. These are specified as follows:

- Lateral boundaries: Left and right are cyclic boundaries

  Cyclic boundary conditions copy all information that propagates through the lateral boundaries (i.e. left, right) to the opposite side of the domain. Hence, an infinitely long coastline is effectively created. This could give modeling issues when a specific feature (i.e. excavation pit) is present within the domain, since the hydrodynamics resulting from this are copied and influence the hydrodynamics at the opposite boundary. Furthemore, a XB NH model with cyclic boundary conditions has to be run with a Message Passing Interface (MPI). This divides the model domain in multiple sub domains and runs every domain on a single core and informations transferred to another domain at the boundaries. Running your model with MPI requires an specification of the number of sub domains and along which axis it will be divided. In this study is chosen for 4 sub domains ($nc = 4$) and a division along the $x-axis$. This is different from the default (i.e. $MPIboundary = y$), since this can place a MPI boundary in wave breaking zone which could lead to erroneous transfer of information between the sub domains.

- Front: 1D non-hydrostatic

  Modeling non hydrostatic requires the usage of the 1D non hydrostatic boundary condition offshore.

- Back : Beach with infinite height, so no over topping.

  The back of the model domain is enclosed by a beach with an infinite height. This means that the boundary does not have to be specified. However, XB NH requires an input in order to run, therefore a 2D absorbing boundary is used.

In Figure 3.3 the schematized depth profile is shown. This profile is based on previous model studies on coral reefs and discussed in Section 2.1.2. The model is forced by different wave heights ($H_{m0,0}$), wave steepnesses (s_0) and directional spreading (s_{dir}). Moreover, the

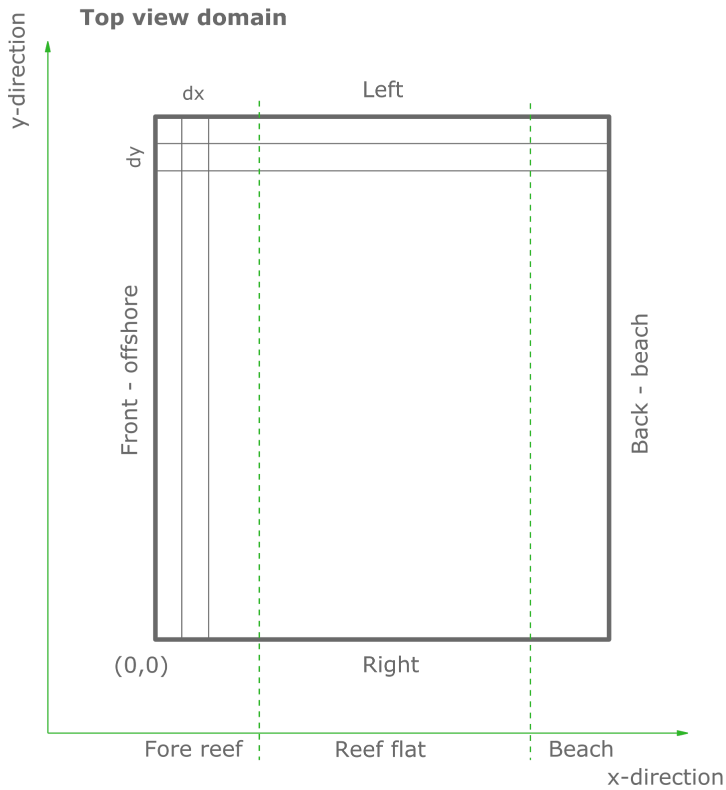

Figure 3.2: The XBeach model domain, where every point is described relative to the coordinate (0,0). y is the alongshore direction and x is the cross-shore direction. Furthermore, the domain is discretized by specifying dx and dy.

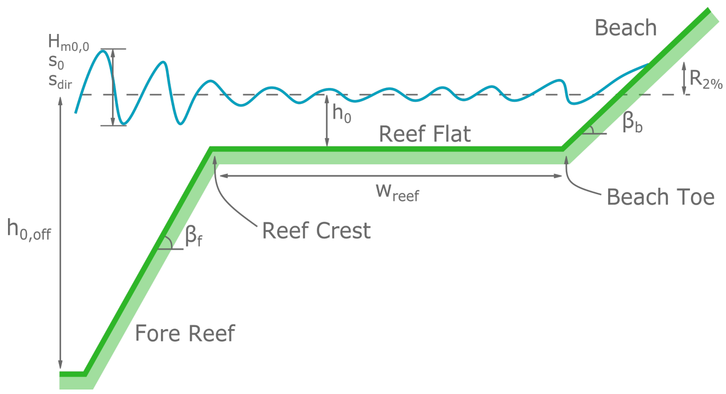

Figure 3.3: A schematization of the depth profile used in XB NH, adapted from Pearson (2016)

Grid

The grid size is important for two reasons: 1) computational stability and 2) accuracy of the model. The stability of a numerical solver can be assessed with the Courant Friedrichs Lewy (CFL) condition, which is a relation between the grid size and the time step. Next to that, the accuracy of the model is assessed with the number of points per wave length or ppwl, since sufficient ppwl are required to describe the shape of a wave.

Furthermore, the grid size in y-direction is mainly dependent on the grid resolution in x-direction, since large dx/dy ratio results inaccurate model output Appendix B. The sensitivity analysis showed that the best results were obtained with $dy = 4.0m$, which is kept constant in every model setup.

In all model runs the default value of $CFL = 0.7$ was used to define the local optimal grid size in x-direction. This value gave sufficient stability in all model runs. The condition was reached trough variable time stepping of the solver, which optimizes the time step at every location. Thus the computational time was optimized, while stability was guaranteed.

The ppwl is set to 20 for the wave length corresponding to the wave component at the peak frequency (f_p). This seemed sufficient to accurately describe wave shape and is able to capture a steepening wave front. However, a ppwl of 20 shows that the high frequency tail of the offshore spectrum is not captured in the XB NH model, since the theory of dispersion relation indicates that a higher frequency means a shorter wave length. These high frequency components was accounted for by defining a cut-off frequency such that at least 95% of the energy was properly entering the domain. This cut-off frequency is shown in Figure 3.4. This cut-off frequency is used to find the corresponding wave length with the dispersion relationship. Subsequently, the cut-off wave length has to be described with at least 15 ppwl, which gives the maximum grid size (dx_{max}). In other words, the grid size has to be sufficiently small to describe short wave lengths, which corresponds to high frequencies (i.e. dispersion relation). The length of the shortest wave is determined with the cut-off frequency in Figure 3.4, subsequently is the dx_{max} is found by assuming that this wave has to be described with at least 15 ppwl.

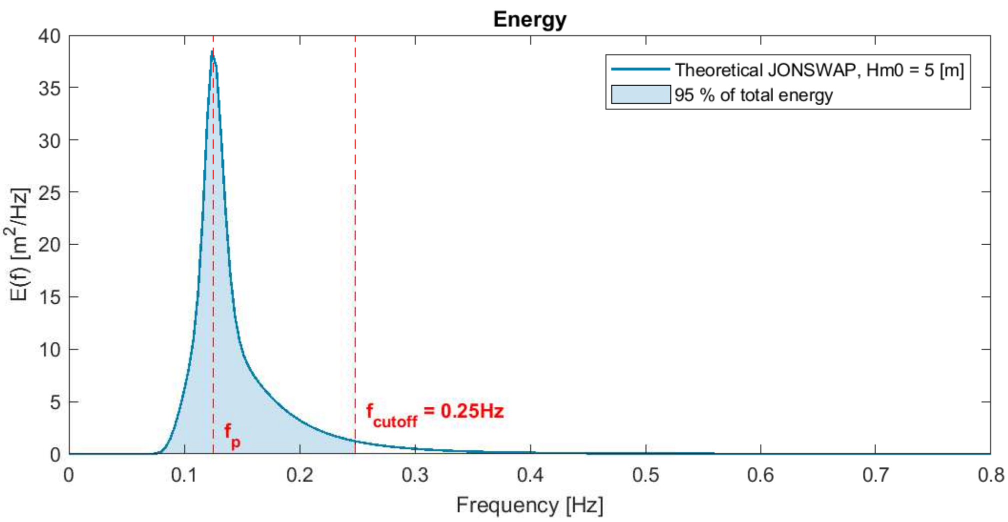

Figure 3.4: Visual explanation of the cut-off frequency. The method was applied on a theoretical JONSWAP spectrum for $H_{m0} = 5.0m$ and $s_0 = 0.05$

To summarize:

- $dy = 4.0$ m, constant throughout the domain
- $dx_{min} = 0.5$ m, trade-off between accuracy and computational time.
- dx_{max} is variable and defined with the method visualized in Figure 3.4.
- dx varies across the domain and was obtained with satisfying the CFL and ppwl condition using a typical time step and the local wave characteristics.

Offshore depth

The depth at the offshore boundary is a trade-off between multiple criteria. First of all, placement of the boundary at a to large relative water depth (kh) will give an inaccurate representation of the dispersive behavior. On the other hand, placement in too shallow water will cause wave breaking when entering the domain. Furthermore, bound long waves are generated at the offshore boundary, but these are better represented when generated in deep water. Lastly, it is preferable to place the offshore boundary at the shallowest point that satisfies the above criteria; in this way the computational time is optimized and the model domain size. All criteria are summarized for convenience.

1. $kh < 5.0$

   de Ridder (2018) found that the dispersive behavior was accurately represented for a relative depth smaller than 5.0.

2. $h > 2 * H_{max}$

   Following the Rayleigh distribution H_{max} is defined as $2 * H_{m0}$. Two times the maximum wave height is a conservative choice, since it corresponds to a breaker parameter of 0.5 ($\gamma = 0.5$), which is generally larger for coral reefs (see Section 2.3.5).

3. $n < 0.8$, where $n = c_g / c$

   Upper limit defined in XBeach.

Wave forcing

A XB NH model is forced by external conditions, like waves, wind and tide. Whereas this study focuses on the wave attack, thus a description of a wave field is required. In this study we describe a 2D wave field with a spectrum, or to be more specific, the variance density spectrum with a JONSWAP model (Equation 3.6) and directional distribution by Mitsuyasu et al. (1975) model (Equation 3.7). These models together form the 2D wave spectrum (Equation 3.5).

$$S(f,\theta) = E(f)D(\theta) \tag{3.5}$$

Where:

$D(\theta)$	Directional function, definition: $\int_{-\pi}^{\pi} D(\theta)d\theta = 1.0$
$E(f)$	Frequency spectrum

$$E_{JONSWAP}(f) = \alpha g^2 (2\pi)^{-4} f^{-5} \exp\left(-\frac{5}{4}\left(\frac{f}{f_p}\right)^{-4}\right)\gamma^{\exp\left(-\frac{1}{2}\left(\frac{(f/f_p)-1}{\sigma}\right)^2\right)} \tag{3.6}$$

Where:

α	Scaling parameter
γ	Peak enhancement factor $1 \le \gamma \le 10$ Usually 3.3
σ	Peak width parameter ($\sigma = 0.07$ for $f \le f_p$, $\sigma = 0.09$ for $f > f_p$)

$$D(\theta) = \cos^{2s}\left(\frac{\theta - \theta_0}{2}\right) \tag{3.7}$$

Where:

s	Directional spreading parameter
θ_0	Mean wave direction

The XB NH offshore model boundary is located in intermediate water depth. Next to that, the depth at this boundary is varying with the type of wave field that is imposed (see Section 3.2.2). This leads to an incorrect comparison of model output under a varying wave forcing, since the wave fields have been subject to refraction and shoaling. For this reason, the wave spectrum is shoaled and refracted from deep water towards the model domain, thus water depth at the offshore boundary. Use the acquired spectrum as wave input at the offshore boundary.

Shoaling of the wave spectrum
Firstly, the offshore frequency spectrum is shoaled. Shoaling is discussed in Section 2.3.3. The shoaled energy of certain wave component can be calculated with the shoaling factor (Equation 3.8 & 3.9).

$$E_{sh}(f) = K_{sh}(f)E(f) \tag{3.8}$$

$$K_{sh}(f) = \frac{c_{g,0}(f)}{c_{g,1}(f)} \tag{3.9}$$

Where:

$c_{g,0}$	Deep water wave group velocity
$c_{g,1}$	Local wave group velocity

The local and deep water wave group velocity can be obtained with the dispersion relationship. The shoaled 2D spectrum is defined as: $S_{sh}(f,\theta) = E_{sh}(f)D(\theta)$.

Refraction of the directional distribution
Secondly, the directional distribution is refracted by applying Snel's law, which is discussed in Section 2.3.4. Refraction of the directional distribution of every single wave component is divided into to three steps:

1. Refraction of every directional component with Snel's law, Equation 3.10. The result is shown in Figure 3.6a. The area below the refracted distribution is reduced (A_1) relative to the original distribution (A_0), this is corrected in step 2.

   $$\theta_1 = \arcsin(\tanh(k_1 h_1)\sin(\theta_0)) \tag{3.10}$$

   Where:

θ_0	Deep water wave angle
θ_1	Local wave angle
k_1	Local wave number
h_1	Local water depth

2. As mentioned in Step 1, a correction factor is applied, which accounts for the energy convergence in every directional bin, see Figure 3.5. Applying the energy correction factor f (Equation 3.11) gives the directional distribution shown in Figure 3.6b. Note that the area below the refracted distribution (A_2) has become equal to the area below the original distribution (A_0), since no energy is lost or added until this step.

   $$f = \frac{d\theta_0}{d\theta_1} \tag{3.11}$$

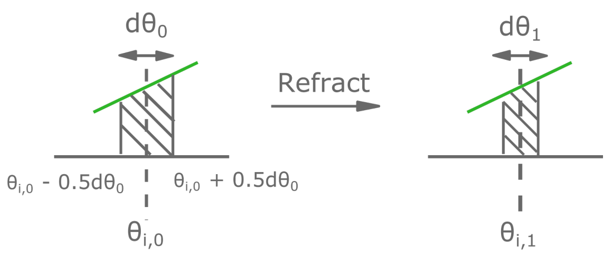

Figure 3.5: Visual explanation of refraction of a directional bin. The green line represents a snapshot of the directional distribution. Refraction of the left and right boundary of the bins cause a convergence of the energy, i.e. a larger wave angle will refract relatively more than a small wave angle.

3. Parallel wave rays propagating over a sloping bottom making an angle with the depth contours will refract. Moreover, the refraction leads to an divergence of the wave rays or an elongation of the wave crest, which is accounted for by a refraction factor, see Equation 3.12. Note that after refraction, the directional distribution is dependent on frequency. A typical refracted distribution is shown in Figure 3.6c. Refraction tends to elongate the wave crest, and therefore reducing the local wave amplitude, which is evident when A_0 and A_3 in Figure 3.6c are compared.

$$D_{ref,fi}(\theta) = K_{ref,fi}(\theta) D_{fi}(\theta) \qquad K_{ref,fi}(\theta) = \frac{\cos(\theta_0)}{\cos(\theta_1)} \tag{3.12}$$

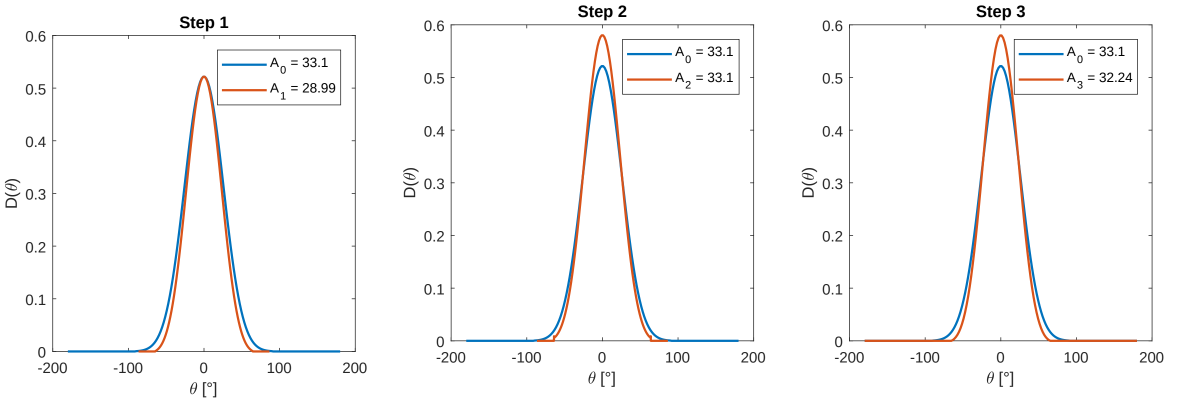

(a) Visualization of Step 1: apply Snel's Law

(b) Visualization of Step 2: apply energy correction factor

(c) Visualization of Step 3: Account for energy divergence of wave energy

Figure 3.6: A visualization of the refraction method. In blue the original directional distribution and in red the new directional distribution obtained in every step. The A_0 indicates the area below the blue graph and A_1,A_2 and A_3 the area below the red graph. The area below the graph can be seen as the energy of a certain frequency component.

Wave input XB NH

Lastly, the directional distribution is interpolated on a grid that can be used as input in the XB NH model. Subsequently, the 2D wave spectrum energy and discretization are written to a $vardens$ file which can be read by XB NH.

Assumptions

The discussed method is based on the following assumptions:

- Slowly varying bottom slope
- Parallel depth contours
- No currents
- No energy dissipation
- No energy input
- Linear waves

Most of the assumptions are valid for the model setup of this study only the first assumptions is in contrast with the model setup. This is only violated when it is assumed that the steep fore reef slope in the XB NH model extents until deep water. It is unknown to what extent it influences the wave refraction and thus the results. It is assumed that every model is slightly influenced by the steep fore reef slopes, hence the influence on the outcome is minimal. The exact influence is not checked in this study and could be checked by using a third generation wave model like SWAN.

Model Output

The output is used as basis of the synthetic database. In order to limit the data output of every single model run only buoy data is used to create a database. The buoy output is time series with an output frequency of 2 Hz of the water level elevation (η), velocity in x-direction (u) and velocity in y-direction (v). The measurement plan is shown in Figure 3.7 and consist of 70 η, u, v buoys and 15 runup gauges. A runup gauge measures the most elevated wet grid cell in positive x direction.

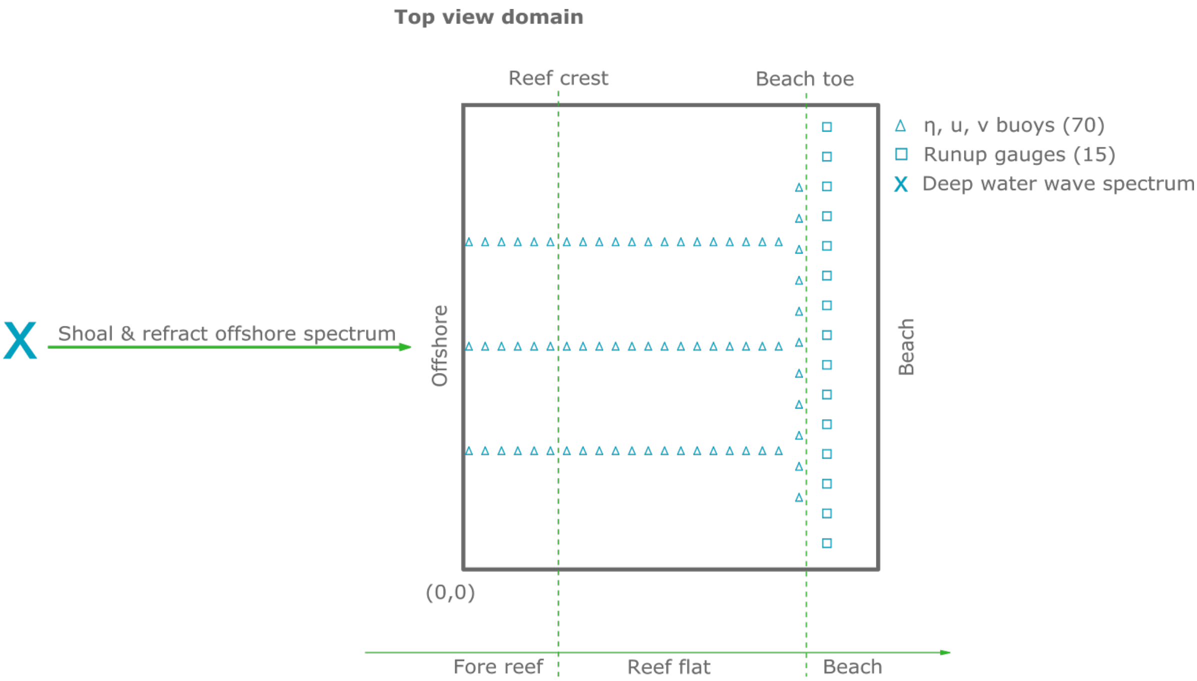

Figure 3.7: Visualization of placement of the measurement points, 3 cross-shore arrays are placed to capture the variability in both x and y direction. At the beach toe alongshore arrays of runup gauges and η, u, v buoys are placed.

3.2.3. Model parameters

The model setup described in subsection 3.2.2 can be used to simulate different hydrodynamic conditions in various reef environments. In this way, the influence of wave characteristics investigated in this study (i.e. directional spread and angle of incidence) on the reef hydrodynamics can be assessed. The reef characteristics and hydrodynamic conditions which have the most significant influence on the runup are selected from a previous study on wave attack in a reef environment (Pearson et al., 2017).

The characteristic reef profile used in this study is shown in Figure 2.2 and is described by a reef flat width (W_{reef}), fore reef slope (β_{fr}), beach slope (β_b), bottom friction (c_f) and reef flat submergence level (h_0). see Table 3.2 for an overview of the selected parameter values.

This study is focused on the safety from flooding due to wind sea and swell waves. Wind sea waves are characterized with a high steepness, and swell with a low steepness. Assigning a wave steepness to a specific wave field can be done by determining the wave age parameter (Equation 3.13). This parameter can be related to an estimation of the wave steepness, with the formulation of Toba (1972) (Equation 3.14). Following the reasoning of Goda (1985), it is possible to couple the directional spreading parameter (s) to the wave age parameter (β) (Equation 3.15), thus to the wave steepness, and thus to the type of wave field.

$$\beta = \frac{c_p}{U_{10}} \tag{3.13}$$

Where:

U_{10}	Wind velocity at 10 meter above the surface
c_p	Wave celerity at the peak frequency

$$s_0 = 0.0268\beta^{-1/2} \tag{3.14}$$

$$s = 11.5\beta^{2.5} \tag{3.15}$$

Large β−values indicate a relatively low wind velocity compared to the wave celerity. This is evident for fully developed sea states, where spectral energy is transfered to lower frequencies, which travel at greater velocities and where little energy input from the wind is present. Smith et al. (1992) defined that a fully developed sea stated has a value of $\beta > 1.2$. Semedo et al. (2014) used this to define a wind sea ($\beta < 1.2$) and a swell dominated wave field ($\beta > 1.2$). Applying this separation value to Equation 3.14 & 3.15 gives:

Table 3.1: Relation between wave steepness and directional spreading.

Wind-sea waves	
Wave steepness	$s_0 > 0.0245$
Directional spread	$s < 18$
Swell waves	
Wave steepness	$s_0 < 0.0245$
Directional spread	$s > 18$

Note that Equation 3.14 & 3.15 only have a clear correlation with the wave age parameter β in wind dominated environments, so relatively accurate predictions are given for $\beta < 1.2$. Additionally, it is assumed that the trend will continue for larger values of β, which is in agreement with the assumption made by Goda (1985).

To conclude, it is assumed that the two wave fields used in this study can be correlated to typical wave steepness and directional spread. These values are the basis of the wave field parametrization and used in the analytical shoaling and refraction model. All model parameters are summarized in Table 3.2.

Table 3.2: A summary of the model parameters. In total 27 different reef geometries are considered, which are exposed to 10 unique wind sea and 10 unique swell wave fields

Reef geometry (27)				
Reef flat width	W_{reef}	50, 200, 500	[m]	3
Fore reef slope	β_{fr}	1/20; 1/10; 1/5	[-]	3
Beach slope	β_b	1/10	[-]	1
Reef flat submergence	h_0	0.5, 2, 4	[m]	3
Bottom friction coefficient	c_f	0.02	[-]	1
Hydrodynamic conditions (20)				
Wind sea (10)				
Wave height	H_{m0}	3.0, 5.0	[m]	2
Wave steepness	s_0	0.05	[-]	1
Directional spreading	s	2, 5, 10, 20, ∞	[-]	5
Swell (10)				
Wave height	H_{m0}	3.0, 5.0	[m]	2
Wave steepness	s_0	0.01	[-]	1
Directional spreading	s	20, 40, 75, 100, ∞	[m]	5

3.3. Post processing model output

The model output has to be post-processed, before it can be stored into a database. At first the wave runup at the coastline is decomposed into setup, swash and a static reef submergence depth. Next to that, the buoy time series are analysed and the valuable data is extracted.

3.3.1. Runup and runup decomposition

Firstly, the $R_{2\%}$ is defined as the water level that is exceeded by 2% of the waves. Thus the runup gauge time series are analysed and individual waves, thus the local maxima are counted. Subsequently, the maxima are analysed and filtered. The first step is to remove the maxima lower than the mean runup. The second step is to select the highest maxima within a certain representative wave period. In this way, the maxima of individual wave runup events are selected. Next, the water level that is exceeded by 2% of the waves is the runup level. The maxima selection method is visualized in Figure 3.8.

Next to that, the setup is defined as the time averaged water level from the runup time series. The runup time series can be analysed and frequency runup components can be obtained by band passing the runup signal. The method is explained in Section 3.3.2.

3.3.2. Time series analysis

A time domain signal can be converted to frequency domain by performing a spectral analysis. A finite time series can be described with a Discrete Fourier Transform (DFT). This breaks a time periodic time series into a finite number of sinusoids. Fast Fourier Transform (FFT) algorithms can be used to compute the DFT. Next, the result of a DFT or FFT can be used to obtain the power density spectrum. Subsequently, the wave height (H_{m0}) can be obtained from a power density spectrum with Equation 3.16.

$$H_{m0} = 4.004\sqrt{m_0} \tag{3.16}$$

Where:

m_0	Zeroth spectral moment, $m_0 = \int_0^\infty f^0 E(f) df$

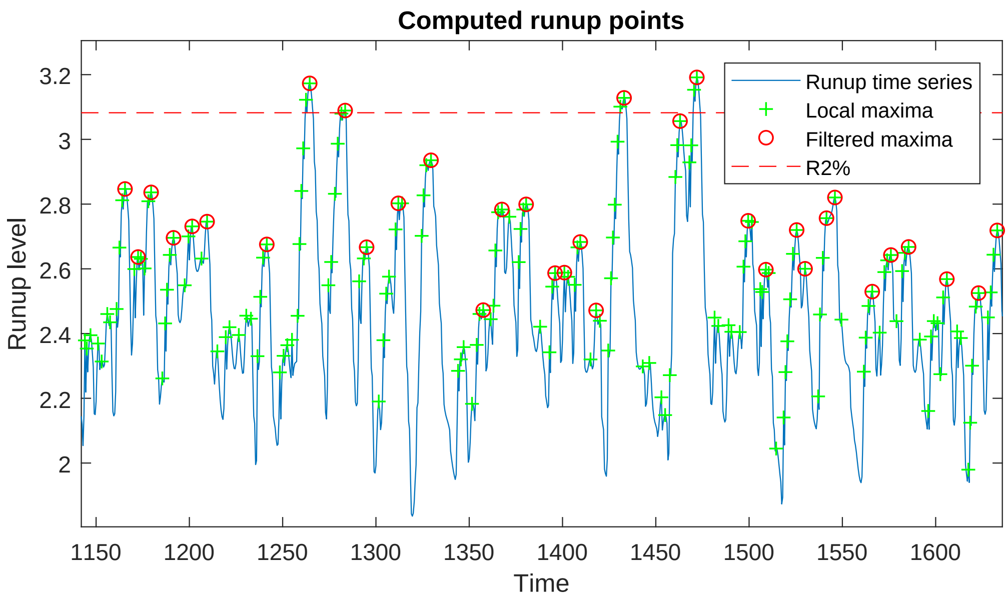

Figure 3.8: Visualization of the runup maxima selection. The runup time signal is shown in blue, green crosses indicate local maxima, red circles the local maxima after filtering and the red dashed line indicates the R2%.

In Section 2.4 the transfer of wave energy to lower frequencies and the importance in coral reef environments is discussed. The lower frequency wave component could contribute significantly to the wave the runup, therefore, the time series at the beach toe are analyzed and spectral wave height estimates are made with Equation 3.16, where the spectral moment (m_0) is found by integrating between the frequency limits:

Table 3.3: Definition of frequency components

High frequency waves (HF)		
Short waves	SW	$0.04 \leq f \leq 0.4$
Low frequency waves (LF)		
Infragravity waves	IG	$0.004 \leq f \leq 0.04$
Very low frequency waves	VLF	$0.001 \leq f \leq 0.004$

Cross-spectral analysis

With a cross-spectral analysis information about the mean wave direction and directional spreading can be obtained, this could be useful for two reasons:

1. In order to check whether the XB model input is correctly represented at the offshore boundary of the domain.
2. To check whether the important physical processes are included in the model, and thus whether XB NH is able to represent the evolution of the mean wave direction and directional spread through the model domain.

As explained in Section 3.2.2 the 2D wave spectrum is described by a variance density spectrum $E(f)$ and a Directional Spreading Function $D(\theta)$ (DSF). The goal of this analysis is to estimate the DSF shape. This can be done by following the method described by Kuik et al. (1988), where the time series of a pitch-and-roll buoy are analysed. This routine analysis is elaborately discussed by Benoit et al. (1997) and applied to an η, u, v time series, which can be obtained from XB output.

First of all, it is assumed that the DSF is a continuous function and thus can be described with a Fourier series decomposition (Equation 3.17). Additionally, the analysis of a single point measurement device (η, u, v) provides sufficient information to estimate the rank 1 and rank 2 Fourier coefficients (a_1, b_1, a_2, b_2). Thus an estimation of the DSF is limited to a truncated Fourier decomposition, see Equation 3.18.

$$D(f,\theta) = \frac{a_0}{2\pi} + \frac{1}{\pi}\sum_{n=1}^{\infty}\left(a_n \cos(n\theta) + b_n \sin(n\theta)\right) \tag{3.17}$$

Where:

a_0	$a_0 = \int_0^{\infty} D(f,\theta)d\theta = 1$
a_n, b_n	Fourier coefficients

$$D(f,\theta) = \frac{1}{2\pi} + \frac{1}{\pi}\left(a_1 \cos(\theta) + b_1 \sin(\theta) + a_2 \cos(2\theta) + b_2 \sin(2\theta)\right) \tag{3.18}$$

So, an estimation of the DSF requires information about the Fourier coefficients. Benoit et al. (1997) showed that the Fourier components can be estimated by using the auto, cross and quad spectra of the time series (Equation 3.19 & 3.20 & 3.21 & 3.22).

$$a_1(f) = \frac{C_{\eta u}}{\sqrt{C_{\eta\eta}(C_{uu} + C_{vv})}} \tag{3.19}$$

$$b_1(f) = \frac{C_{\eta v}}{\sqrt{C_{\eta\eta}(C_{uu} + C_{vv})}} \tag{3.20}$$

$$a_2(f) = \frac{C_{uu} - C_{vv}}{C_{uu} + C_{vv}} \tag{3.21}$$

$$b_2(f) = \frac{2C_{uv}}{C_{uu} + C_{vv}} \tag{3.22}$$

In Equation 3.19 & 3.20 & 3.21 & 3.22 C_{xy} is defined as the cross spectrum between two time series. The cross spectrum is determined by taking the real part of the complex cross spectrum, the definition of this complex cross spectrum is shown in Equation 3.23. Thus, the power density spectrum of both time series have to be computed, to get the cross spectrum. The power density spectra P_x and P_y can be obtained with a routine analysis of the time series as explained earlier.

$$P_{xy} = P_x P_y^*, \qquad C_{xy} = \mathrm{Re}(P_{xy}) \tag{3.23}$$

Where:

P_{xy}	The complex cross spectrum
P_x	Power density spectrum of time series x(t)
P_y^*	Complex conjugate of the power density spectrum of time series y(t)
C_{xy}	The cross spectrum

Besides the assumption that the DSF is continuous function, it also assumed to be unimodal. Hence, it can be described with the (Mitsuyasu et al., 1975) model. The model describes the DSF by means of a mean wave direction (θ_0) and a directional spreading parameter (s), see Equation 3.7. Furthermore, Kuik et al. (1988) defined formulations to estimate the Mitsuyasu et al. (1975) model parameters by using the rank 1 Fourier coefficients (a_1, b_1), see Equation 3.24 & 3.25, and the rank 2 estimates are given in Equation 3.26 & 3.27 (Benoit et al., 1997). In theory, the rank 1 and rank 2 estimates should give the same results. However, practice reveals that these estimates could differ, especially estimations of the directional spread. Note that σ and s can be related to each with the following expression $\sigma = \sqrt{2/(s+1)}$ (Barstow et al., 2005).

$$\theta_{0,1}(f) = \arctan\left(\frac{b_1}{a_1}\right) \tag{3.24}$$

$$\sigma_1(f) = (2(1-r_1))^{1/2} \tag{3.25}$$

Where:
$r_1 = \sqrt{a_1^2 + b_1^2}$

$$\theta_{0,2}(f) = \frac{1}{2}\arctan\left(\frac{b_2}{a_2}\right) \tag{3.26}$$

$$\sigma_2(f) = \left(\frac{1}{2}(1-r_2)\right)^{1/2} \tag{3.27}$$

Where:
$r_2 = \sqrt{a_2^2 + b_2^2}$

Estimations of the Mitsuyasu model parameters are dependent on frequency. It is chosen to limit the analysis to the short wave frequency range, thus $0.04Hz \leq f \leq 0.4Hz$ (indicated in red in Figure 3.9). Furthermore, noise is generated when the energy density of a specific frequency component is very low. Therefore, the analysis is cut-off when the energy density drops below 0.5% of the energy at the peak frequency (indicated in black in Figure 3.9).

In the last step representative values of θ_0 and s are calculated. As mentioned before, the estimations depend on frequency and these fluctuate. For this reason, single value estimations are made by taking the energy weighted average. Such an average gives more weight to an estimation at the peak frequency than others. Herbers et al. (1999) also used this method to obtain a wave field representative estimation of θ_0 and s.

$$\overline{\theta}_{0,1} = \frac{\sum \theta_{0,1}(f)E(f)}{\sum E(f)}, \qquad \overline{\sigma}_1 = \frac{\sum \sigma_1(f)E(f)}{\sum E(f)} \tag{3.28}$$

Where:

$\overline{\theta}_{0,1}$	Energy weighted average of the mean wave direction
$\overline{\sigma}_1$	Energy weighted average of directional spread
$E(f)$	Energy density spectrum

The mean wave angle $\overline{\theta}$ and mean directional spreading $\overline{\sigma}$ can be used to investigate the evolution of these parameter throughout the domain.

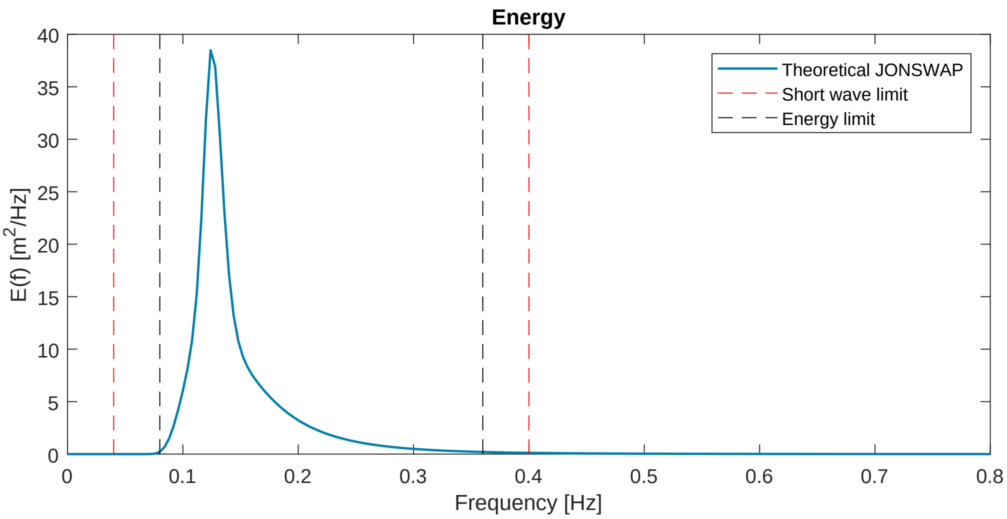

Figure 3.9: A JONSWAP spectrum with $H_{m0} = 5.0m$, In red the short wave limit ($0.04Hz \leq f \leq 0.4Hz$) and in black the energy cutoff

3.4. Data analysis

The last step of this study is to analyze the database. A common way to investigate large dataset is to perform a regression analysis. The importance of model variables can easily be assessed by performing such an analysis. A multivariate linear regression analysis is used to investigate the influence of individual parameters on the runup. The analysis is demonstrated with a simple multivariate linear regression model presented in Equation 3.29 (Rawlings et al., 1998). A model is called linear when it can be written at as a linear combination of β-parameters, thus the relation could be non-linear in x.

$$y = \beta_0 + \beta_1 x_1 + \beta_2 x_2 + \epsilon \tag{3.29}$$

Where:

y	Response variable
x_1, x_2	Predictor variables
$\beta_0, \beta_1, \beta_2$	Regression coefficients
ϵ	Residual term

The goal of this analysis is to find the regression coefficients (β) that provide the best estimation of the response variable. Firstly, the linear relation will be written in the form of a vector and matrix summation, see Equation 3.30. Where $\mathbf{X}$ are the predictor variables and $\mathbf{y}$ is the response variable, β is called the regression coefficient or the weighing factor of the predictors. The regression model is applied to a dataset with n data points.

$$\mathbf{y} = \mathbf{X}\beta + \epsilon \tag{3.30}$$

Where:

$$\mathbf{y} = \begin{bmatrix} y_1 \\ y_2 \\ \vdots \\ y_n \end{bmatrix} \quad \mathbf{X} = \begin{bmatrix} 1 & x_{11} & x_{21} \\ 1 & x_{12} & x_{22} \\ \vdots & \vdots & \vdots \\ 1 & x_{1n} & x_{2n} \end{bmatrix} \quad \beta = \begin{bmatrix} \beta_0 \\ \beta_1 \\ \beta_2 \end{bmatrix} \quad \epsilon = \begin{bmatrix} \epsilon_1 \\ \epsilon_2 \\ \vdots \\ \epsilon_n \end{bmatrix}$$

Next, the ordinary least squares (OLS) method can be used, to find the best linear combination of predictor variables that estimate the response variable. The OLS method calculates the best linear fit by minimizing the sum of squares, in other words, it optimizes the residual term (ϵ-parameter). Thus, the best estimation results in a residual term that equals zero, which mean that Equation 3.30 can be written as:

$$\hat{\mathbf{y}} = \mathbf{X}\hat{\beta} \tag{3.31}$$

Where:
$\hat{\beta} = (\mathbf{X'X})^{-1}\mathbf{X'y}$
$\hat{y}$ is estimation of y

In Equation 3.31 is **X'** defined as the transpose of **X**. The residual term can be found by calculating the difference between **y** and $\hat{\mathbf{y}}$ (Equation 3.32). The residual term can be used to compare different types of regression models, i.e. a low residual term indicates a good prediction of **y**.

$$\epsilon = \mathbf{y} - \hat{\mathbf{y}} = (\mathbf{I} - \mathbf{H})\mathbf{y} \tag{3.32}$$

Where:
$\mathbf{H} = \mathbf{X}(\mathbf{X'X})^{-1}\mathbf{X'}$

Furthermore, the accuracy of the regression model can be assessed with the correlation coefficient (Equation 3.33). Note that, the correlation will increase with every predictor parameter added to the regression model. For this reason, the adjusted correlation coefficient can be used, this parameter corrects for the number of model predictors (Equation 3.34).

$$R^2 = \frac{SS_{reg}}{SS_T} \tag{3.33}$$

Where:

SS_T	Total sum of squares, Equation 3.35
SS_{reg}	Sum of squares from the regression model, Equation 3.36

$$R^2_{adj} = 1 - \left(\frac{n-1}{n-k}\right)\left(1 - R^2\right) \tag{3.34}$$

Where:

n	Number of data points or sample size
k	The number of predictors

The total sum of squares (Equation 3.35), the sum of squares from the regression model (Equation 3.36) and the residual sum of squares (Equation 3.37) are defined as:

$$SS_T = \sum_{i=1}^{n} (y_i - \overline{y})^2 \tag{3.35}$$

$$SS_{reg} = \sum_{i=1}^{n} (\hat{y}_i - \overline{y})^2 \tag{3.36}$$

$$SS_{res} = \sum_{i=1}^{n} (y_i - \hat{y}_i)^2 = SS_T - SS_{reg} \tag{3.37}$$

At last, it could be useful to standardize the data set, such that every predictor and response parameter is scaled and dimensionless. With a standardized data set it is possible to access the influence of each parameter on the estimation, thus, it gives insight whether a parameter should be incorporated in a regression model. Two common methods are unit normal scaling (Equation 3.38) and unit length scaling (Equation 3.39).

$$z_{ij} = \frac{x_{ij} - \overline{x}_j}{s_j}, \qquad y_i^* = \frac{y_i - \overline{y}}{s_y} \tag{3.38}$$

Where:

z_{ij}	Unit normal scaled parameter of predictor x_j
$\overline{x}_j$	Mean of predictor x_j
s_j	Estimated sample standard deviation of predictor x_j
y_i^i	Unit normalized and scaled response variable y
y_i	Response variable
$\overline{y}$	Mean value of the response variable
s_y	Estimated sample standard deviation

$$w_{ij} = \frac{x_{ij} - \overline{x}_j}{\sqrt{S_{jj}}}, \qquad y_i^0 = \frac{y_i - \overline{y}}{\sqrt{SS_T}} \tag{3.39}$$

Where:

w_{ij}	Unit length scaled parameter of predictor x_j
S_{jj}	Corrected sum of squares $S_{jj} = \sum(x_{ij} - \overline{x}_j)^2$

Another type of model is the non-linear regression model, an example is given in Equation 3.40. The linear regression model described above is not applicable on this type of relations between the response and predictor parameters. Hence, Equation 3.40 has to be written in its linear form, this is obtained by applying the logarithmic laws to the non-linear relation.

$$y = \beta_0 x_1^{\beta_1} x_2^{\beta_2} \quad \rightarrow \quad \ln(y) = \ln\left(\beta_0 x_1^{\beta_1} x_2^{\beta_2}\right) \quad \rightarrow \quad \ln(y) = \ln(\beta_0) + \beta_1 \ln(x_1) + \beta_2 \ln(x_2) \tag{3.40}$$

Lastly, the influence of a parameter on the predictive power can be assessed by performing a F test. This test compares the regression analysis of the full model with a reduced model. The F values can be used in a F test look up table in order to find whether the addition of a predictor added value to the predictive skill of the model.

$$F_{diff} = \frac{(SS_{reg,full} - SS_{reg,red})/p}{SS_{res,full}/(n-k-1)} \tag{3.41}$$

In Equation 3.41 is p the number of predictors removed from the full model, or the degrees of freedom in the numerator. And $(n-k-1)$ the degrees of freedom in the denominator. These degrees of freedom together make up the shape of your F distribution and thus the F-value for a five percent significance test. In general means a large value of F_{diff} means that the full regression model is preforming better than the reduced regression model. The F_{diff} and R^2_{adj} can be used to assess the influence of a predictor on the predictive skill of a model.

4

Results - Wave transformation

The goal of this chapter is to describe the wave transformation in a coral reef environment. Firstly, the cross-shore wave energy evolution is discussed. Secondly, the transformation of the cross-shore wave energy density spectrum is treated. Thirdly, the evolution of the directional spreading within the domain is treated. Lastly, the evolution of wave directional spread in different reef environments is discussed.

The chapter is split into two parts, firstly the results from wind sea wave conditions is treated. Subsequently, the model results from swell wave conditions are discussed. The results from wind sea and swell waves are split, since they represent a different type of wave field. For instance, a wind sea wave field is characterized by relatively short waves and a broad wave spectrum (i.e. large s_{dir} values). And a swell wave field is characterized by relatively long waves with a narrow directional spectrum (i.e. large s_{dir} values). In Figure 4.1(a),(b) the surface elevation of wind sea and swell waves is shown. The wind sea waves (Figure 4.1(a)) are characterized by short wave lengths in x-direction (i.e. can be seen by the succession of blue and yellow regions in Figure 4.1) and relatively short wave crest lengths in y-direction (i.e. yellow regions in Figure 4.1). Such a wave field can be seen as a more chaotic distribution of water surface peaks and troughs. In contrast, Swell waves (Figure 4.1(b)) have relatively long wave lengths in x-direction and have long wave crests in y-direction.

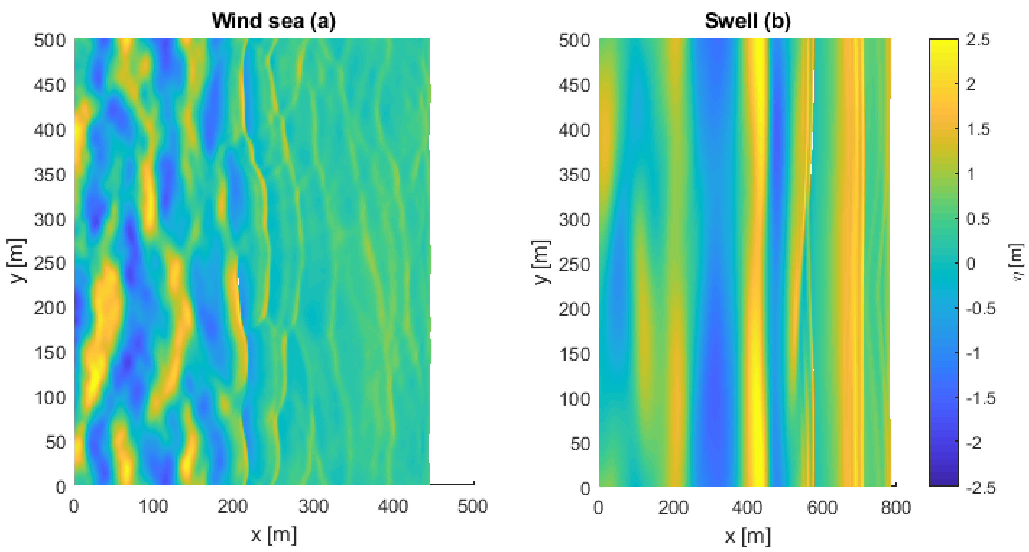

Figure 4.1: In both figures the instantaneous surface elevation is shown. The reef geometry has a β_f = 0.01, W_{reef} = 200 m and h_0 = 2.0 m . (a) the surface elevation of a wind sea wave field with $H_{m0,0}$ = 5 m and s_{dir} = 10. (b) the surface elevation of a wind sea wave field with $H_{m0,0}$ = 5 m and s_{dir} = 40. Note that swell waves have a narrower directional distribution, this is explained in Section 3.2.3. Furthermore, the scale on the x-axis is different, this is due to the placement of the offshore boundary, see Section 3.2.2.

4.1. Wind sea waves

In this first section the evolution of wind sea waves in a coral reef environment is discussed. The forcing parameters and reef geometry are presented in Table 4.1, this setup will be used to show the wave evolution. Note that, the cross-shore evolution is averaged over three cross-shore buoy arrays (see Figure 3.7 for the location).

Table 4.1: Model setup for the qualitative analysis of wave evolution

Reef geometry			
Reef flat width	W_{reef}	200	[m]
Fore reef slope	β_{fr}	1/10	[-]
Beach slope	β_b	1/10	[-]
Reef flat submergence	h_0	2	[m]
Bottom friction coefficient	c_f	0.02	[-]
Hydrodynamic conditions			
Wave height	H_{m0}	5.0	[m]
Wave steepness	s_0	0.05	[-]
Directional spread	s	10.0	[-]

4.1.1. Wave height transformation

Evolution of spectral wave height H_{m0} is indicated in Figure 4.2(b). Firstly, the wave height H_{m0} is slightly lower than the deep water wave height of 5.0 m as presented in Table 4.1. This is due to the refraction and shoaling model prior to the XB NH model domain. Furthermore, the wave spectrum calculated with the shoaling and refraction model has a correlation of $R = 0.99$ with the spectrum obtained at the offshore buoy. Therefore, it is assumed that the wave energy is correctly entering the model domain. Within the first 30 meters of the model domain the wave height is reduced. This slight reduction is common problem in XB NH and could be explained by a transition area where the NLSW equations have to take over the waves that are generated at the boundary. At roughly $x \approx 200$ m waves are breaking and thus wave height is reduced. On the reef flat the wave height is further decreased due to the bottom friction. At the most inshore buoy, waves are only 14% of the incident wave height ($H_{m0}HF$) (Figure 4.2(b)). So there could be stated that the coral reef is attenuating the incident short waves, hence protecting the coastline. This is in line with the findings of Ferrario et al. (2014), who found that up to 95% of the incident wave energy can dissipated by the coral reef.

Furthermore, the literature study showed that the LF motions can dominate wave runup in a reef environment. Besides that, it showed that two processes are mainly responsible for the generation of LF wave energy; 1) long bound waves and 2) the break-point mechanism. In Figure 4.2(b) it can be seen that the LF wave height increases in the wave breaking region, which suggests that LF wave energy is generated by the break-point mechanism. Furthermore, the HF wave height decreases due to wave breaking and frictional dissipation. This leads to an increased importance of the LF motions on the reef flat and close to beach, since most HF wave energy is dissipated (see Figure 4.2(c)). The dissipation of HF wave energy and gradual increase of the LF wave motion domination is well established for fringing reefs and shown by Pomeroy et al. (2012a).

Lastly, the mean frequency (f_{mean}) of the wave field is constant until the wave breaking point (see Figure 4.2(d)), after which the mean frequency increases and subsequently decreases across the reef flat. The increase of the f_{mean} could be due to the growth of super harmonics as the waves steepen on the fore reef slope. The reduction of f_{mean} on the reef flat can be due to the dissipation of short wave energy, hence increased domination of LF waves. This dominance is also evident from Figure 4.2(c).

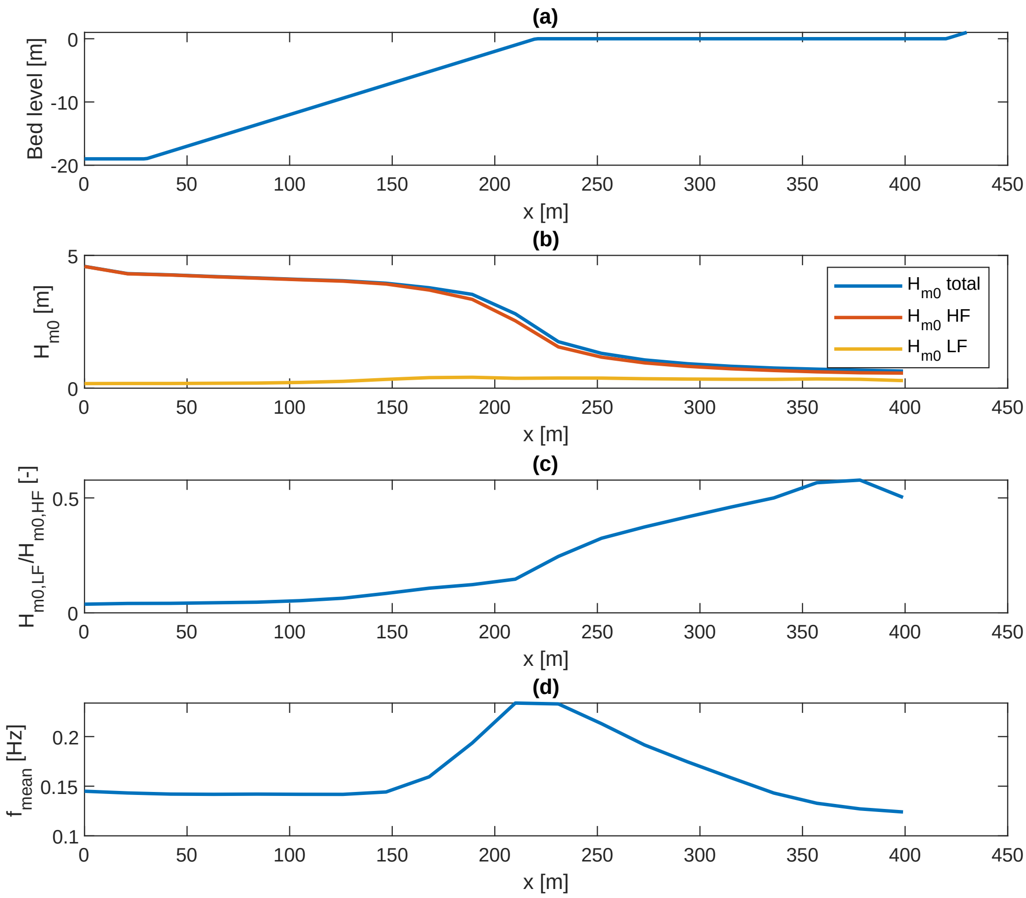

Figure 4.2: (a) the coral reef bathymetry is shown. This geometry consists of $\beta_f = 0.1$, $W_{reef} = 200m$ and $h_0 = 2.0$. (b) shows the wave height evolution in cross-shore direction. (c) shows the evolution of the ratio between HF and LF wave height. (d) shows the cross-shore evolution of the mean wave period (f_{mean}) which is calculated for $0.001 \leq f \leq 0.04$.

4.1.2. Spectral evolution

In the previous Section the evolution of the wave spectrum parameters is discussed. The break point of waves is identified and the generation of LF waves is evident. In this Section the cross-shore spectral evolution of η, u, v is discussed and is shown in Figure 4.3. These spectra are found with a routine analysis of the buoy time signal, this is discussed in Section 3.3.2. Furthermore, the wave spectra are normalized with the local E_{max}, this creates insight in the distribution of wave energy over frequency.

It is evident that the variance spectrum of η does not change until the reef crest (indicated with the green line in Figure 4.3(a)). At the reef crest wave breaking is initiated, which is already shown in Figure 4.2(b). During wave breaking wave energy is dissipated and LF waves motions are generated. At $x \approx 300m$ the LF wave motions become more dominant, which could be due short wave energy dissipation by wave breaking at the reef crest and bottom friction on the reef flat. Furthermore, it is evident that high frequency energy is generated on the reef flat, these could be transmitted incident waves. This high frequency energy can also be undular bores, which are observed on the reef flat.

The power density spectrum of the u-velocities is evolving similar to the surface elevation, which is in accordance with linear wave theory. However, the oscillations at the peak frequency are directly damped at the reef crest and LF motions dominate the reef flat.

The spectral evolution of the v-velocities is similar to the u-velocities. The oscillations at the peak frequency are damped when wave breaking is initiated, and is located in deeper water than the u-velocities. From this point LF oscillation of the v-velocity become more dominant.

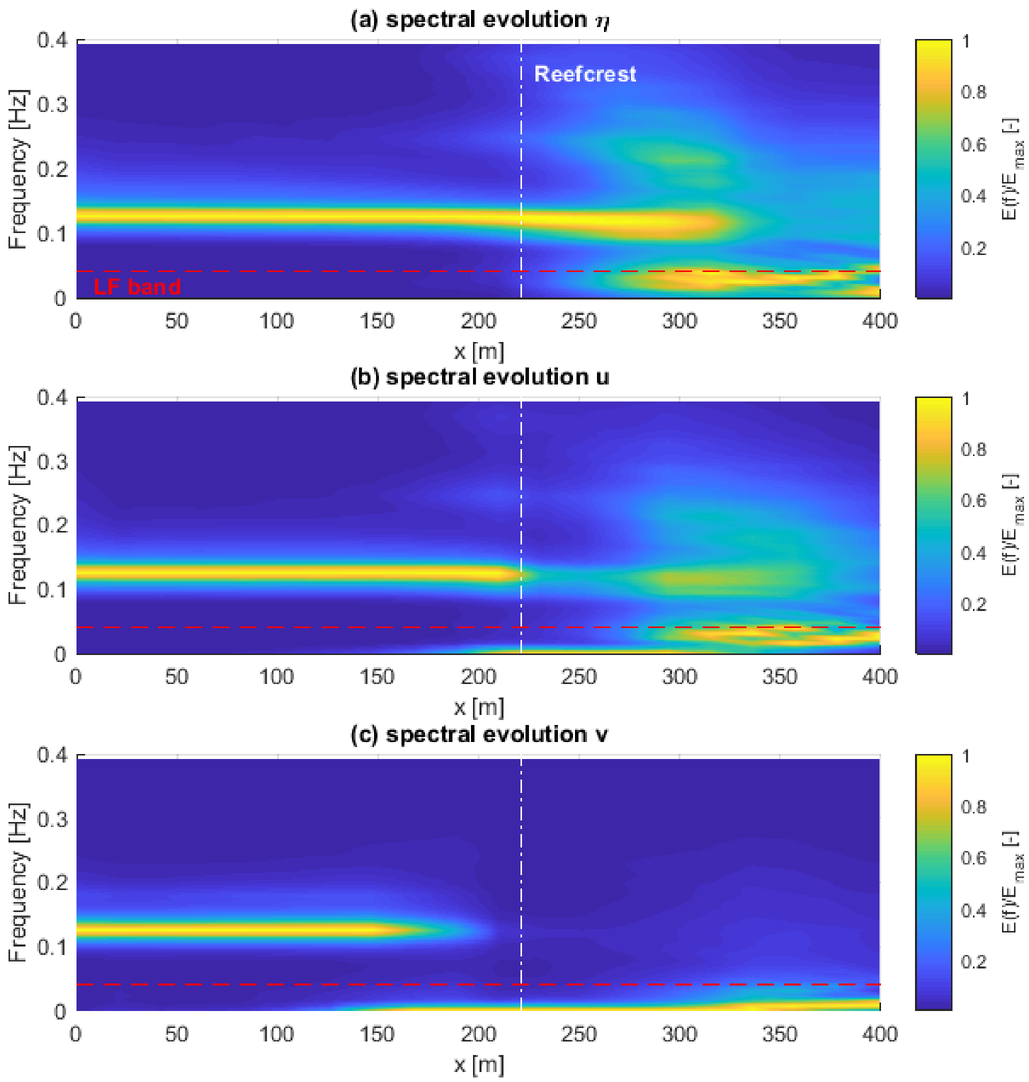

Figure 4.3: The evolution of the spectral variance density in cross-shore direction. (a) the water level η, (b) the u-velocity and (c) v-velocity. The spectra are obtained with the method described in Section 3.3.2. Furthermore, the wave spectra are normalized with the local E_{max}, this gives a clear insight in the distribution of wave energy over frequency.

The analysis of Figure 4.2 and Figure 4.3 show that most of the HF wave energy is dissipated on the reef crest and reef flat. In Figure 4.2(b) it is evident that the HF wave height is reduced due to wave breaking on the fore reef slope and crest. Furthermore, on the reef flat it is assumed that the wave field is saturated, hence most energy is dissipated through bottom dissipation. So, the two important mechanisms of HF wave dissipation are wave breaking and bottom friction. Next to that, Figure 4.2(c) showed that the low frequency wave motions become more dominant closer to shore, due the frictional dissipation of short wave energy on the reef flat and the generation of LF motions in the breaker zone, through the break point mechanism.

4.1.3. Evolution of directional spread

Next, the evolution of directional spreading is discussed. The directional spreading of a wave field is calculated with the method of Kuik et al. (1988) and is treated in Section 3.3.2. The results are shown in Figure 4.4(d). The cross-shore evolution of the directional spread is averaged over three cross-shore buoy arrays placed in the model domain. Furthermore, the results do not extent until the beach toe due to the placement of the buoy arrays.

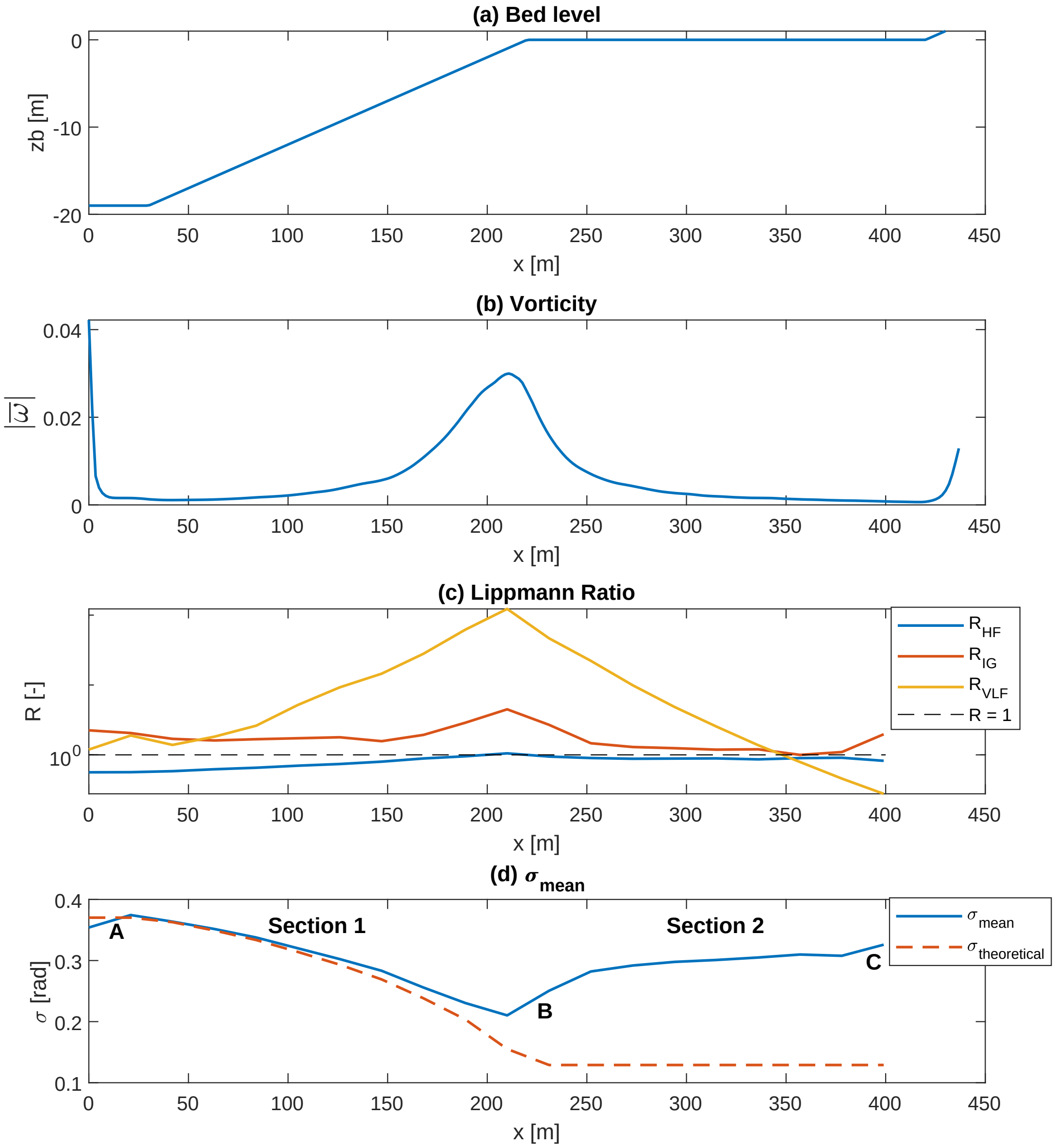

Figure 4.4: Cross-shore wave evolution. (a) the bathymetry, (b) the absolute and time averaged horizontal vorticity (c) the Lippmann ratios (Equation 2.14) calculated for different frequency bands and (d) the evolution of directional spreading from XB NH output (σ_{mean}) and from a theoretical model described in Section 3.2.2

Firstly, in Figure 4.4(b) the cross-shore evolution of vorticity is shown. Vorticity is composed of the pure rotation (swirl) and the shear motions in a velocity field. The vorticity is calculated with Equation 2.13. Note that the absolute vorticity is considered and it is time averaged over 2 hours (i.e. runtime XB NH models). From this figure can be concluded that vorticity is mainly generated in wave breaking zone, this is in line with the findings of Clark et al. (2012), who found that vorticity is generated due to preferential breaking of short crested waves. In other words, the vorticity is generated by along-crest variations in the breaking force. As mentioned before, the vorticity is a combination of eddies and mean current. In order to exclude the mean current from your analysis the ratio defined by Lippmann et al. (1999) can be used.

The ratio defined by Lippmann et al. (1999), here called Lippmann ratio, is discussed in Section 2.5.1. In Figure 4.4(c) (note the log-scale) cross-shore distribution of the Lippmann ratio is shown. This is defined as a ratio between the gravity and shear motions, i.e. an area is dominated by shear motions when $R >> 1$. The Lippmann ratio is determined for the HF, IG and VLF frequency band, which are defined earlier.

HF band: The Lippmann ratio of the HF motions is less than one offshore and moves towards one closer to shore. This shows that the HF motions are mainly dominated by gravity waves.
IG band: The Lippmann ratio of the IG motions offshore is larger than 1. In contrast, Lippmann et al. (1999) found that these values should equal one and will increase inside the surf zone. Furthermore, a increase of R_{IG} is found in the wave breaking zone, which is also found by (Lippmann et al., 1999).
VLF band: The Lippmann ratio of the VLF band R_{VLF} shows that the shear motions are dominating at a large part of domain.

Lastly, the evolution of directional spreading within the domain is investigated. The background study showed that directional spreading has an influence on the radiation stresses S_{xx}. Furthermore, it showed that the radiation stresses influence the setup, hence LF wave generation via the break-point mechanism. This suggests that it is interesting to know how directional spreading changes within the model domain. The evolution of the directional spreading can be subdivided into two sections, namely before breaking ($x < 200$) and after breaking ($x > 200$), see Figure 4.2(d). Next to that, a theoretical evolution of the directional spreading is shown. The theoretical directional distribution is found with linear wave theory where it is assumed that Snel's Law is valid. The theoretical refraction of the directional distribution is discussed in Section 3.2.2.

Section 1: The directional spreading is decreasing until breaking point. This is expected when theory is followed. Snel's law implies that obliquely incident wave components traveling over a sloping bottom will refract and become shore normal; thus, directional spreading will decrease. This phenomena is observed in Figure 4.4(d), where the theoretical model and the (i.e. based on Snel's Law) and XB NH model output is compared. In the first section the theoretical model and the XB NH model output start to deviate closer to the wave breaking point. This is also the region where the vorticity and thus currents are increasing.

Section 2: After wave breaking and thus on the reef flat waves will not experience any refraction due a sloping bed. Hence, it is expected that the directional spread will stay equal (i.e. Red line Figure 4.4(d)), however this is not evident for the directional spreading in the XB NH model output. In contrast, it indicates an increasing spread inside the surf zone. In this section the largest deviation between the theoretical and the model output is observed, since the model run experiences directional broadening. This phenomena is also observed in nature by Herbers et al. (1999) & Henderson et al. (2006), who analyzed data of wave evolution on sandy beaches. Henderson et al. (2006) stated that the directional broadening is occurring due to the refraction on currents inside the surf zone. The results in Figure 4.2(d) suggest that the directional broadening is occurring due the increased vorticity inside the surf zone, which is generated due to preferential wave breaking.

To summarize, Henderson et al. (2006) argued that the directional broadening inside the surf zone is due to refraction of the waves on currents. They found that a strong directional broadening often coincided with a strong domination of the LF shear motions ($0.001 \leq f \leq 0.05$). In this analysis it seems that directional broadening is occurring when 2 criteria are met: 1) the absence of a sloping bottom, thus no refraction on depth contours, and 2) the presence of horizontal vorticity. The first is evident when the theoretical and XB NH model output is compared, the deviation commences when the vorticity is increasing. Subsequently, the absence of a sloping bottom on the reef flat and the presence of vorticity leads to directional broadening, which largely deviates from the theory. A calculation of the Lippmann ratios indicate that the shear waves in the IG and VLF band are responsible for the broadening. This agrees with the findings of Henderson et al. (2006), who also found large Lippmann ratios for the LF band. A contrast between the findings of Henderson et al. (2006) and this investigation is the order of magnitude of these ratios, i.e. the Lippmann ratios found by Henderson et al. (2006) are a order of magnitude larger.

4.2. Swell waves

In this section the transformation of swell waves is discussed. The structure of this section will be same as the previous. Firstly, wave transformation and spectral evolution are discussed. Lastly, the evolution of the directional spreading is discussed. The model setup is shown in Table 4.2.

Table 4.2: Model setup for the analysis of swell wave transformation in a coral reef environment.

Reef geometry			
Reef flat width	W_{reef}	200	[m]
Fore reef slope	β_{fr}	1/10	[-]
Beach slope	β_b	1/10	[-]
Reef flat submergence	h_0	2	[m]
Bottom friction coefficient	c_f	0.02	[-]
Hydrodynamic conditions			
Wave height	H_{m0}	5.0	[m]
Wave steepness	s_0	0.01	[-]
Directional spread	s	40.0	[-]

4.2.1. Wave height transformation

In Figure 4.5 the evolution of swell waves is shown. It is clearly visible that the waves shoal on the fore reef slope and a clear wave height reduction is located at the reef crest. This is in line with the theory of shoaling waves. Furthermore, the LF wave height is substantial at the offshore boundary, this could be due to the bound long wave generated at the offshore boundary or due to the reflection of long waves on reef crest and beach slope. Next to that, the LF wave height increases when entering the breaking zone, this could indicate LF wave generation due to the break point mechanism (Symonds et al., 1982). In contrast with wind sea waves the LF wave height is larger, this could be due to the larger wave length and smaller directional spread of the swell waves.

Close to shore the water level fluctuations are mainly dominated by LF motions, which is similar to the wind sea model (Figure 4.5(c)). Nevertheless, the dominance of LF waves is larger than 1 whereas wind sea waves remained below 1.

The evolution of mean wave frequency (f_{mean}) is shown in Figure 4.5(d). The evolution is has the same shape as the wind sea model (Figure 4.2(d)) and no significant differences are found with wind sea wave is found.

4.2.2. Spectral evolution

In Figure 4.6 the variance density spectral evolution is shown of the η, u, v time series. The shape spectral evolution is already discussed in Section 4.1. This section will focus on the differences.

The surface elevation variance density spectrum shows that the LF wave motions start dominating the HF wave motions, which was also shown in Figure 4.5(c). In contrast to the wind sea model, most energy is located in the VLF region.

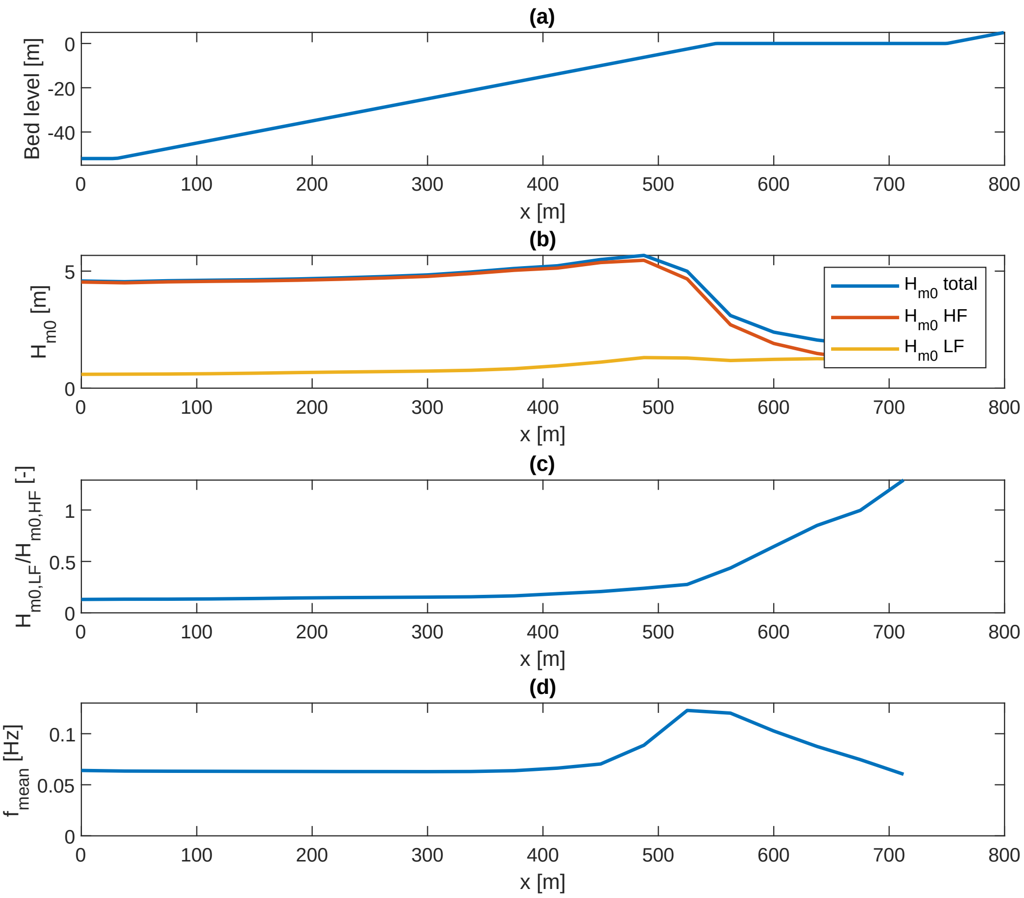

Figure 4.5: (a) the coral reef bathymetry is shown. This geometry consists of $\beta_f = 0.1$, $W_{reef} = 200m$ and $h_0 = 2.0$. (b) shows the wave height evolution in cross-shore direction. (c) shows the evolution of the ratio between HF and LF wave height. (d) shows the cross-shore evolution of the mean wave period (f_{mean}).

The spectral evolution of the u, v-velocities is similar to evolution in the wind sea model, namely the oscillations in the LF band are dominating during and after wave breaking.

4.2.3. Evolution of Directional spreading

The evolution of directional spreading is shown in Figure 4.7. At first the absolute horizontal vorticity and Lippmann ratios are calculated and discussed. In Figure 4.7(b) the absolute vertical vorticity is shown $|\overline{\omega}|$. Similar to the wind sea model, most vorticity is generated in the wave breaking zone. Nevertheless, the maximum vorticity generated in the surf zone is one order of magnitude smaller for swell waves. An analysis of the vorticity fields showed that swell waves generate less vorticity than wind sea waves. Moreover, swell waves have a lower directional spreading which also reduces the amount of vorticity (Appendix C).

The Lippmann ratios are determined for the HF, IG and VLF band (Figure 4.7(c)). The physical explanation of these ratios is explained in Section 4.1. The ratios indicate only a shear wave domination in the VLF band, where wind sea waves indicate a shear wave domination in the IG and VLF band. This indicates that most fluctuations in the velocity field, that are not a results of the waves, are located in the VLF band for swell waves.

Lastly, the evolution of directional spreading of HF waves is shown in Figure 4.5(d). The evolution is similar to the wind sea model, namely directional narrowing on the fore reef slope and directional broadening inside

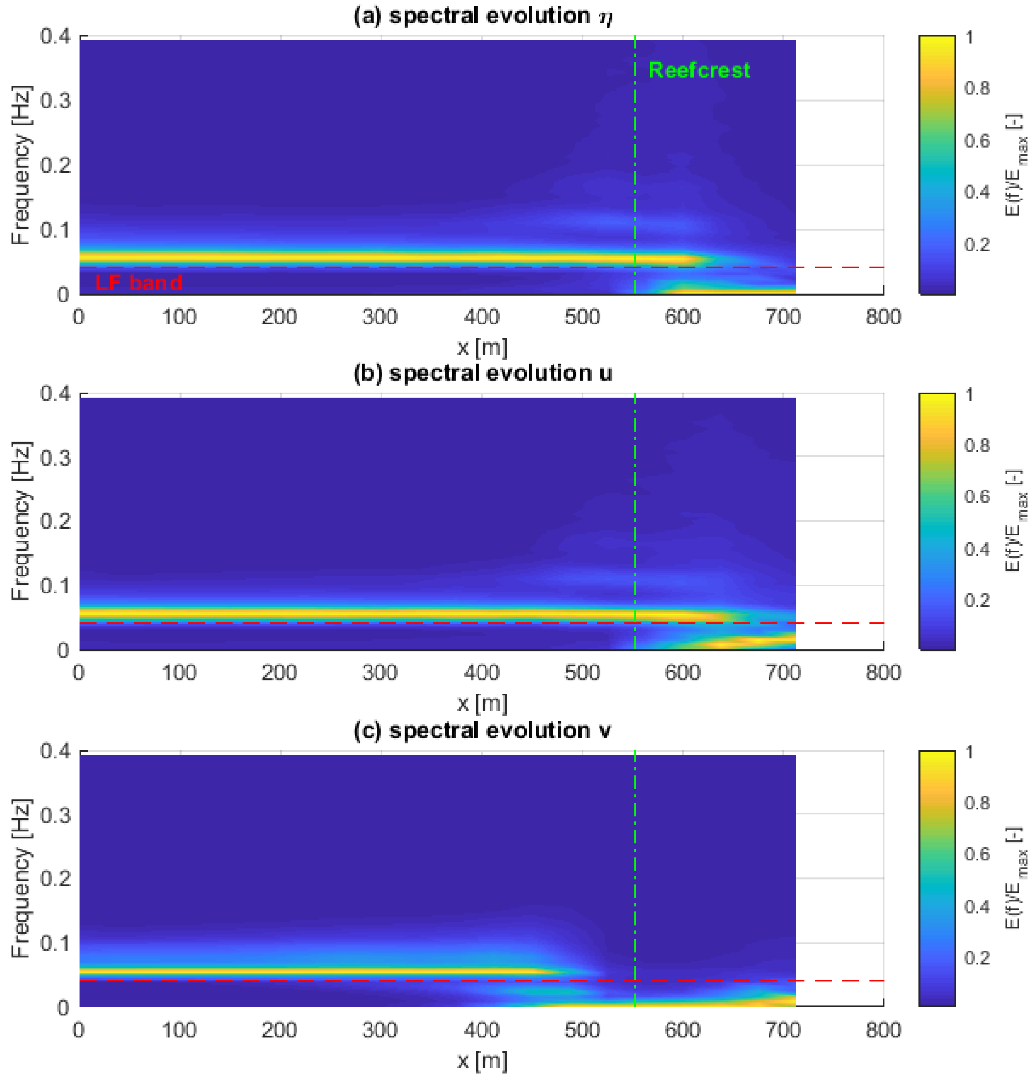

Figure 4.6: The evolution of the spectral variance density in cross-shore direction. (a) the water level η, (b) the u-velocity and (c) v-velocity. The spectra are obtained with the method described in Section 3.3.2

the surf zone.

Thus, Figure 4.7(b & c) indicate that in the wave breaking zone vorticity is generated, which could be shear and pure swirl motions. From the analysis of wind sea waves (Section 4.1) it seems that the absence of a slope and the dominance of vorticity leads to directional broadening. This is in line with the findings presented here. However, the calculation in of the Lippmann ratios shows a domination of VLF shear motions which could indicate the importance of VLF horizontal circulations. This is different for wind sea wave, since the IG and VLF shear motions are dominating.

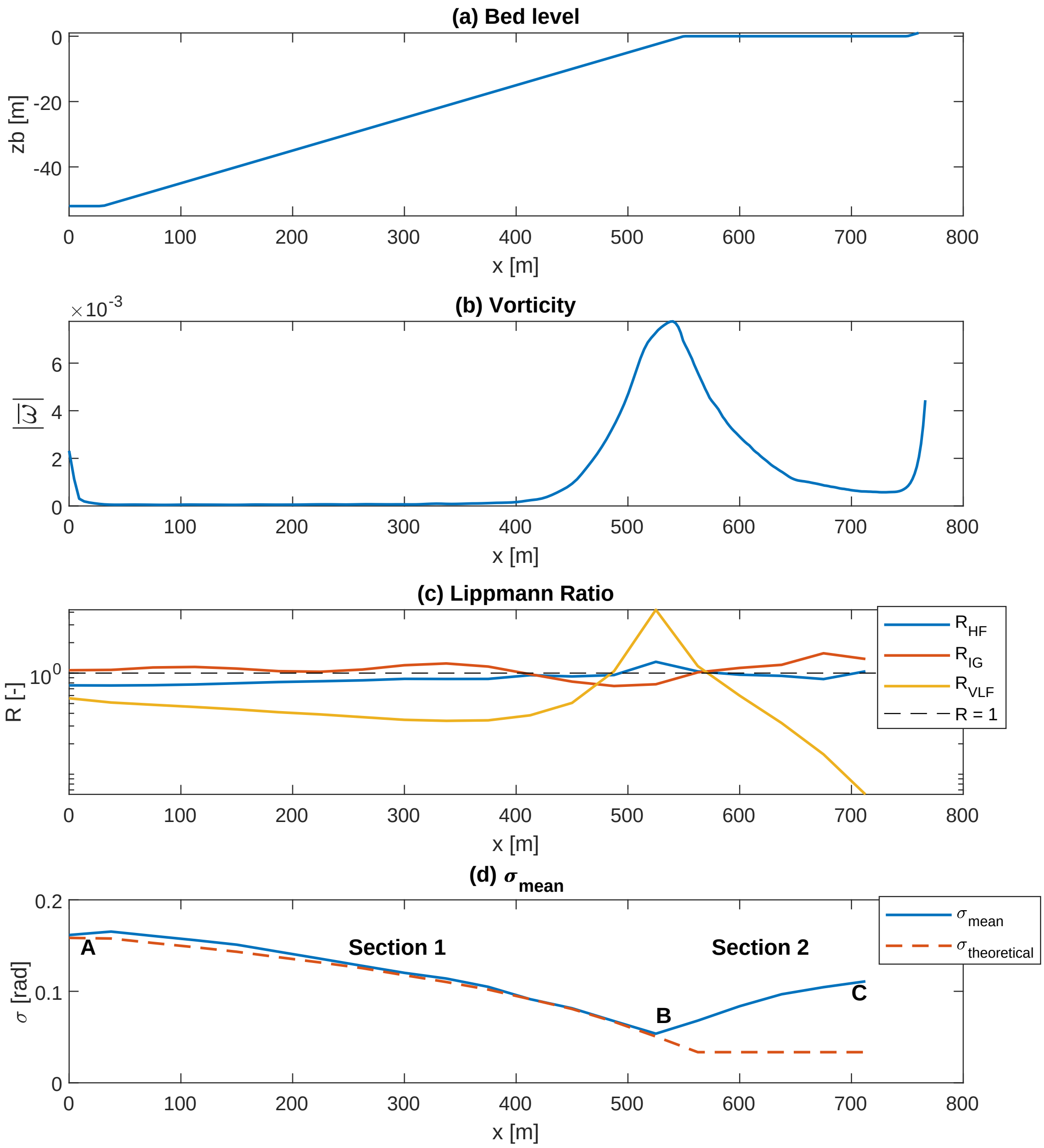

Figure 4.7: Cross-shore wave evolution. (a) the bathymetry, (b) the time averaged vertical vorticity (c) the Lippmann ratios calculated for every frequency band and (d) the evolution of directional spreading calculated with the method described in Section 3.2.2

4.3. Influence of Reef Geometry and Wave Forcing the Evolution of Directional spread

In the previous Sections directional narrowing and broadening is found. This Section focuses on the relation between the reef geometry and wave forcing and the directional spread evolution. The relations create insight in which parameters are controlling directional narrowing and broadening.

In Figure 4.8 the relation between directional evolution and model parameters is shown. In order to calculate these ratios it is assumed that the shape of σ evolution is equal in every simulation (see Figure 4.4(d)), and

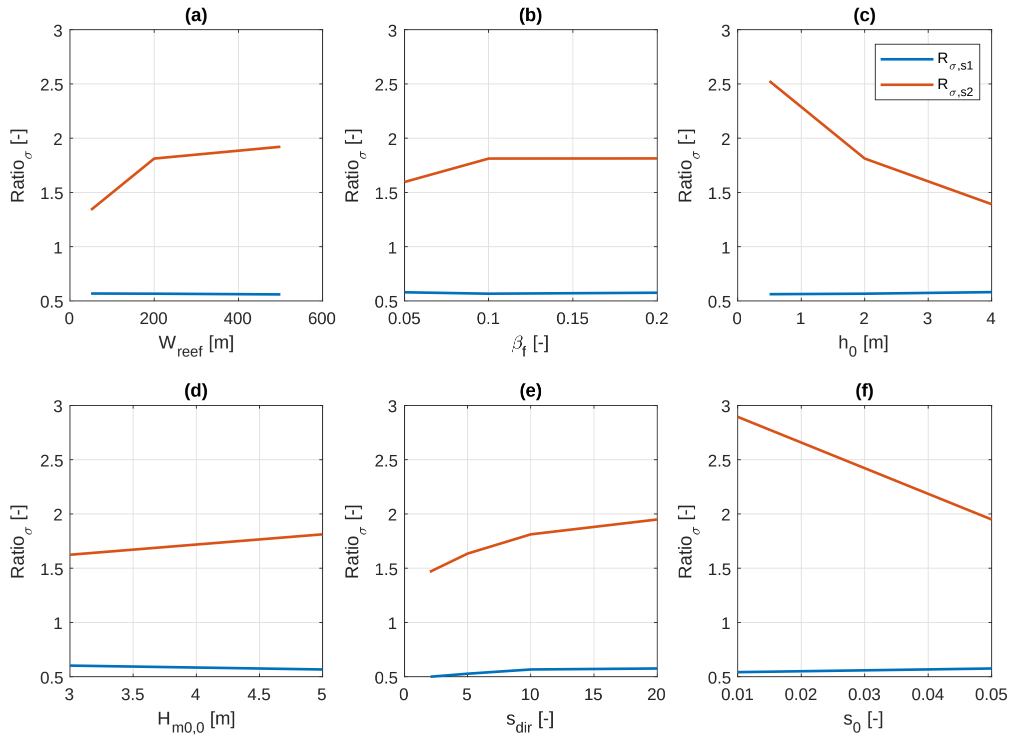

Figure 4.8: The directional narrowing (blue) and broadening (red) explained with ratios. $R_{\sigma,1}$ is the ratio between σ offshore and the lowest σ, which is located in the wave breaking zone. $R_{\sigma,2}$ is the ratio between σ at the beach toe and the lowest point. These ratios are calculated for different values of the model parameters.

the points used for calculation of $R_{\sigma,1}$ and $R_{\sigma,2}$ are marked by A,B and C, see Equation 4.1 and 4.2. So $R_{\sigma,1}$ is a measure of the directional narrowing on the fore reef slope. Next to that, $R_{\sigma,2}$ is measure of the directional broadening on the reef edge and reef flat.

$$R_{\sigma,1} = \frac{\sigma_B}{\sigma_A} \tag{4.1}$$

$$R_{\sigma,2} = \frac{\sigma_C}{\sigma_B} \tag{4.2}$$

Firstly, it can be seen that the directional narrowing ($R_{\sigma,p1}$, blue lines) is insensitive to changes in W_{reef}, β_f, h_0 and H_{m0}. Only directional spreading has a slight effect on the directional narrowing. This confirms the expectations that a wider spectrum will refract more, and thus will become more narrow than the refraction of a narrow banded spectrum.

Secondly, the model parameters seem to have an effect on the directional broadening ($R_{\sigma,p2}$, red lines). Every variable will briefly be discussed below.

W$_{\mathbf{reef}}$: An increased reef flat width leads to more directional broadening. In the previous section it was shown that the directional broadening seemed to be controlled by the vorticity that is generated within the surf zone. This leads to the hypothesis that horizontal vorticity can develop over a larger area (i.e. longer reef width) and thus could affect the directional broadening for a long distance. An analysis of the cross-shore vorticity profiles showed that the vorticity is not equal to zero at the beach for the short reefs, see Appendix C. This means that a longer reef width (W_{reef}) provides more space for the eddies to develop and thus a longer distance to influence the directional spreading.

$\boldsymbol{\beta_f}$: An steep fore reef slope leads to more directional broadening. Again a connection with the vorticity generation can be made. It is hypothesized that a steep reef fore reef slope will lead to a more confined wave breaking zone. This leads to larger gradients in the radiations stresses (i.e. S_{xx}/dx) and thus enhances the alongshore variation wave forces, which leads to the generation of horizontal eddies or vorticity (Clark et al., 2012). An analysis of the vorticity profiles for different fore reef slopes and under constant forcing showed that the amount of vorticity increases with an increasing steepness of the fore reef slope (Appendix C). This increased vorticity leads to more directional broadening inside the surf zone.

$\mathbf{h_0}$: An increased reef flat submergence level leads to a reduced broadening of the directional spectrum. At low reef flat submergence levels (h_0) more short wave energy will be dissipated on the reef crest. More energy dissipation on the reef crest will lead to larger gradients in the radiation stress (i.e. S_{xx}/dx), or wave forcing. This cross-shore increase of the wave forcing could lead to larger gradients in the alongshore wave forcing, hence more vorticity is generated according to the theory. An analysis of the vorticity profiles for different reef flat submergence levels (h_0) showed that more vorticity is generated in the wave breaking zone for a lower reef flat submergence level. This can be seen as the cause of the increased directional broadening.

$\mathbf{H_{m0,0}}$: An increased wave height leads to more directional broadening of the wave spectrum. It is hypothesized that a larger wave height leads to larger wave forces, this cross-shore increase of the wave forces could also lead to a larger gradient in the alongshore wave forces and thus more vorticity. An analysis of the horizontal vorticity for different wave heights showed that the vorticity is not increasing but is stretching over a larger area and thus influencing the waves to a larger extent, see Appendix C.

$\mathbf{s_{dir}}$: A broader incident directional spectrum (i.e. low values of s_{dir}) leads to less directional broadening. However, it is expected that a broader directional spectrum will lead to more vorticity, since the alongshore variability of the wave forcing is larger. This hypothesis is substantiated with an analysis of the horizontal vorticity and is shown in Appendix C. So a broader spectrum leads to more vorticity and following the previous analogy, hence more directional broadening. However, the opposite is found in Figure 4.8. When the vorticity fields are compared to each other it is found that the vorticity fields are smaller compared to the vorticity fields of a narrow directional spectrum, see Appendix C. This suggests that the size of the vorticity fields is also important for directional broadening. This is also logical, since a small horizontal eddy is not able to refract a wave, whereas larger eddies are expected to have more impact on the wave's propagation.

$\mathbf{s_0}$: It is evident that directional broadening of swell waves is larger than the directional broadening of wind sea waves. This against priori expectations, since the vorticity reduces for swell waves, see Appendix C. Furthermore, the analyses showed that the size of the vorticity fields increased. So, it expected that the size of the amount and the size of the vorticity field is important for directional broadening.

5

Results - Runup analysis

In this section the dataset is analyzed, which is created with the method described in Section 3.2. After post processing the data it can be used to analyse the influence of wave forcing and reef geometry on the wave runup. These results will be compared with results from previous research on runup in coral reef environments. This can be seen as a verification of the model output and will create confidence in the model's capabilities. Lastly, the influence of directional spreading on wave runup will be treated. This will give us insight in how directional spreading is influencing the runup and how important it is for runup predictions.

5.1. Influence of Coral Reef Geometry and Wave Forcing on Wave Runup

In this first Section the influence of the reef geometry and wave forcing on the wave runup is discussed. The purpose of this section is to verify the model output by elaborating on the relations and connect the findings to existing literature and the physics.

In Figure 5.1 the relation between model parameters (i.e. reef geometry and forcing) and runup are shown. The runup is decomposed into: setup (R_{setup}), HF swash (R_{HF}) and LF swash (R_{LF}) and the relation between the model parameters is discussed below.

First of all, it can be seen that the highest runup is expected at reefs with a narrow reef flat width (W_{reef}), steep fore reef slope (β_f), a large reef flat submergence level, forced by high waves (H_{m0}) with a small wave steepness (i.e. low s_0, so swell waves). This is in agreement with previous research, e.g. Pearson et al. (2017); Quataert et al. (2015); Shimozono et al. (2015).

Reef flat width (W_{reef})

In Figure 5.1(a) is the influence of W_{reef} on the runup shown. The reef flat functions as a wave energy attenuator, hence it protects the coastline against wave driven flooding.

R_{Setup}: There exists a slightly negative relation between the reef flat width (W_{reef}) and the setup (R_{setup}), which is in line with the findings of Pearson et al. (2017). A wider reef increases the bottom friction forces in the cross-shore momentum balance and thus reduces the setup (Equation 2.4). However, Quataert et al. (2015) did not find a relation and argued that setup is generated on the fore reef slope and thus independent of the reef flat width.

$R_{HF,2\%}$: The contribution of short incident waves towards the runup are slightly reduced with an increased reef width (W_{reef}). This is expected since most short wave energy is dissipated by breaking on the reef crest, where only the transmitted wave height experiences bottom friction. A longer reef flat width will lead to more dissipation of the HF wave energy, hence reduced HF wave runup. This coincides with findings of Pearson et al. (2017); Shimozono et al. (2015).

$R_{LF,2\%}$: The R_{LF} component decreases with an increased reef width. The relation between these can be explained by the strong frictional energy dissipation on the reef flat, which is larger for LF wave than for HF waves due to their increased wave length. An increased wave length leads to a lower relative depth

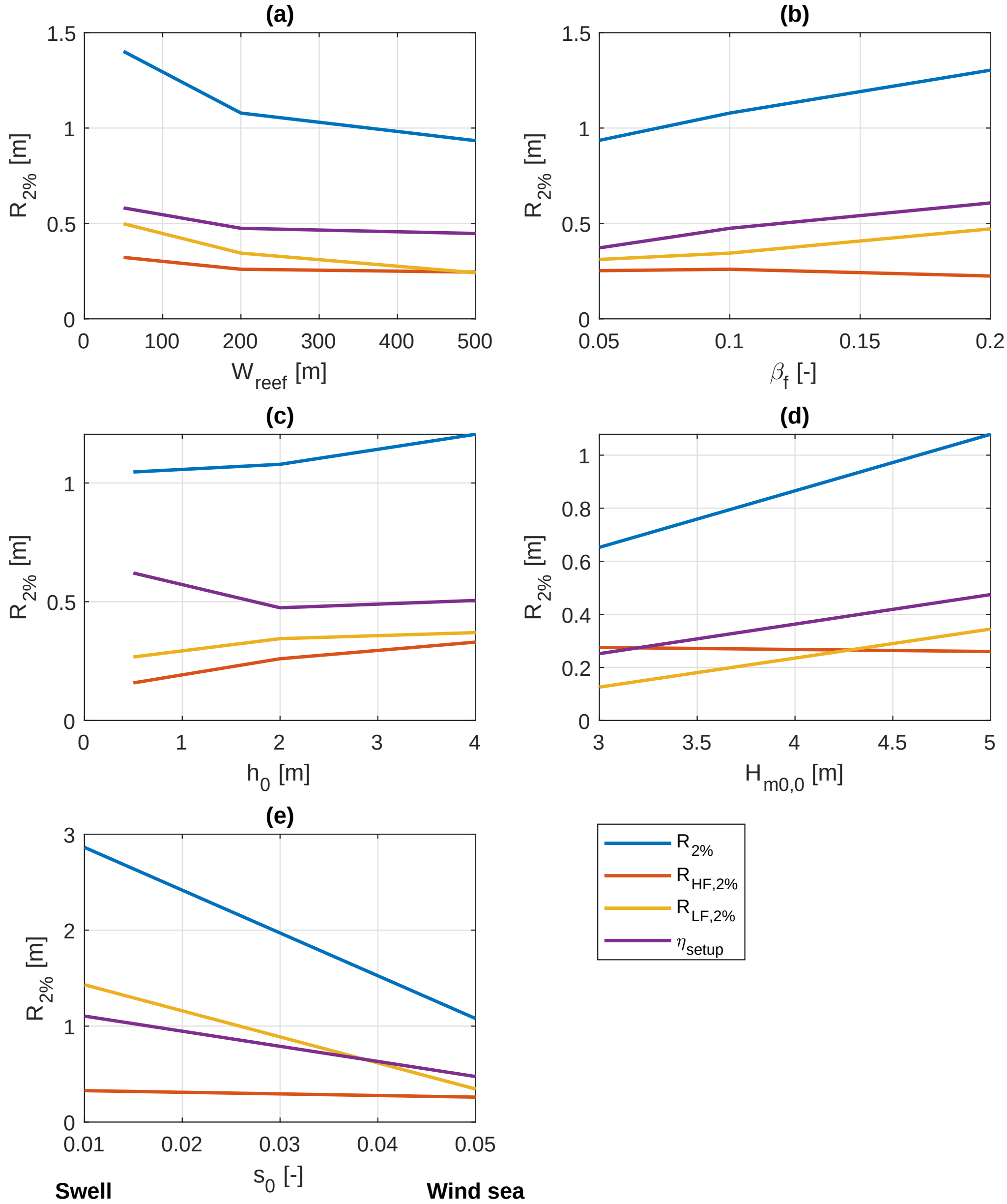

Figure 5.1: The influence of wave forcing and reef geometry on the runup is shown. The runup ($R_{2\%}$) is decomposed into HF runup ($R_{HF,2\%}$), LF runup ($R_{HF,2\%}$) and setup (η_{setup}). These components are found with the analysis explained in Section 3.3.1 and the time series of all 15 runup gauges is used in order to obtain an alongshore average. The results presented here are given for a certain model there is chosen for W_{reef} = 200 m, $beta_f$ = 0.01, h_0 = 2.0 m, H_{m0} = 5.0 m, s_0 = 0.05 and s_{dir} = 20. (a) The relation between the reef flat width (W_{reef}) and runup, (b) the relation between the fore reef slope (β_f) and runup, (c) the relation between reef flat submergence level (h_0) and runup, (d) the relation between the offshore wave height ($H_{m0,0}$) and the runup, and (e) the relation between the wave steepness (s_0) and runup. Note that a s_0 = 0.05 corresponds to a swell wave field and s_0 = 0.01 a wind sea wave field.

(kh), which actually means that the wave is experiencing more bottom friction and thus more frictional dissipation than HF waves. For this reason, a long reef flat will dissipate more LF wave energy and thus lowers the LF wave runup. This relation is in line with findings of Pearson et al. (2017); Quataert et al. (2015); Shimozono et al. (2015).

Fore reef slope (β_f)
In Figure 5.1(b) the relation between runup and the fore reef slope is shown. A steeper fore slope leads an increased wave runup. Every single runup component is discussed in order to explain this relation.

$\mathbf{R_{Setup}}$: The setup at the reef coastline increases with an increase fore reef slope angle (β_f). The fore reef slope has an effect on the wave breaking zone, since a steeper slope induces wave breaking in shallower water and in a more confined area, which increases the setup for steeper slopes. This relation between the fore reef slope and setup is in agreement with the findings of Pearson et al. (2017); Quataert et al. (2015).
$\mathbf{R_{HF,2\%}}$: The fore slope (β_f) has no influence on the HF wave runup. Quataert et al. (2015) argued that this is due saturation of the HF wave band. The absence of a connection between fore reef slope (β_f) and R_{HF} is in line with findings of Pearson et al. (2017).
$\mathbf{R_{LF,2\%}}$: A positive relation between the R_{LF} runup component and the fore reef slope (β_f) is evident. Where a steeper slope leads to a higher LF runup component. This finding is in agreement with relation between the setup and β_f, since in Section 4.1 is shown that IG wave generation is dominated by the break-point mechanism, which is also called the dynamic setup. Pomeroy et al. (2012a) has shown that the break-point mechanism is strongly dependent on the fore reef slope, which confirms the relation between β_f and R_{LF}. The relation between fore reef slope and the generation of LF wave motions is well established in literature, e.g. Pearson et al. (2017); Quataert et al. (2015).

Reef flat submergence level (h_0)
In Figure 5.1(c) the relation between the reef flat submergence level and the runup is shown. It seems that the runup is insensitive to a increase of h_0, since it only slightly increases.

$\mathbf{R_{Setup}}$: The setup decreases with an increasing reef flat submergence level (h_0). A larger h_0 induces less short-period wave breaking at the reef crest, which leads to a smaller change of the radiation stress in cross-shore direction, thus lower wave setup (See Equation 2.4, cross-shore momentum balance). This relation is well established in literature, e.g. Becker et al. (2016); Beetham et al. (2015); Pearson et al. (2017); Quataert et al. (2015); Vetter et al. (2010). Furthermore, this relation is not evident for h_0 = 2.0 m to h_0 = 4.0 m. For these values the setup seems to be stable, while a further reduction of setup is expected. This could be explained with the influence of bottom friction. In the cross-shore momentum balance wave forces are balanced by the hydrostatic pressure and bottom friction (Equation 2.4). A larger relative depth (kh), i.e. increasing h_0, leads to a reduction of the bottom friction forces. Thus wave forces are mainly balanced by hydrostatic pressure. The role of bottom friction forces on the setup in a reef environment is also discussed by Buckley et al. (2016); Quataert et al. (2015).
$\mathbf{R_{HF,2\%}}$: The runup as a result of HF waves increases with an increasing water depth (h_0). The effect of an increasing water depth is two fold: 1) lower HF waves energy dissipation due to breaking on the reef crest, and 2) the relative depth (kh) increases thus less energy is dissipated by bottom friction. This relation between the water level and short period wave runup is in agreement with findings of Beetham et al. (2015); Pearson et al. (2017); Quataert et al. (2015)
$\mathbf{R_{LF,2\%}}$: An increasing reef flat submergence level (h_0) leads to an increased LF runup (R_{LF}). This is in contrast with the relation found for the R_{setup}, since this decreases with an increasing h_0. This means that the increased h_0 leads to an increased kh and thus a reduced LF wave dissipation due to bottom friction. The latter process is more dominant than the reduced generation mechanism. Furthermore, there could be cases where the first process is dominant, and thus a different relation can be found. Pearson et al. (2017) found a slight increase of the LF runup component, whereas Beetham et al. (2015) argued that the IG runup component (f < 0.04) is relatively insensitive to tidal modulations. The findings here suggest that it could be a unique case where the two processes balance each other.

Offshore wave height ($H_{m0,0}$)
In Figure 5.1(d) the relation between runup and offshore wave height is shown. The wave height and runup are positively correlated, thus an increased wave height will lead to an increased runup.

$\mathbf{R_{Setup}}$: The setup increases with an increasing incident wave height $H_{m0,0}$. An increased wave height induces higher wave forces in the wave breaking zone and thus has to balanced by a larger setup (Appendix D).
$\mathbf{R_{HF,2\%}}$: The HF runup component is relatively insensitive to a variation in the wave height. This is ex-

pected, since the wave field is saturated on the reef flat, due to depth limited wave breaking on the fore reef slope.
$R_{LF,2\%}$: An increased wave height ($H_{m0,0}$) leads to an increased LF runup component. This is in line with the theory of the break-point mechanism, since the setup also increases.

Offshore wave steepness (s_0)
In Figure 5.1(e) the relation between runup and the offshore wave steepness (s_0) is shown. The wave steepness and runup are negatively correlated, thus an increased wave wave steepness will lead to a decreased runup. In other words, the runup is higher for swell waves than wind sea waves. This relation will be explained by decomposing the runup.

R_{Setup}: The wave setup is larger for swell waves than for wind sea waves. These findings are in line with the findings of Pearson et al. (2017), and are due to larger gradients in the radiation stresses.
$R_{HF,2\%}$: The HF wave runup is not sensitive to any changes in the wave steepness, which is in line with expectations. Waves break due to a sloping bottom (i.e. depth limited breaking). So any changes in the wave steepness will not change the transmitted wave height on the reef flat.
$R_{LF,2\%}$: The LF runup is larger for Swell waves than for wind sea waves. This increase is larger than the increase in setup, this could be attributed to the strong groupiness of swell waves, since the background study showed that the break-point mechanism is enhanced by a strong groupiness of the incident waves. The increased LF wave runup for the swell waves is in line with the findings of Pearson et al. (2017).

5.2. Influence of Directional Spreading on Wave Runup

The previous section showed that the model is producing results which are in line with the findings in other literature on coral reef hydrodynamics. This created confidence in the model's capabilities. This section will focus on the influence of directional spreading on the runup. Again the runup is decomposed in different components and the evolution of every component is briefly discussed.

Runup of directionally spread wind sea waves
The relation between the directional spreading of wind sea waves and runup ($R_{2\%}$) is shown in Figure 5.2(a). This indicates a positive correlation between $R_{2\%}$ and s_{dir}. The $R_{2\%}$ is decomposed into its components which are briefly discussed below.

R_{Setup}: The setup (R_{setup}) increases slightly with an increasing s-value or with a less directionally spread wave field. A narrower directional wave spectrum means that more waves are normally incident, which could enhance the radiation stress in x-direction (S_{xx}). Feddersen (2004) investigated the dependence of radiation stress and the directional spectrum. He suggests that directional spreading should be included in radiation stress estimations. For this reason, calculations of the radiation stress for different directional spread is executed and the results are compared, see Appendix D. This analysis shows that the directional spreading is influencing the evolution of S_{xx}. Furthermore, setup is a result of gradients in the radiation stresses ($\frac{\delta S_{xx}}{\delta x}$). When these are compared it is found that these gradients are smaller for broader spectra which leads to less setup.
$R_{HF,2\%}$: The HF runup component is insensitive to any changes in the directional spreading (s_{dir}). No literature is found that in contrast with nor support the relation described. Furthermore, this finding confirms the expectations, since most HF wave energy is dissipated on the reef edge and flat.
$R_{LF,2\%}$: The LF runup component increases for larger values of s_{dir}. As explained, a reduction of the directional spread resulted in an increased setup, which was due to the changes in the radiation stresses, see Appendix D. This means that the forcing term of the LF waves increases with an increasing s_{dir}, hence an increased R_{LF} is expected form the radiation stress analysis. This finding is in line with the findings of Guza and Feddersen (2012). In this article a new parameterization of R_{LF} is suggested which includes directional spreading, and is argued to improve the runup predictions. Guza and Feddersen (2012) focused on the relation between R_{LF} and s_{dir} on dissipative beaches, whereas the findings in Figure 5.2(a) suggest that it should also be incorporated in R_{LF} predictions in coral reef environments.

Furthermore, the dashed lines in Figure 5.2(a) indicate the model results forced with a $s_{dir} = \infty$. This can be

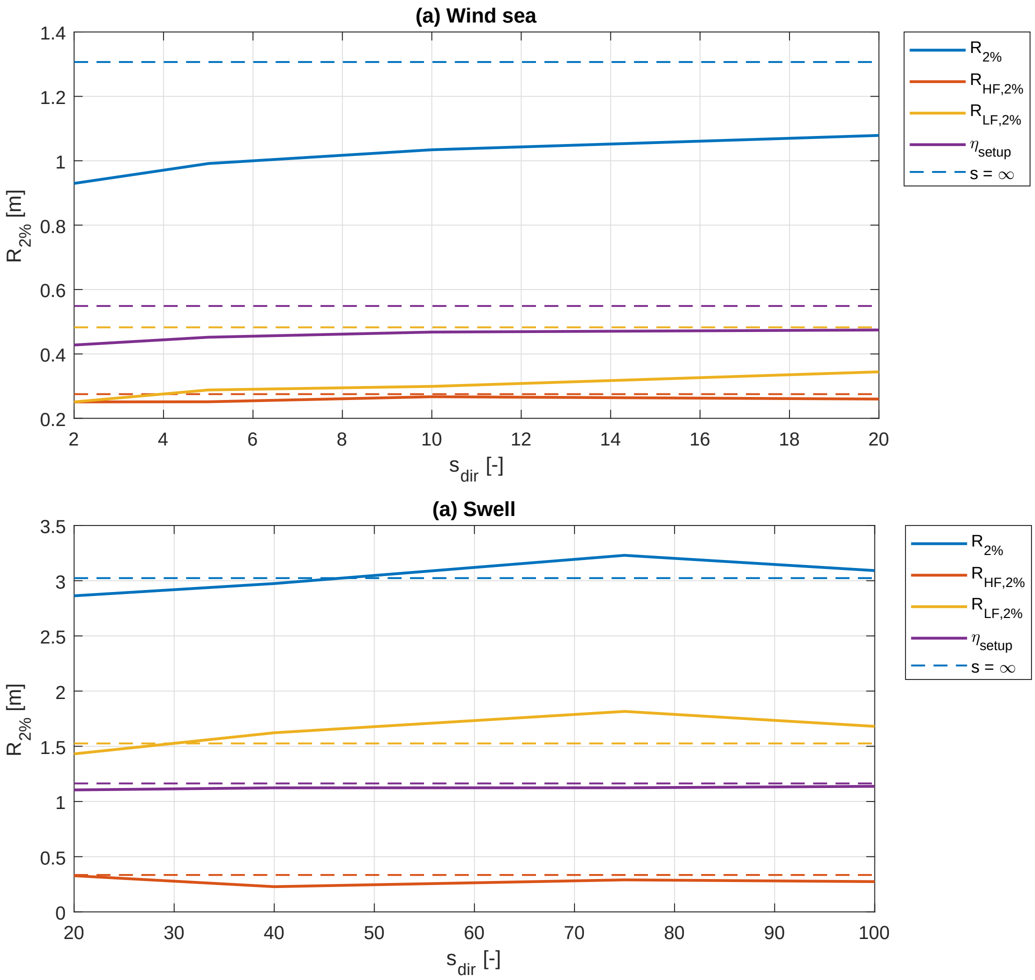

Figure 5.2: The influence of offshore directional spreading (s_{dir}) on the runup. (a) shows the results for models forced with wind sea waves, and (b) the runup for models forced with swell waves. The runup ($R_{2\%}$) is decomposed into a setup (R_{setup}), HF runup component (R_{HF}) and a LF runup component (R_{LF}). The decomposition of the runup signal is explained in Section 3.3.1. Dashed lines indicate the runup and the runup components of models runs with $s_{dir} = \infty$, this can be seen as 1D model runs. These figures are produced with the following reef geometry and forcing: $W_{reef} = 200m$, $\beta_f = 0.1$, $h_0 = 2.0m$ and $H_{m0,0} = 5.0m$

seen as a 1D model wave model, thus without directional spreading. Figure 5.2 shows a strong overestimation (i.e. approximately 25%) of the $R_{2\%}$ when the wind sea wave forcing has a value of $s_{dir} = \infty$. Below every runup component with or without directional spreading is discussed. In appendix D an analysis of the true radiation stress ($S_{xx,tr}$, i.e. with directional spreading) and narrow banded radiation stress ($S_{xx,nb}$) is made. The $S_{xx,nb}$ is the same as the S_{xx} of $s_{dir} = \infty$.

R_{Setup}: The setup is slightly overestimated when wind sea waves without directional spreading (i.e. $s_{dir} = \infty$) are modeled. The analysis of S_{xx} in Appendix D showed that the wave forcing reduces (i.e. $\frac{\delta S_{xx}}{\delta x}$ reduces) with a broader spectrum or lower values of s_{dir}. This again explains that the setup is underestimated.

$R_{HF,2\%}$: The HF runup component is well represented when wind sea waves are modeled without directional spreading.

$R_{LF,2\%}$: Modeling wind sea waves without directional spreading has a significant effect on the LF runup component. In a 1D model this component is overestimated with approximately 60%, when the R_{LF} at $s_{dir} = 10$ is compared with $s_{dir} = \infty$. The radiation stress analysis showed that the forcing term of LF waves is reduced by including directional spreading in the model.

Runup of directionally spread swell waves

The relation between runup and directional spreading of swell waves is shown in Figure 5.2(b). Note, that swell waves are characterized with a different directional spreading, see Section 3.2.3 for a explanation. In general it can be seen that runup ($R_{2\%}$) of swell waves is insensitive to variation in the directional spreading.

$R_{\mathbf{Setup}}$: The setup of swell waves is insensitive to any changes in the directional spreading. This is contrast with the findings and the explanation given for the wind sea model. Firstly, swell waves are assumed to have less directional spreading, which leads to less dependence of S_{xx} on directional spreading, see analysis Appendix D. Secondly, the analysis showed that the wave forces are barely influenced by variations in s_{dir}, which explains the low influence on setup.
$R_{\mathbf{HF,2\%}}$: Similar to the model forced by wind sea waves is the HF runup component insensitive to any changes in the directional spreading.
$R_{\mathbf{LF,2\%}}$: The LF runup component is slightly influenced by changes in the directional spreading, where a slight positive correlation is found until $s_{dir} = 75$, higher values give a negative correlation. Slight influence of s_{dir} on the LF runup is in line with the expectations, since we have already shown that the forcing term is barely influenced by directional spreading.

Furthermore, at $s_{dir} = 75$ LF runup is larger than the LF runup for $s_{dir} = \infty$, this is contrast with the theory and the expectations. The S_{xx} analysis showed that no discrepancies with the theory. This instability is not yet resolved, however it is suggest to look at the wave groupiness. LF wave generation via the break-point mechanism is not only dependent on the wave forcing, but also on the groupiness of the waves, so an analysis of the wave groupiness of the incident wave field could give insight in this issue. It is not expected that the radiation stresses are responsible for this, since the setup is correctly represented.

Lastly, the runup of swell waves with and without directional spreading are compared (dashed lines in Figure 5.2(b)). This figures shows that the runup ($R_{2\%}$) is influenced by the directional spreading, however no large differences are found. Furthermore, it is expected that the model runs without directional spreading would give the highest runup, which is not evident in Figure 5.2(b). Every runup component is briefly discussed in order to find the discrepancy.

$R_{\mathbf{Setup}}$: There is almost no difference between the setup of swell waves with or without directional spreading. This is in line with analysis performed in Appendix D.
$R_{\mathbf{HF,2\%}}$: The HF runup component is well represented when swell waves are modeled without directional spreading.
$R_{\mathbf{LF,2\%}}$: The LF runup component is mainly lower for swell waves without spreading compared with model runs with spreading. This is in contrast with the theory, where is expected that $s_{dir} = \infty$ should give the highest LF runup. In order to analyze this discrepancy there could be looked at the wave groupiness.

Next, the influence of directional spreading on wave runup in different reef environments and with different wave forcing is investigated. The wave runup components of $s_{dir} = 10$ are divided by the wave runup of components of $s_{dir} = \infty$, see Figure 5.3(a-d). These components are calculated for different the parameter range of the reef geometry and wave forcing. Note that for wave steepness the wave runup of $s_{dir} = 20$ and $s_{dir} = \infty$ are compared, see Figure 5.3(e). The runup is decomposed into runup components, which are discussed below. In general the following statements can be made over the runup components.

$R_{\mathbf{Setup}}$: A low setup ratio indicates a large overestimation of the runup in a 1D model. This ratio is smallest for a low β_f, large h_0 and the influence of W_{reef} and $H_{m0,0}$ is insignificant.
$R_{\mathbf{HF,2\%}}$: The HF runup is smallest for a small W_{reef}, large β_f, large h_0 and small $H_{m0,0}$. Thus a 1D model overestimates the runup in the most under this forcing and in these environments.
$R_{\mathbf{LF,2\%}}$: The LF runup ratio is smallest for $W_{reef} = 200$, small β_f, large h_0 and insensitive to changes in $H_{m0,0}$. Thus a 1D model overestimates the runup in the most under this forcing and in these environments.

Furthermore, it is evident that the influence of s_dir on LF runup is much larger than the effect on setup. This indicates that there could be an other mechanism that is influenced by s_{dir} and is influencing the LF wave generation. The literature study showed that the wave groupiness is important for the break-point mechanism. Therefore, it suggested to also incorporate the wave groupiness in a future study, the method of List

(1991) can be used to investigate the groupiness.

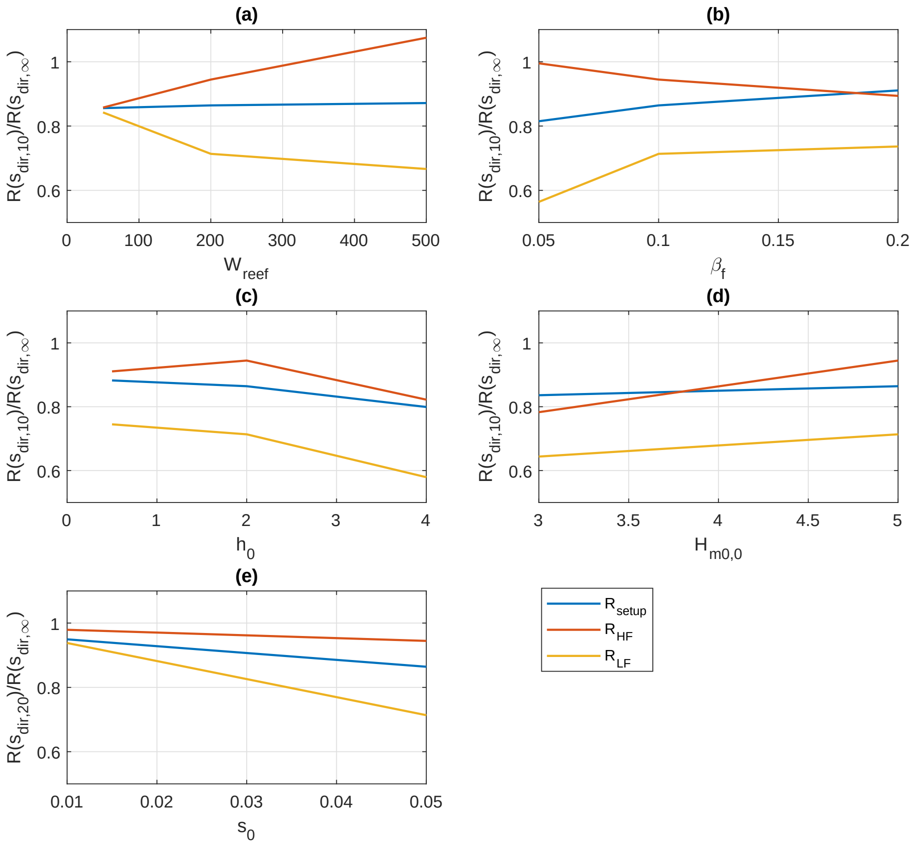

Figure 5.3: The influence of directional spreading on wave runup components in different reef environments and under different wave forcing. The ratio between the $s_{dir} = 10$ wave runup component and the $s_{dir=\infty}$ wave runup component is calculated, see a-d. The influence of wave steepness is assessed by calculating the ratio between $s_{dir} = 20$ wave runup component and the $s_{dir=\infty}$ wave runup component, see e. The ratios shown here are calculated for $W_{reef} = 200m$, $\beta_f = 0.1$, $h_0 = 2.0m$, $s_0 = 0.05$ and $H_{m0,0} = 5.0m$

Reef flat width (W_{reef})
The relation between the runup ratios and W_{reef} is shown in Figure 5.3(a), and every runup component ratio is discussed.

R_{Setup}: This overestimation of the setup is constant and seems to be independent of the W_{reef}. An analyses of radiation stresses and wave setup showed that the gradients in radiations stresses do not change with a changing reef width, see Appendix D. This is in line with the findings presented here.
$R_{HF,2\%}$: The HF runup ratio is influenced by the W_{reef}. Firstly, A small W_{reef} shows a large overestimation of the HF runup, this could be due to wave energy dissipation on the W_{reef} and the influence of directional spreading on runup. So, when less energy HF wave energy is dissipated, it is expected that the influence of directional spreading on runup is large. Secondly, a long W_{reef} shows a, this is not yet well understood.
$R_{LF,2\%}$: The LF runup ratio is influenced by variations in W_{reef}. The largest ratio is found at the smallest W_{reef}, which means that the influence of directional spreading is the least for this reef width. Furthermore, the influence of directional spreading increases when W_{reef} increases, i.e. smaller ratios are found. The increased influence of directional spreading for longer reef is not expected, since setup is not influenced. This means another process is causing the this. An hypothesis is that the LF waves generated with $s_{dir} = \infty$ are damped more than the LF waves generated with $s_{dir} = 10$. This is not investigated in this study.

Fore reef slope (β_f)
The relation between the runup ratios and β_f is shown in Figure 5.3(b), and every runup component ratio is discussed.

R_{Setup}: The setup ratio is influenced by β_f. The lowest ratio is found for a flat slope and increases for a steeper fore reef slope. The radiation stress analysis showed an opposite behavior of the radiation stresses, see Appendix D. This means that another process is responsible for the trend shown here. It is hypothesized that the flow velocities generated under a changing directional spread are causing this difference.
$R_{HF,2\%}$: The HF runup ratio slightly reduces with a steeper β_f. A steeper β_f means a larger setup, which could enhance the HF wave transmission onto the reef flat. Larger HF waves on the reef flat could explain the larger influence of directional spreading on the HF runup component.
$R_{LF,2\%}$: The LF runup ratio is smallest for a flat fore reef slope and increases with an increasing steepness. This is conform the evolution of setup ratio, where R_{LF} is the dynamic setup generated in the wave breaking zone.

Reef flat submergence depth (h_0)
The relation between the runup ratios and h_0 is shown in Figure 5.3(c), and every runup component ratio is discussed.

R_{Setup}: The highest setup ratio is found for the smallest h_0 and decreases with an increasing h_0. A comparison of the setup at the beach toe and from the runup gauge indicates that the difference in influence of s_{dir} is mainly caused on the beach slope. So, due to wave breaking at the beach slope the s_{dir} influence increases. This cannot be shown with the analysis in Appendix D, since the measurement buoys reach until the beach toe. So, an increased h_0 leads to less wave breaking and thus more influence of directional spreading on the wave setup generated at the beach toe.
$R_{HF,2\%}$: An increased water level leads to a decreased R_{HF} ratio. A higher water level on the reef flat increases the HF wave transmission. These directionally spread waves will probably have a lower runup than long crested waves, since there are wave components arriving under an angle.
$R_{LF,2\%}$: The LF runup ratio are following the same relation that is found for setup. This is in line with theory, that suggests that LF waves are generated by dynamic setup.

Wave height ($H_{m0,0}$)
The relation between the runup ratios and H_{m0} is shown in Figure 5.3(d). The influence of directional spreading on runup is generally lower for higher waves. Every runup component ratio is discussed.

R_{Setup}: The setup ratio increases slightly when $H_{m0,0}$ increases, however the effect seems to be minimal. This means that the influence of s_{dir} on the wave setup is hardly influenced by the wave height.
$R_{HF,2\%}$: The HF runup ratio increases with an increasing $H_{m0,0}$. A smaller wave height means less HF wave breaking, which could enhance the effect of directional spreading on the transmitted HF wave runup.
$R_{LF,2\%}$: The LF runup ratio are following the same relation that is found for setup. This is in line with theory, that suggests that LF waves are generated by dynamic setup.

Wave steepness (s_0)
The relation between the runup ratios and s_0 is shown in Figure 5.3(e). This shows that the influence of s_{dir} is much lower for wind sea waves than for swell waves. Below, every runup component ratio is discussed.

R_{Setup}: The influence of s_{dir} is influenced by the wave steepness. This finding is in line with the analysis of the radiation stresses and wave setup (see Appendix D).
$R_{HF,2\%}$: The influence of s_{dir} barely changes with a different wave steepness. This is in line with priori expectations.
$R_{LF,2\%}$: The wind sea LF wave runup is more influence by s_{dir} than the swell wave runup. It seems that the difference cannot completely be attributed to influence on setup. Therefore, it is interesting to further investigate the influence of s_{dir} on LF wave generation in different environments.

To summarize, the results presented in this section it is shown that the wave runup is influenced by wave directional spread. This is mainly due to the effect of wave directional spread on setup and LF runup and to a lesser extent HF runup. The analysis of Figure 5.3 showed that the influence of s_{dir} is changing in different reef environments. Assuming that setup and LF runup are the most important runup components in reef environments, it is evident that wave directional spread becomes more important when the runup components are reduced. In other words, the influence of directional spreading is largest in coral reef environment where the lowest wave runup is expected.

5.3. Quantifying the Influence of Directional Spread on Wave Runup

In Section 5.2 is shown that directional spreading has an influence on the runup. After decomposition of the runup it was evident that mainly the setup (R_{setup}) and LF runup component (R_{LF}) were influenced. This section will focus on the importance of directional spreading in runup predictions in a coral reef environment. Firstly, a regression model is made. Subsequently, directional spreading is added to the model and the predictive skill is tested. An explanation of the method is given in Section 3.4. This method is applied to every single runup component and again a distinction is made between wind sea and swell waves, due to their different parameter range of s_{dir}.

5.3.1. Regression model wind sea waves

Firstly, a regression model is set up for the XB NH data output forced with wind sea wave conditions. This model consists of the parameters that have a significant influence on the runup or runup component. The influence is investigated by performing a single variable linear regression analysis (See Appendix E), which gave insight in the dependence of the variables. The results are summarized in Table 5.1. From this analysis it is evident that wind sea directional spreading limit (i.e. $2 \leq s_{dir} \leq 20$) has little influence on the runup components. To further investigate this influence a regression model is made without directional spreading, subsequently spreading is added and the predictive skill of the model is assessed. This skill is assessed by calculating the square of the correlation (R^2) and a F-test, see Section 3.4 for an explanation.

Table 5.1: Summary of the linear single variate regression analysis on storm waves. The R^2 of single variate regression analysis on every runup component is obtained and compared.

$\mathbf{R_{setup}}$		$\mathbf{R_{HF}}$	$\mathbf{R_{LF}}$
Parameter	R^2	R^2	R^2
W_{reef}	0.04	0.08	0.20
β_f	0.18	0.0	0.06
h_0	0.03	0.75	0.06
$H_{m0,0}$	0.04	0.0	0.40
s_{dir}	0.01	0.004	0.02

From Section 5.1 & 5.2 it was evident that the runup components had different relations with the model parameter. For this reason a regression analysis is performed on every runup component. The best fit with the data is found by optimizing the R^2, i.e. closest to 1. Furthermore, the added value of directional spreading to the prediction of wave runup components is assessed by F_{diff}. This is a statical measure to test the null hypothesis that a full regression model (i.e. with directional spreading) is performing better than the reduced regression model (i.e. without directional spreading). The calculated $Fdiff$ can be used to show whether the wave directional spread has a significant influence on predictive skill of the response variable. In general, a high F value indicates that the addition of s_{dir} as predictor is significant. The addition of s_{dir} has an insignificant influence when $F < 3.89$, this value can be found by using a F distribution look up table for 1 and 210 degrees of freedom, which is used throughout this analysis.

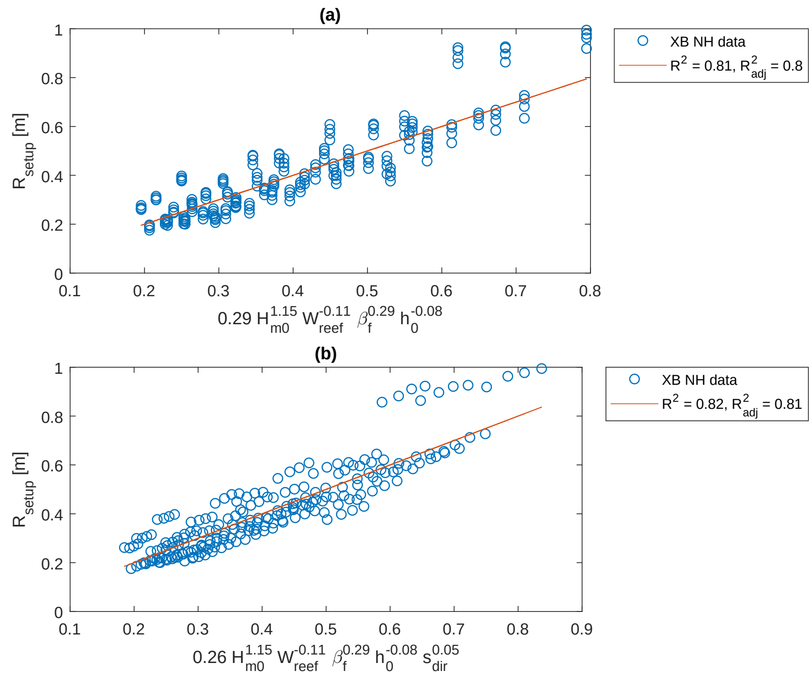

Figure 5.4: Non-linear multivariate regression model for R_{setup}. The non-linear relation is given on the x-axis and the response variable on y-axis. In (a) the reduced regression model optimized on the R^2, (b) the non-linear regression model with directional spreading.

Setup ($\mathbf{R_{setup}}$)

Combining the information obtained in Section 5.1 and the single variable linear regression analysis presented in Appendix E showed that; $H_{m0,0}$, β_f, h_0, W_{reef} have a relation with R_{setup}. Where $H_{m0,0}$ showed the highest correlation and W_{reef} the lowest. The setup is best estimated with a non-linear regression model, see Figure 5.4(a). This model showed the best predictive skill, or highest R^2. This confirms the findings in Section 5.1, which showed that most relation are non-linear.

The variable $R^2 = 0.81$ can be interpreted as 81% of the variance in the response variable ($y = R_{2\%}$) is presented by the model. $R = \sqrt{R^2}$ is the correlation coefficient, in this case the $R = 0.90$. Which indicates a strong linear relation between the data and model.

The regression model seems to perform well on the XB NH data, however the model tends to have a poor predictive skill for large setup values. These values are obtained from model runs with low h_0, narrow W_{reef}, steep β_f and high wave ($H_{m0,0}$). A more extensive research in the regression analysis is necessary in order to incorporate these extreme values into the analysis.

In Figure 5.4(b) the regression model with directional spreading is given. The predictive skill of the two models can be compared by comparing the R^2. A better comparison can be made with the R^2_{adj}, in this variable is corrected for the number of predictors (see Section 3.4). It can be seen that the R^2_{adj} slightly increases with the addition of s_{dir}, i.e. $R^2_{adj} = 0.80$ and $R^2_{adj} = 0.81$.

Lastly, the F_{diff} test gives a value of 11.7, this means that the addition of directional spreading increased the predictive skill of the model (See Table 5.2). The influence of directional spreading on setup was shown in Section 5.2 and is in line with this finding.

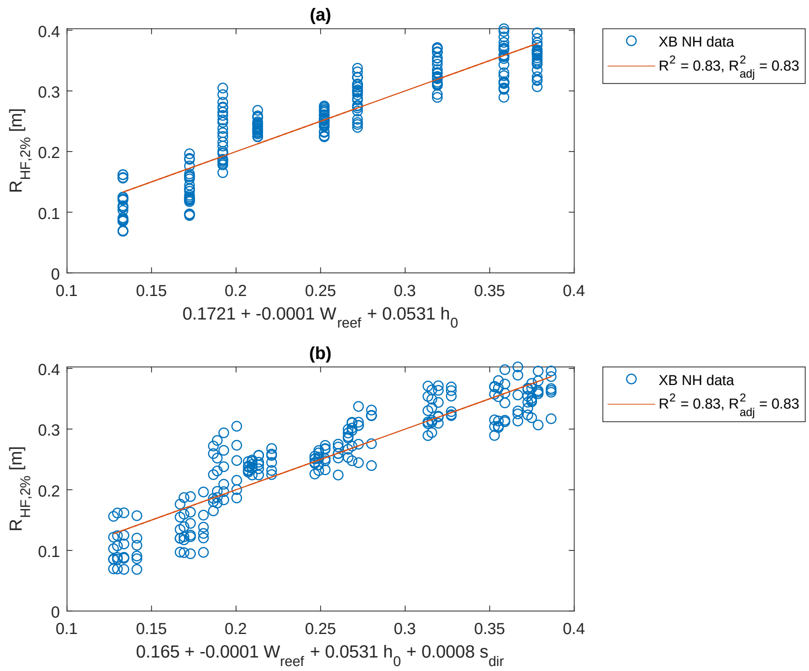

Figure 5.5: Linear multivariate regression model for R_{HF}. The linear relation is given on the x-axis and the response variable on y-axis. (a) the reduced regression model optimized on the R^2, (b) the linear regression model with directional spreading.

High frequency runup ($\mathbf{R_{HF}}$)
Combining the information obtained in Section 5.1 and the single variable linear regression analysis presented in Appendix E showed that; h_0, W_{reef} have a relation with R_{HF}. Where h_0 showed the highest correlation and W_{reef} the lowest. The other variables do not influence the HF runup component. The R_{HF} is best predicted with a linear multivariate regression analysis, see Figure 5.5(a). The $R^2 = 0.83$ which is indicates a relatively good fit, and $R = 0.91$ indicating a strong linear relation between the response and linear combination of predictors.

In Figure 5.5(b) the regression model with directional spreading is shown. It can be seen that the R^2_{adj} does not increases after the addition of s_{dir}. This finding is in line with the findings in Section 5.2.

Lastly, the F_{diff} gives a value of 4.45. This means that the addition of directional spreading has a significant effect on the predictive skill of the model (See Table 5.2). This linear regression model shows that directional spreading has a slight effect on HF runup component.

Low frequency runup ($\mathbf{R_{LF}}$)
Combining the information obtained in Section 5.1 and the single variable linear regression analysis presented in Appendix E showed that; $H_{m0,0}$,, W_{reef}, β_f and h_0 have a relation with R_{LF}. Where $H_{m0,0}$ showed the highest correlation and h_0 the lowest. The LF runup component is best estimated with a linear regression model, see Figure 5.4(a). Note that the response variable is transformed by taking natural logarithm, this showed the best predictive skill, i.e. highest R^2 of 0.79.

In Figure 5.5(b) the regression model with directional spreading is shown. The model including directional spreading as predictor variable slightly increases from $R^2_{adj} = 0.79$ to $R^2_{adj} = 0.81$. In contrary, the F_{diff} test gives a value of 18.99. This means that the addition of directional spreading has a significant effect on the predictive skill of the model (See Table 5.2). So, effect of directional spreading on the prediction of LF runup component is significant and in line with the findings in Section 5.2.

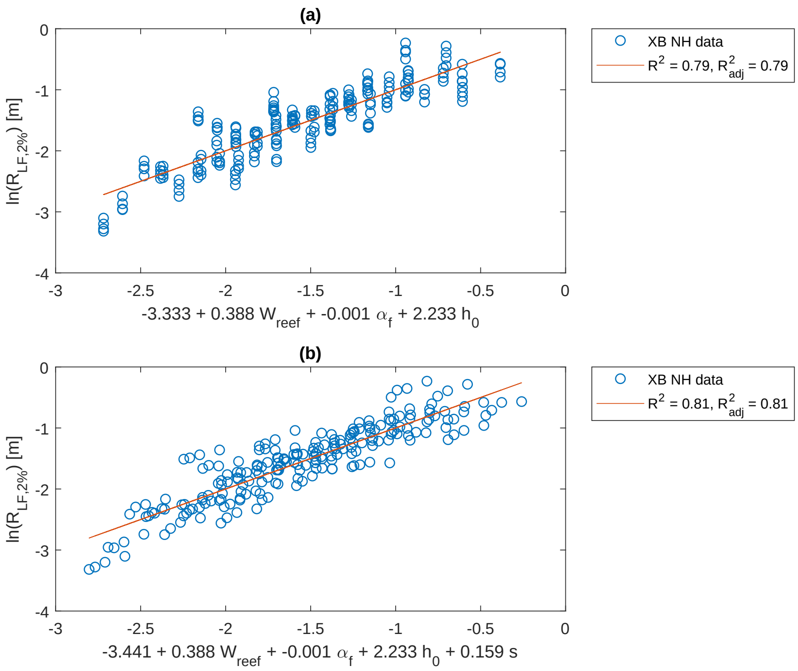

Figure 5.6: Linear multivariate regression model for R_{LF}. The linear relation between the predictor variables is given on the x-axis and the response variable is given on y-axis. (a) the reduced regression model optimized on the R^2, best fit is found by taking the $\ln(R_{LF})$, (b) the linear regression model with directional spreading.

Table 5.2: Summary of the linear regression model on storm waves. The variables in this table are discussed in Section 3.4. Model 1 refers to the models without directional spreading, model 2 refers to the models including directional spreading. Note that the parameter range of wind sea wave directional spreading is $2 \leq s_{dir} \leq 20$

Regression model Setup R_{setup}							
Model	k	R^2	R^2_{adj}	Change R^2_{adj}	SS_{reg}	SS_{res}	F_{diff}
1	4	0.81	0.80	-	4.70	1.38	-
2	5	0.82	0.81	0.01	4.77	1.30	11.7
Regression model HF runup R_{HF}							
1	2	0.83	0.83	-	1.38	0.29	-
2	3	0.83	0.83	0.0	1.39	0.28	4.45
Regression model LF runup R_{LF}							
1	4	0.79	0.79	-	64.50	16.65	-
2	5	0.81	0.81	0.02	65.89	15.27	18.99

5.3.2. Difference 1D and 2DH runup for wind sea waves

The previous section focused on the influence of directional spreading in a 2DH model. This section focuses on the influence under- or overestimation of runup in 1D models when this is compared with 2DH models including directional spreading. This is done for every runup component and the runup of $s_{dir} = \infty$ (dashed line in Figure 5.2) is compared with the runup of $s_{dir} = 10$. This value is assumed to be a representative value for wind sea waves.

In Figure 5.7 the runup of $s_{dir} = \infty$ is divided by runup at $s_{dir} = 10$ which is shown on the y-axis. On the x-axis you find all model runs forced by wind sea waves. On average, every runup component is overestimated in a 1D model ($s_{dir} = \infty$) when compared to a 2DH model including directional spreading. On average is the R_{HF} with 12%, R_{LF} with 37% and the R_{setup} with 20 % over estimated. It is clear that the runup is generally

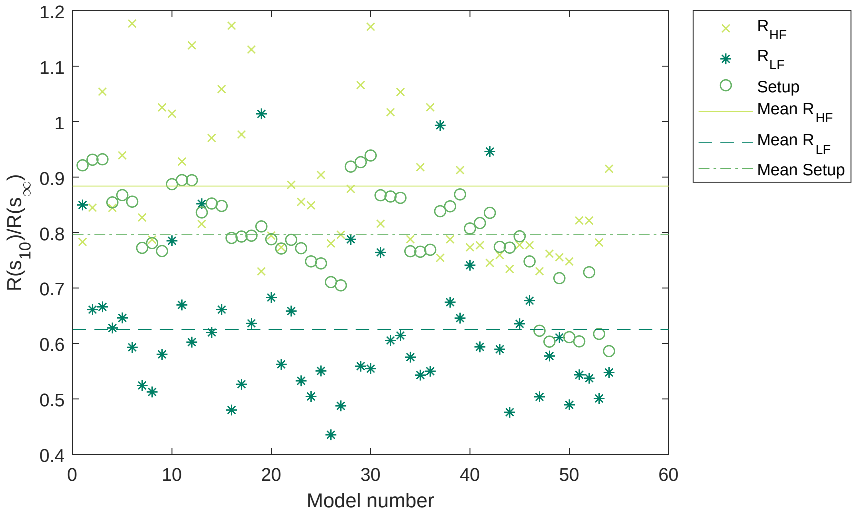

Figure 5.7: The runup of a 1D model (i.e. $s_{dir} = \infty$) is compared with the runup of a 2DH model (i.e. $s_{dir} = 10$). For the 2DH model a representative value of $s_{dir} = 10$ for a wind sea wave field is chosen. On the y-axis the ratio between the runup in a 1D model and 2DH model, and on the x-axis the wind sea models.

reduced when directional spreading is included in the 2DH model. Furthermore, there is a large scatter of the runup component ratios, which makes it interesting to investigated how these ratios are influenced, see the analysis in Section 5.2.

5.3.3. Regression Model Swell Waves

Next, the influence of directional spreading in swell waves is investigated. Again, the influence of each predictor variable is assessed by performing a single variate regression analysis (Appendix E) and summarized in Table 5.3. Note that the parameter range of swell wave directional spreading of $20 \leq s_{dir} \leq 100$ is used in this regression analysis. This analysis shows that directional spreading has the lowest relation with all runup components compared to the other parameters.

Table 5.3: Summary of the linear single variate regression analysis on XB NH model output of swell waves. The R^2 of single variate regression analysis on every runup component is obtained and compared.

$\mathbf{R_{setup}}$		$\mathbf{R_{HF}}$	$\mathbf{R_{LF}}$
Parameter	R^2	R^2	R^2
W_{reef}	0.09	0.57	0.19
β_f	0.21	0.05	0.12
h_0	0.06	0.06	0.01
$H_{m0,0}$	0.45	0.004	0.53
s_{dir}	0.0	0.0	0.0

Subsequently, a regression models with and without directional spreading are made. Next the predictive skill is tested by comparing R^2_{adj} values and performing the F-test. Note that the figures of the regression models are not presented here, but are presented in Appendix E.

The results of these models is summarized in Table 5.4. The predictive skill of all models is tested on the addition of directional spreading to the regression. First of all, it is evident that for any of the regression models the explanatory power does not increase when adding s_{dir}. This is evident when the change of R^2_{adj} is close to zero. Note that R^2_{adj} is compared, since this variable takes the number of predictors (k) into account. For

R_{HF} negative change of R^2_{adj} is found, this means that the addition of directional spreading less variance of the response variable can be explained. However, the R^2_{adj} does not give information about the model significance, which can be assessed with the F tests.

At last the F_{diff} are shown. These values explain whether the incorporation of directional spreading increases the significance of the model. In other words does the model a better job in predicting the response variable with directional spreading. The runup component R_{HF} shows a low F_{diff} value, this means that the regression model does not perform better than the model without directional spreading. Moreover, R_{HF} and R_{LF} show a value of $F_{diff} = 3.90$ and $F_{diff} = 5.44$ respectively. Firstly, this indicates that the addition of s_dir in setup and LF runup predictions is less important for swell waves than for wind sea waves. Secondly, the values are higher than the critical F-value of 3.89 so the addition of s_{dir} will improve the predictive skill of the models.

Table 5.4: Summary of the linear regression model on swell waves. The variables in this table are discussed in Section 3.4. Model 1 refers to the models without directional spreading, model 2 refers to the models including directional spreading. Note that the parameter range of swell wave directional spreading is $20 \leq s_{dir} \leq 100$

Regression model Setup R_{setup}							
Model	k	R^2	R^2_{adj}	Change R^2_{adj}	SS_{reg}	SS_{res}	F_{diff}
1	4	0.93	0.93	-	42.47	3.58	-
2	5	0.93	0.93	0.0	42.54	3.55	3.90
Regression model HF runup R_{HF}							
1	2	0.66	0.66	-	29.53	15.41	-
2	3	0.66	0.65	-0.01	29.54	15.41	0.10
Regression model LF runup R_{LF}							
1	4	0.87	0.87	-	60.13	9.74	-
2	5	0.87	0.87	0.0	59.54	8.70	5.44

5.3.4. Difference 1D and 2DH runup for swell

The previous section focused on the influence of directional spreading in a 2DH model. This section focuses on the under- or overestimation of runup in 1D models. This is done for every runup component and the runup of $s_{dir} = \infty$ (dashed line in Figure 5.2) is compared with the runup at $s_{dir} = 40$, this value is assumed to be representative for swell waves.

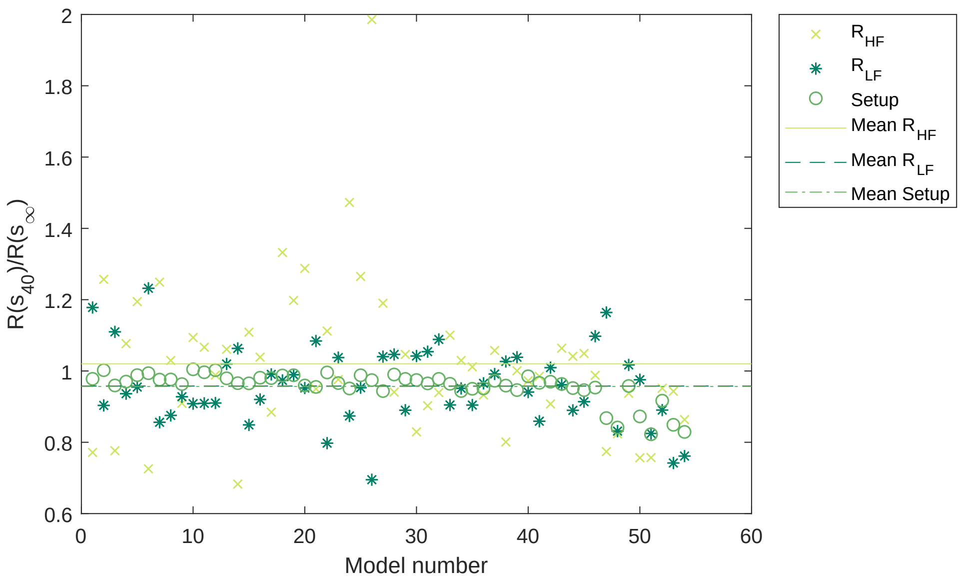

Figure 5.8: The runup of a 1D model (i.e. $s_{dir} = \infty$) is compared with the runup of a 2DH model (i.e. $s_{dir} = 40$). For the 2DH model a representative value of $s_{dir} = 40$ for a swell wave field is chosen. On the y-axis the ratio between the runup in a 1D model and 2DH model, and on the x-axis the wind sea models.

The runup component ratios are shown in Figure 5.8. The markers indicated model output and the dashed lines the average ratios for every runup component. Firstly, the average ratios of the runup components (i.e. dashed lines) are close to one. Thus on average the runup components are extremely overestimated in a 1D model compared to a 2DH model. This is different when these results are compared with wind sea waves, where larger average values were found. Furthermore, scatter around these mean values is found for the R_{HF} and R_{LF} runup components, and is the least for R_{setup}.

Remarkable is the ratio at model 26 where the R_{HF} is two times larger in the $s_{dir} = 40$ than the $s_{dir} = \infty$ model. This also corresponds to a low ratio of R_{LF}, this could indicate that the band pass filter is not preforming well and thus LF energy is band passed to HF energy.

6
Discussion

In this study an attempt is made to investigate the influence of wave directional spreading on coastal hazards at coastlines fronted by a coral reef. In the introduction a connection between coastal hazards and runup is made and was therefore used as a proxy. This made it possible to investigate the influence of wave directional spread on runup by performing digital experiments with XB NH. The model output is post-processed and analyzed. The main findings of these analyses are summed up below.

1. The evolution of directional spreading within the model domain is analyzed with a routine time series analysis. This showed that the directional spectrum narrows on the fore reef slope and broadens inside the surf zone, the latter is against priori expectations.

2. The influence of directional spreading on the runup components (R_{setup}, R_{HF} and R_{LF}) is investigated. This analysis showed that s_{dir} mainly influences the setup (R_{setup}) and Low Frequency runup (R_{LF}), and has a limited impact on the High Frequency runup (R_{HF}).

3. The regression analysis of the dataset showed that incorporating directional spreading in a runup model will improve the runup predictions. Furthermore, the influence of directional spreading on the setup and LF runup is the lowest compared to the influence of H_{m0}, s_0, W_{reef}, h_0, and β_f.

4. A comparison of runup data from an XB NH model with and without directional spreading (i.e. 2DH compared with a 1D model) showed that the addition of directional spreading leads to a reduction wave runup. Hence, a 1D model makes a conservative prediction of the runup.

These are the main findings of the research and are elaborately discussed below. Subsequently, a connection between these main findings and the research objective is made.

6.1. Evolution of directional spreading

During this study the evolution of directional spreading is discussed. It was found the directional spread reduces on the fore reef slope and subsequently increases on the reef flat. The first process, directional narrowing, is compared to a theoretical refraction model based on Snel's Law. This showed that the first process is mainly due to refraction on a sloping bottom. Furthermore, it was found that the theoretical model and the XB NH model start to deviate from each other inside the surf zone and directional broadening was found on the reef flat. This directional broadening is also observed by Herbers et al. (1999), who investigated the evolution of directional spreading on dissipative beaches, and found an increase of the directional spreading for certain cases. However, they were not able to identify the driving mechanism. They were able to connect the directional broadening to an increased incident wave height and decreased water depth on the sand bar.

These findings are in line with the findings of Section 4.1; directional broadening increases with increasing $H_{m0,0}$ and decreasing h_0, see Figure 4.8.

Furthermore, in this research the broadening commences on the reef flat, which might suggest that directional broadening only occurs in the absence of a slope. This is in contrast with the findings of Herbers et al. (1999); they found directional broadening on a sloping bathymetry. Note that they looked at dissipative beaches which are characterized by very mild slopes, hence less influence on directional narrowing. This suggests that there is a balance between the bed slope that tends to narrow the directional spectrum and mechanisms that try to broaden the directional spectrum.

It is expected that the broadening of the directional spectrum is mainly a result of the refraction of waves on currents. This is in line with the hypothesis of Henderson et al. (2006), who suggested that the directional broadening is due to wave-current interaction. Where the waves refract on the currents inside surf zone which are generated by wave breaking, this is analyzed by calculating the vorticity inside the surf zone.

In Section 4.1 is shown that most horizontal vorticity (i.e. circulations in the horizontal 2DH plane) is generated at the reef crest where most waves are breaking. Clark et al. (2012) hypothesized that vorticity is generated when the short crested waves break, note that short crested is linked to directional spreading. Furthermore, the theory used by Clark et al. (2012) states that circulations in the horizontal plane occur due to a gradient in the forcing along the wave crest, see Equation 6.1. They found that vorticity is generated and that it depends on the temporal and spatial scale of wave breaking. Furthermore, the generated vorticity persisted for 40-60 seconds which was much longer than the mean wave period of 8 seconds.

$$\frac{d\omega}{dt} = -\frac{dF_{br}}{dy_c} \tag{6.1}$$

Where:

ω	Vorticity [1/s]
t	Time [s]
F_{br}	Cross-shore breaking force $[N/m^2]$
y_c	Wave crest length [m]

So, the vorticity in the wave breaking zone is a result of the along crest variation in the wave forcing. These gradients lead to horizontal circulations. A comparison of the theoretical and XB NH evolution of directional spreading showed that the deviation commences when the vorticity increases. Furthermore, the largest gradient in the directional spreading is found close to the wave breaking zone where the vorticity is large. These findings are in line with the findings of (Henderson et al., 2006) and suggest that it is due to the wave-current interaction. In order to further investigate this hypothesis an extensive analysis of the directional evolution and vorticity fields is performed.

The influence of reef geometry and wave forcing on the directional narrowing at the fore slope and broadening at the reef flat is investigated. This showed that narrowing was insensitive to any changes in geometry and forcing. In contrast, directional broadening was influenced by changes in reef geometry and wave forcing. The influence of H_{m0} and h_0 on the directional broadening is in line with the findings of Herbers et al. (1999). However, we can take this one step further by analyzing the vorticity. An analysis of the cross-shore evolution of vorticity (see Appendix C) showed that the vorticity is influenced by H_{m0}, h_0, β_f and W_{reef}. These findings confirm the hypothesis that horizontal eddies are responsible for the directional broadening and that more broadening occurs with more vorticity. However, the vorticity analysis of s_{dir} and s_0 contradict with the hypothesis. For these parameters the directional broadening increases with a decreasing amount vorticity. This suggests that the broadening is not only a result of the amount of vorticity. For this reason, vorticity fields are compared (see Appendix C) and it was found that a narrower directional spectrum and swell waves lead to larger vorticity fields. These findings suggest that not only the amount of vorticity, but also the size of the vorticity fields controls the directional broadening. This can be further investigated by decomposing the vorticity into frequency bands and analyze the vorticity in each band. It is expected that an increased IG and VLF vorticity will have more effect on directional spreading than the HF vorticity. Furthermore, it is expected that the s_0 and s_{dir} influence the amount of vorticity in the lower frequency bands.

6.2. Influence of directional spreading on wave runup

In the previous section we have seen that directional spreading changes within the surf zone. In this section there is focused on the influence of directional spreading on wave runup. The findings of Section 5.2 show that directional spreading influences the wave runup. It was found that directional spreading mainly influences the R_{setup} and the R_{LF} and it barely affects the R_{HF}. This effect is further investigated.

Setup is generated due to a cross-shore gradient in the radiation stresses (S_{xx}). A gradient in the radiation stresses is obtained when the wave energy or H_{rms} changes. However, this is valid when it is assumed that the incident wave field has no directional spreading, which is only true in 1D models. The true radiation stresses can be calculated with the equation presented in the background study (Feddersen, 2004), and is for convenience repeated here:

$$S_{xx} = E_0 \left(n(1+S) - \frac{1}{2} \right) \tag{6.2}$$

Where:

S_{xx}	Radiation stresses $[kg/s^2]$
E_0	Wave energy $(1/8\rho g H_{rms})$
S	Correction for directional spreading $(\cos^2(\overline{\theta})(1-\sigma^{*2}) + \sin^2(\overline{\theta})\sigma^{*2})$
σ^*	Directional spreading given by Kuik et al. (1988)
$\overline{\theta}$	Mean wave direction

This equation indicates that S_{xx} is not only a function of H_{rms} and n, but is also influenced by directional spreading inside the domain. The evolution of directional spreading is discussed in Section 6.1 and it seems to influence the S_{xx} evolution. We have seen that the directional width tends to decrease and then increase inside the domain. Combining this with a changing wave height (Figure 4.2(b)) and wave celerity an estimation of the S_{xx} inside the model domain can be made. This analysis of the radiation stresses and their cross-shore gradient is performed and shown in Appendix D. Next to that, the influence of wind sea wave directional spread on the evolution of S_{xx} is shown here.

The analysis of Figure 6.1 shows that an inclusion of s_{dir} in the cross-shore radiation stresses is affecting the amount and evolution of S_{xx}. The amount of S_{xx} influences the generation of the bound long wave at the offshore boundary, however, it is expected that this effect on runup is minimal since the break-point mechanism is the dominating type of generation in a coral reef environment (Pomeroy et al., 2012a). Furthermore, this analysis also indicated an influence of directional spreading on the gradient of the radiation stresses. From the cross-shore momentum balance it is evident that a gradient in the radiation stresses leads to wave setup. A comparison of the radiation stress gradients shows that the peak of the gradient reduces with an increased width of the directional spectrum (i.e. increased value of s_{dir}). This explains the dependence of wave setup on the directional spreading of wind sea waves.

The literature review showed that the R_{LF} is important for the runup estimations in a coral reef environment. Next to that, previous studies on wave transformation in coral reef environments showed that the break-point mechanism is the dominating LF wave generation mechanism (Pomeroy et al., 2012a). The break-point mechanism is basically the time variation of the setup (Bertin et al., 2018; Symonds et al., 1982). We have already seen that the directional spreading influences the wave induced setup, hence it influences the R_{LF}. In other words, the increased directional spread leads to an reduced forcing of the LF wave motions and thus a reduced LF runup. Guza and Feddersen (2012) showed with a wave modeling study that directional spreading influences R_{IG} component ($0.004 \leq f \leq 0.04$). This is in line with the findings presented in this study.

Lastly, the influence of swell wave directional spread on the LF runup component is in contrast with the assumption that these are generated by time varying setup. Namely, the R_{LF} for $s_{dir} = 75$ is higher than the R_{LF} for $s_{dir} = 100$, see Figure 5.2(b). Firstly, the forcing term of the LF waves is investigated, i.e. the wave

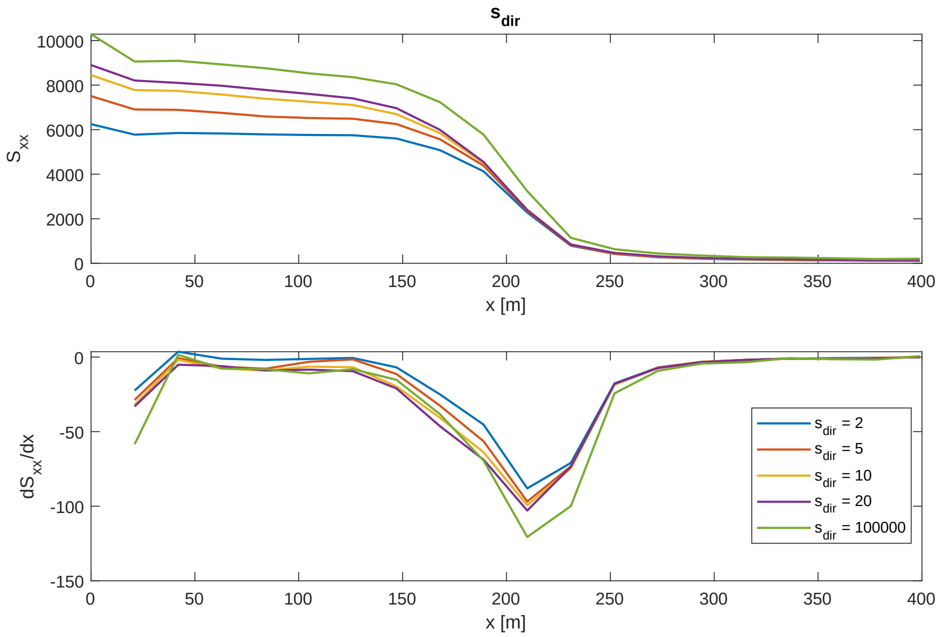

Figure 6.1: The influence of directional spreading on the radiation stresses for wind sea waves. In the top figure the radiation stress evolution in x-direction is shown for different directional spreading. In the lower figure the radiation stress gradients are shown. The model setup; W_{reef} = 200 m, β_f = 0.1, h_0 = 2.0 m and $H_{m0,0}$ = 5 m.

setup. This shows no abnormalities, since the wave setup is correctly represented in the XB NH model. This indicates that the evolution of S_{xx} is correctly represented, hence the forcing term of LF waves. Besides the forcing term is the wave groupiness important for LF wave generation via break-point mechanism (Symonds et al., 1982). So, the discrepancy with the theory can be due to an error in the representation of the wave groupiness for larger values of s_{dir}. In order to analyze this, the groupiness factor can be calculated and compared with multiple XB NH model simulations. The wave groupiness can be assessed with the method described by List (1991).

6.3. The Importance of directional spreading in wave runup predictions

It is evident that directional spreading influences the wave runup in reef environments. This analysis is focusing on the importance of directional spreading in runup predictions, which is assessed with a regression analysis. Firstly, a single variate regression analysis is performed. This analysis gives insight in the relation between, for instance, W_{reef} and R_{setup} and is presented in Appendix E. These results showed that directional spreading has the lowest correlation with the R_{setup} and R_{LF}. This means that the influence of directional spreading on R_{setup} and R_{LF} is the lowest compared to W_{reef}, β_f, h_0 and $H_{m0,0}$. These parameters were selected due to their influence on wave runup, which was shown by other studies on wave runup in coral reef environments, e.g. (Pearson et al., 2017; Quataert et al., 2015). These results suggest that it is more important to first incorporate W_{reef}, β_f, h_0 and $H_{m0,0}$ in your runup analysis before s_{dir}.

However, the previous analysis showed that the directional spreading influences runup. So, the question remains whether incorporating directional spreading will improve the runup prediction. For this reason, a regression model with and without directional spreading is compared. These results showed that the inclusion of directional spreading in the regression models significantly improved the predictive skill of R_{setup} and R_{LF}. Furthermore, the regression model for the HF runup component was less sensitive to the addition of directional spreading. These finding are in line with the theory we discussed and the findings of Guza and Feddersen (2012).

Lastly, it is evident that the influence of directional spreading on the swell wave runup components is less compared to wind sea wave runup. This difference is attributed to the lower directional spreading of swell waves, which was assumed by following a theoretical model, presented in Section 3.2.2. This assumption is not always valid, e.g. Ewans (2002) found a large directional spread of swell waves at the coastline of New Zealand. Furthermore, he found that the directional spread of swell is dependent on the wave height. For wave heights $3.0 \leq H_{m0} \leq 5.0$ m they found a directional spreading of $10° \leq \sigma \leq 27°$, which corresponds to $8 \leq s_{dir} \leq 65$. This is lower than the range used in the current study. However, it is expected that this minor difference will not significantly influence the findings presented here.

6.4. Comparison wave runup with or without directional spreading

As mentioned in the introduction many studies are focused on 1D simplifications of a coral reef. These studies do not include directional spreading, so it is interesting to compare those results. The results show, on average, an overestimation of every runup component in a 1D model. This is especially evident for the wind sea models and leads to a slight overestimation in the swell wave models. This means that 1D modeling is a conservative way of determining the wave runup, which in the case of swell waves is even a good approximation.

It is evident that s_{dir} influences R_{setup} and R_{LF} and these show the largest deviation with the 1D model runup estimations. Furthermore, there is a large difference between the influence of s_{dir} for winds sea waves and swell waves. This suggests that it is worthwhile to incorporate a reduction factor that is depended on the wave steepness. Subsequently, the wave steepness can be connected to a certain representative directional spreading, by using the relation of Goda (1985). This relation is not exact, however we have shown that the exact value of directional spreading is not of great importance to the prediction of the setup and LF runup.

6.5. Limitations

The aim of this section is to elaborate on the method and the assumptions behind it. Some assumptions have an influence on the outcome of this study and therefore should be discussed.

6.5.1. XBeach Non-Hydrostatic Model

In this study XB NH is used as a digital experimental environment. This provided flexibility in the experimental setup and was of a great value to this study. In this way it was possible to test over 27 different kind of coral reefs forced by 20 different types of wave fields. So it was possible to perform 540 different model runs and to investigate the influence of directional spreading in different coral reef environments. XB NH has been used in coral reef environments multiple times and showed great potential. Pearson et al. (2017) validated the model against data of Nwogu and Demirbilek (2010). Klaver (2018) used the model to investigate the effect of excavation pits on reef hydrodynamics. In short, all studies were able to capture the important reef hydrodynamics. However, all these studies focused on 1D processes, whereas this study is focusing on 2DH model runs. This implies that 2D processes are important, which are not included in the validation of the 1D models. In order to overcome this, wave runup relations found in existing literature (e.g. (Pearson et al., 2017; Quataert et al., 2015)) are compared to the relations found in Section 5.1; it was shown that the 2DH XB NH wave runup relations were comparable with previous 1D XB NH studies on wave runup. This created confidence in the 2DH XB NH model performance in a 2DH coral reef environment.

The XB NH modeling approach used in this study lead to some limitations. The main limitation of this study is the lack of model validation, due to the scarce availability of field data or experimental data. Especially data that can be used to validate the 2D processes found in this study. For instance, it would be valuable to validate the directional narrowing and broadening on existing data, since this process is important for the determination of radiation stresses. This can be obtained by placing a cross-shore array of η, u, v buoys in a coral reef environment. Together with these buoys it is interesting to include runup gauges to validate the wave runup. Furthermore, tracer studies can be executed to identify and validate the generation of vorticity in the wave breaking zone. Nevertheless, measurement campaigns are expensive, therefore it is suggested to compare the findings in this study with model output of other numerical software like SWASH. This software is based on the same formulations, however multiple vertical layers can be included to increase the dispersive behavior. This study is performed without any validation, therefore many findings are connected to findings in literature.

The $maxbrsteep$ parameter in XB NH model is used to calibrate the model on data. Lashley et al. (2018) calibrated XB NH model on experimental data in a coral reef environment from Demirbilek et al. (2007) and Buckley et al. (2015). They obtained a best fit with a value of $maxbrsteep = 0.4$, this value is used in the current modeling study. However, both datasets do not include directional spreading, hence it would be interesting to find the optimal $maxbrsteep$ for directionally spread wave fields. This would improve the model's output, since wave breaking is an important variable for LF wave runup. Furthermore, it is expected that this will have little effect on the findings in this report, since it is a relative comparison of model results.

Next to that, a synthetic database is created with 27 different kind of coral reefs forced by 20 different wave fields. These variables are selected from previous research on wave runup in coral reef environments in order to limit the parameter range. This keeps the computational time manageable. The statements made in this study are valid within the range of the dataset. So, caution is needed when using the current findings outside the parameter range presented here. The dataset can be extended and the same method can be used to generate and analyze the data.

In this study a simplified cross-section of a fringing coral reef is used. This is done to limit the number of models, and thus reduce computational time. In literature many different types of coral reef are identified. For instance, (Gourlay, 1996b) defined a coral reef with a coral reef face, i.e. a mild sloping transition between the fore reef slope and reef flat. This reef face is expected to significantly influence the model results, since many processes in this study are influenced by the physical processes in the wave breaking zone.

The analysis of wave runup for different swell wave directional spread showed a discrepancy between the theory and the model output, see Figure 5.2. It was found that this was mainly due to an fault representation of the LF wave generation. It is advised to further investigate these results by analyzing the wave groupiness with the method of List (1991), since this influences LF wave generation (Symonds et al., 1995).

Lastly, it is shown that XB NH is able to model wave runup in a 2DH environment. Furthermore, XB NH was able to model the wave-current interaction, hence represent directional broadening within the surf zone. It also provided flexibility to model different reef geometries under different wave forcing. So, with XB NH it was possible the significantly increase the knowledge about the influence of wave directional spread in a coral reef environment.

6.5.2. Shoaling and refraction model

In Section 3.2.2 the shoaling and refraction model is presented. This model is used to ensure that every XB NH model has the same deep water wave data as input. However, this is a simplification of the reality, since no bottom friction is used and a mild bottom slope is assumed. It is found that the latter assumption is not influencing the model results, since the theoretical model is similar to the XB NH model output. Furthermore, it is expected that bottom friction will not have significant effect, since the model boundaries are located in relatively deep water. However, to confirm this a model like SWAN can be used to calculated the spectral change.

6.6. Significance Of This Research

Lastly, the significance of this research is discussed. Multiple coastal hazards in coral reef environments are often a result of wave driven flooding. Therefore, multiple studies focus on the understanding of wave driven flooding in reef environments by analyzing the wave runup. A shortcoming of these studies is that 2D processes are neglected. For this reason, an attempt is made to understand the influence of wave directional spreading on coastal hazards in coral reef environments.

Firstly, it was evident that the directional spreading increases within the surf zone due to wave-current interaction. The evolution of the directional spread is important for the understanding and assessment of radiation stresses, and ultimately the setup at a coral reef coastline. Furthermore, it was shown that horizontal circulations are generated in the surf zone. These are important for distribution of matter within the surf zone and transfer outside the surf zone, e.g. larvae, nutrients, contaminations and temperature. This research provided insight in the control of vorticity generation, and it showed a reduced vorticity generation for larger reef flat submergence level, see Appendix C. Based on the findings in this research it is suggested that SLR will lead to less transfer of matter across the surf zone, which could affect the coral reefs.

Furthermore, it is found that the wave directional spread influences the wave setup and LF runup. Thus incorporating directional spreading will improve runup predictions and give a better understanding of the threat at a coastline fronted by a coral reef. However, if a choice between different variables must be made due to budget, it is suggested to exclude the specific value of wave directional spread in the analysis, since it has the least influence on runup compared to the reef flat width, reef flat submergence level, fore reef slope and wave height. Moreover, determination of exact directional spreading is expensive, since multiple measurement buoys are necessary, where data about the wave height, reef flat width, fore reef slope and reef flat submergence level is more easily accessible.

However, completely excluding the influence of directional spreading from the analysis will lead to a significant overestimation of wind sea wave runup and a slight overestimation for swell wave runup. Therefore, it is suggested to determine the type of wave field (i.e. wind sea or swell) you are dealing with and take that into account. Furthermore, it is more relevant to account for directional spreading in your runup predictions for wind sea waves than for swell waves. This also suggests that it is less relevant to include directional spreading in 1D modeling studies that look at swell waves.

7 Conclusions

In this study an attempt is made to understand and quantify the influence of wave directional spread on coastal hazards in coral reef environments. This is investigated by using the XBeach Non-Hydrostatic wave model as a tool to executed digital experiments. The model output is post-processed and analyzed. This analysis lead the several key findings and are presented in this chapter.

What is the effect of wave directional spread on the wave runup at coastlines fronted by a coral reef?

This study shows that an increased directional spreading leads to a reduced wave runup on coastlines fronted by a coral reef. A decomposition of the runup signal showed that mainly the wave setup and Low Frequency ($f < 0.04$ Hz) wave runup are reduced with an increased wave directional spread and that the High Frequency ($f > 0.04$ Hz) runup is barely affected. So, waves with a very low directional spreading will lead to the highest runup and thus are the largest threat to a coastline fronted by a coral reef.

How does wave directional spread evolve in a coral reef environment?

It is found that the directional spreading changes within a coral reef environment. At the fore reef slope the directional width reduces due to the refraction of oblique wave components, which is in line with Snel's Law. Inside the surf zone wave directional spread increases while there is an absence of a sloping bottom. The largest increase of the directional width can be expected at wide reef flats, low reef flat submergence level, large wave height and steep fore reef slopes. This broadening is attributed to the wave-current interaction and is due the presence of vorticity. Furthermore, the directional broadening was linked to the absolute amount of vorticity and the size of the vorticity fields.

Does directional spreading influence wave runup in a coral reef environment and how does wave directional spread influence the wave runup?

This research showed that directional spreading influences the wave runup in coral reef environments. Next to that, it mainly influences the wave setup and the Low Frequency wave runup, and it barely influences the High Frequency wave runup. The radiation stresses are analyzed by using the 'true' radiation stress defined by Feddersen (2004). This analysis showed that the influence of wave directional spread on setup is mainly caused by the influence of the spreading on the radiation stresses (S_{xx}), i.e. a broad spectrum leads to lower gradients in the radiation stress and thus lower wave setup. When this lower wave setup is connected to the generation of LF waves via the break-point mechanism, and thus a broader spectrum will also lead to a reduced LF wave runup at coastlines fronted by a coral reef.

How important is it to include directional spreading in the prediction of wave runup?

This study used regression models to investigate the influence of directional spreading on the runup. This analysis showed that wave directional spread improves the prediction of wave setup and Low

Frequency wave runup. So, for an accurate runup predictions it is necessary to incorporate the exact directional spreading in your model. However, it is evident that the influence of directional spreading on wave setup and Low frequency runup is the lowest when it is compared to the influence of W_{reef}, h_0, β_f and H_{m0}. So, directional spreading improves the setup and Low Frequency runup predictions, but is the least important parameter in the predictive model.

What is the difference between wave runup including wave directional spread and wave runup excluding wave directional spread?

This study showed that the runup of waves without directional spreading (i.e. a 1D XB NH model) is overestimated when it is compared with the runup of waves with directional spreading (i.e. 2DH XB NH model). This is mainly due to the overestimation of the wave setup and low frequency wave runup. Furthermore, the overestimation of the setup and Low Frequency runup in 1D models is larger for wind sea waves than for swell waves. For this reason, it is important to incorporate a runup reduction when modeling wind sea waves, and less important to have information about the specific directional width of spectrum. For swell waves it is less important to account for the overestimation of the runup, since these are, on average, slightly overestimated which only leads to a slightly more conservative prediction of the runup.

To conclude, the development of directional spreading inside the domain affects the gradient of the radiation stresses. In this way setup and low frequency runup are influenced. The results imply that directional spreading could improve setup and low frequency runup predictions, however it is the least influential parameter considered in this study. In 1D modeling the setup and LF runup are overestimated during wind sea wave conditions. Modeling swell waves in 1D gives a slight overestimation of the wave runup and thus it is more important to know which wave field you want to model and account for that, than information about the precise directional spread of this wave field.

8 Recommendations

In this study it is shown for wind sea and swell waves that the wave directional spread influences the wave runup in coral reef environments. Furthermore, we were able the understand the wave directional spread transformation in a coral reef environment. This is a novel work focused on the analysis of 2DH processes in relation with wave runup in coral reef environments. Additionally, the findings in this study can be used for the assessments of coastal hazards in coral reef environments, and some recommendations are given. Lastly, the method described here can be used to analyze other 2DH features that influence wave runup.

8.1. Application

Based on the findings presented in this study, it is evident that wave directional spread of wind sea waves and swell waves influence wave runup. Furthermore, the regression analysis showed that incorporating the specific directional spreading leads to better predictions of the wave setup and Low Frequency wave runup in coral reef environments. However, it has the least influence on these runup components compared to the reef flat width, fore reef slope, reef flat submergence level and wave height.

The usage of these results depends on the type of coastal hazard assessment that is executed. If an accurate representation of wave runup is required, based on this study, it is advised to include this in the runup analysis, which is especially important for wind sea waves. However, data about wave directional spreading has to be available in order to include it in the analysis. The areas of interest in this study are characterized by scarce availability of field data and especially data about the directional spreading. So, if the assessment has a limited amount resources, it is advised to determine the wave height, reef flat width, reef flat submergence level and fore reef slope first, before considering directional spreading.

Furthermore, excluding directional spreading completely from the analysis will provide conservative estimations of the wave runup, since it will give an overestimation of the wave runup for wind sea waves and a slight overestimation of the runup for swell waves. Based on this study, it is advised to determine the type of wave field that is threatening the coral reef coastline and include this in the analysis.

8.2. Future work

Firstly, it is of great value to validate the 2DH XB NH model on field data. The first step would be the comparison of XB NH model output with the data from 1 η, u, v buoy in the near shore and wave runup data. Next, it would be interesting to compare the evolution of wave directional spread with a cross-shore array of wave buoys starting at the edge of the surf zone. When the evolution of directional spreading is correctly represented then it could be assumed that the vorticity is also correctly represented. With a larger budget the array of buoys can be extended with runup gauges on the coral reef beach.

The findings presented here can be used in the assessment of coastal hazards. BEWARE (Pearson et al., 2017) is a tool to assess the wave runup in coral reef environments. In this study a Bayesian network is trained with

1D XB NH model run output. The current findings can be used to increase the accuracy of this tool. Based on this study, it is advised to incorporate runup reduction factors for the wave setup and Low frequency wave runup, e.g. Section 5.3.2. However, some steps are necessary. Firstly, the current parameter range must be extended to match te parameter range of BEWARE. In Section 5.3.2 it was evident that the influence of wave directional spread is influenced by the reef flat width, fore reef slope and reef flat submergence level. These parameters should be included in the extension of the database. The number of model runs can be limited by connecting the wave steepness with a typical directional spreading by using the wave age parameter. A practical tool would be the relation given by Goda (1985). The relation between wave steepness and directional spreading does not have to be precise, since it has already been proven that the parameter space of directional spreading for wind sea and swell waves has a relative low influence on runup predictions.

Furthermore, the method used in this study can be used for analysis of other 2D mechanisms that influence the wave runup. Firstly, this method can be used to analyze the influence of obliquely incident waves on the wave runup. Van der Meer (2002) investigated the safety of dikes under wave different type of wave forcing. He found that obliquely incident waves influence the runup on a dike (see Figure 8.1). The approach used in this study can be used to model and analyze the influence of obliquely incident waves on the wave runup. It is important to use XBeachX version 1.23.5526 or newer, since an older version does not correctly represent the obliquely incident waves. Furthermore, it is advised to start with long crested waves and low incident wave angles and increase the model complexity when satisfactory results are obtained. Extra attention is required at the Message Passing Interface boundaries. Lastly, the shoaling and refraction model is also applicable for obliquely incident waves. However, it will lead to skewed directional spectra, so extra attention should be paid to the influence of skewed directional spectra on the reef hydrodynamics.

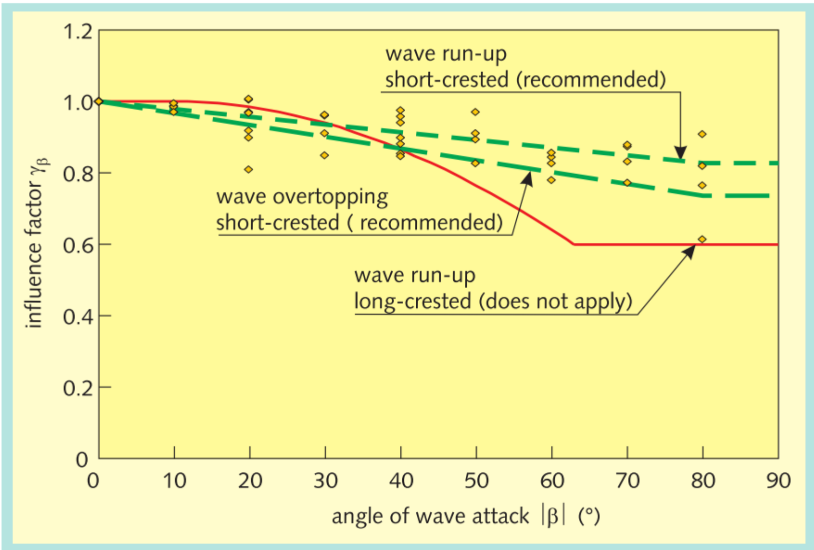

Figure 8.1: A reduction factor for oblique wave attack on a dike, the angle β is measured at the beach toe. This reduction factor is used for wave runup and overtopping calculations on dutch dikes (From Van der Meer (2002))

Secondly, the methodology in this study can be used to investigate the influence of curved coastlines on the wave runup. Tajima et al. (2017) found an alongshore variation of the wave runup by performing post storm field measurements. These alongshore variations seem to coincide with a curved reef edge and coastline, see Figure 8.2. An analysis of this phenomenon would be a valuable addition to the current knowledge about wave runup in coral reef environments. The first step would be to create a curved bathymetry profile, shown in Figure 8.2. Next, the bathymetry has to be discretized and it is advised to compare the results of a curved linear and rectangular grid. Keep the model complexity low by modeling normally incident long crested waves. Furthermore, the use of cyclic boundary conditions at the lateral boundaries has to be investigated. It is expected that the hydrodynamics are influenced by the curved depth contours. The cyclic boundary will copy these hydrodynamics to the opposite lateral boundary and thus influence the hydrodynamics at the other side of the model. Therefore, it is suggested to investigate the use of Neumann boundary conditions or extent the model in y-direction such that the hydrodynamics resulting from the curvature will be damped before traveling out of the domain.

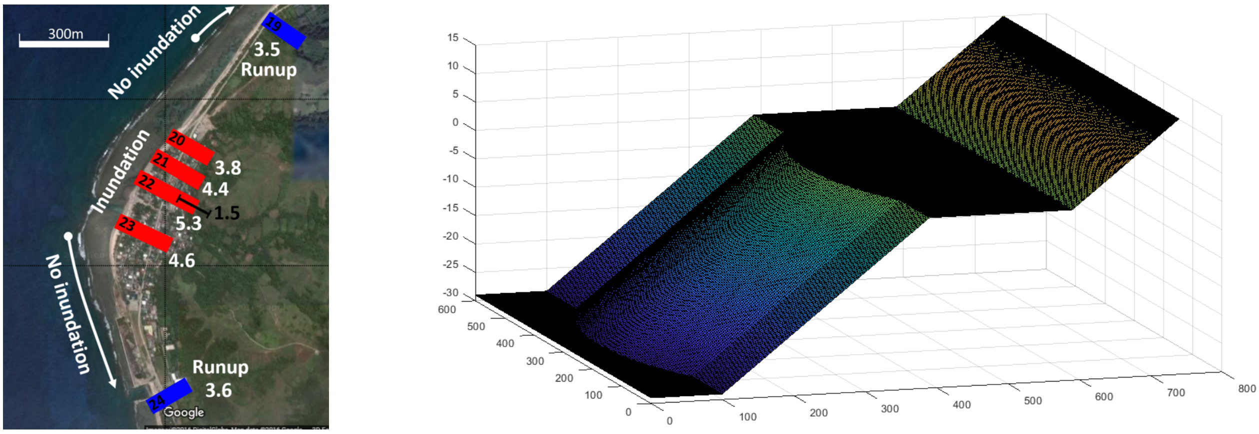

Figure 8.2: Left: Post storm (Typhoon) measurements of inundation levels which show great variability alongshore, inundation levels (red) and runup (blue) at Ivana, Batanes (From Tajima et al. (2017)). Right: Schematization of a curved fore reef slope at coral reefs. A parabola formulation is used to define the curvature.

Lastly, it was found that the LF wave runup calculations for directionally narrow swell waves leads to abnormalities which cannot be explained by theoretical models. Therefore, it is expected that these are a result of an inaccuracy in XB NH. The analysis of setup showed that the forcing of LF wave motions is correctly represented in the model. So it is hypothesized that the wave groupiness could influence the LF wave generation and thus an erroneous representation of the wave groupiness could lead to incorrect LF runup calculation. For this reason, it is suggested to investigate the wave groupiness by using the method described by List (1991).

Bibliography

Arthur, R. (1946). Refraction of water waves by islands and shoals with circular bottom-contours. *American Geophysical Union*, 27(2).

Barstow, S. F., Bidlot, J.-r., Caires, S., Donelan, M. A., Drennan, W. M., Graber, H. C., Green, J. J., Gu, C., Barstow, S. F., Bidlot, J.-r., Caires, S., Donelan, M. A., and Dren, W. M. (2005). *Measuring and Analysing the directional spectrum of ocean waves*. COST Office.

Battjes, J. (1974). Surf Similarity. In *Coastal Engineering 1974*, Methods in Molecular Biology, pages 466–480, New York, NY. American Society of Civil Engineers.

Battjes, J. A. (2004). Shoaling of subharmonic gravity waves. *Journal of Geophysical Research*, 109(C2):C02009.

Becker, J. M., Merrifield, M. A., and Ford, M. (2014). Water level effects on breaking wave setup for Pacific Island fringing reefs. *Journal of Geophysical Research: Oceans*, 119(2):914–932.

Becker, J. M., Merrifield, M. A., and Yoon, H. (2016). Infragravity waves on fringing reefs in the tropical Pacific: Dynamic setup. *Journal of Geophysical Research : Oceans*, pages 3010–3028.

Beetham, E., Kench, P. S., O'Callaghan, J., and Popinet, S. (2015). Wave transformation and shoreline water level on Funafuti Atoll, Tuvalu. *Journal of Geophysical Research : Oceans*.

Benoit, M., Frigaard, P., and Schaffer, H. (1997). Analyzing multidirectional wave spectra: a tentative classification of available methods. In *Proceedings of the 1997 IAHR conference*, number January 1997.

Bertin, X., de Bakker, A., van Dongeren, A., Coco, G., André, G., Ardhuin, F., Bonneton, P., Bouchette, F., Castelle, B., Crawford, W. C., Davidson, M., Deen, M., Dodet, G., Guérin, T., Inch, K., Leckler, F., McCall, R., Muller, H., Olabarrieta, M., Roelvink, D., Ruessink, G., Sous, D., Stutzmann, É., and Tissier, M. (2018). Infragravity waves: From driving mechanisms to impacts. *Earth-Science Reviews*, 177(December 2017):774–799.

Buckley, M. L., Lowe, R. J., Hansen, J. E., and Van Dongeren, A. R. (2015). Dynamics of Wave Setup over a Steeply Sloping Fringing Reef. *Journal of Physical Oceanography*, 45(12):3005–3023.

Buckley, M. L., Lowe, R. J., Hansen, J. E., and Van Dongeren, A. R. (2016). Wave Setup over a Fringing Reef with Large Bottom Roughness. *Journal of Physical Oceanography*, 46(8):2317–2333.

Cheriton, O. M., Storlazzi, C. D., and Rosenberger, K. J. (2016). Observations of wave transformation over a fringing coral reef and the importance of low-frequency waves and offshore water levels to runup, overwash, and coastal flooding. *Journal of Geophysical Research: Oceans*, pages 1–15.

Clark, D. B., Elgar, S., and Raubenheimer, B. (2012). Vorticity generation by short-crested wave breaking. *Geophysical Research Letters*, 39(24):1–6.

Costa, M. B., Araújo, M., Araújo, T. C., and Siegle, E. (2016). Influence of reef geometry on wave attenuation on a Brazilian coral reef. *Geomorphology*, 253:318–327.

Cui, H., Pietrzak, J. D., and Stelling, G. S. (2014). Optimal dispersion with minimized Poisson equations for non-hydrostatic free surface flows. *Ocean Modelling*, 81:1–12.

Da Silva, G. V., Murray, T., and Strauss, D. (2018). Longshore wave variability along non-straight coastlines. *Estuarine, Coastal and Shelf Science*, 212(February):318–328.

Dalrymple, R. A., MacMahan, J. H., Reniers, A. J., and Nelko, V. (2011). Rip Currents. *Annual Review of Fluid Mechanics*, 43(1):551–581.

de Ridder, M. (2018). *Non-hydrostatic wave modelling of coral reefs with the addition of a porous in- canopy model*. Master thesis, Delft University of Technology.

Demirbilek, Z., Nwogu, O. G., Ward, D. L., Zeki Demirbilek, Nwogu, O. G., and Ward, D. L. (2007). Laboratory Study of Wind Effect on Runup over Fringing Reefs. *Test*, (July):1–83.

Ewans, K. C. (2002). Directional Spreading in Ocean Swell. In *Ocean Wave Measurement and Analysis (2001)*, volume 40604, pages 517–529, Reston, VA. American Society of Civil Engineers.

Feddersen, F. (2004). Effect of wave directional spread on the radiation stress: Comparing theory and observations. *Coastal Engineering*, 51(5-6):472–482.

Ferrario, F., Beck, M. W., Storlazzi, C. D., Micheli, F., Shepard, C. C., and Airoldi, L. (2014). The effectiveness of coral reefs for coastal hazard risk reduction and adaptation. *Nature Communications*, 5(May):1–9.

Gawehn, M., van Dongeren, A., van Rooijen, A., Storlazzi, C. D., Cheriton, O. M., and Reniers, A. (2016). Identification and classification of very low frequency waves on a coral reef flat. *Journal of Geophysical Research: Oceans*, (November):7560–7574.

Goda, Y. (1985). *Random Seas and Design of Maritime Structures*. University of Tokyo Press, Tokyo.

Gourlay, M. R. (1996a). Wave set-up on coral reefs. 1. Set-up and wave-generated flow on an idealised two dimensional horizontal reef. *Coastal Engineering*, 27(3-4):161–193.

Gourlay, M. R. (1996b). Wave set-up on coral reefs. 2. Set-up on reefs with various profiles. *Coastal Engineering*, 28(1-4):17–55.

Guza, R. T. and Feddersen, F. (2012). Effect of wave frequency and directional spread on shoreline runup. *Geophysical Research Letters*, 39(11):1–5.

Hasselmann, K., Barnett, T. P., Bouws, E., Carlson, H., Cartwright, D. E., Enke, K., Ewing, J. A., Gienapp, H., Hasselmann, D. E., Kruseman, P., Meerburg, A., Muller, P., Olbers, D. J., Richter, K., Sell, W., and Walden, H. (1973). Measurements of Wind-Wave Growth and Swell Decay during the Joint North Sea Wave Project (JONSWAP). *Ergnzungsheft zur Deutschen Hydrographischen Zeitschrift Reihe*, A(8)(8 0):p.95.

Hearn, C. J. (1999). Wave-breaking hydrodynamics within coral reef systems and the effect of changing relative sea level. *Journal of Geophysical Research: Oceans*, 104(C12):30007–30019.

Henderson, S. M., Guza, R. T., Elgar, S., and Herbers, T. H. C. (2006). Refraction of Surface Gravity Waves by Shear Waves. *Journal of Physical Oceanography*, 36(4):629–635.

Herbers, T. H. C., Elgar, S., and Guza, R. T. (1999). Directional spreading of waves in the nearshore zone. *Journal of Geophysical Research*, 104:7683–7693.

Hoeke, R. K., McInnes, K. L., Kruger, J. C., McNaught, R. J., Hunter, J. R., and Smithers, S. G. (2013a). Widespread inundation of Pacific islands triggered by distant-source wind-waves. *Global and Planetary Change*, 108:1–11.

Hoeke, R. K., Storlazzi, C. D., and Ridd, P. V. (2013b). Drivers of circulation in a fringing coral reef embayment: A wave-flow coupled numerical modeling study of Hanalei Bay, Hawaii. *Continental Shelf Research*, 58:79–95.

Hunt, I. A. (1959). Design of seawalls and breakwaters. *Journal of the Waterways and Harbors Division*, 85(3):123–152.

Johnson, J. W., O'Brien, M. P., and Isaacs, J. D. (1948). Graphical Construction of Wave Refraction Diagams. Technical report, Hydrographic Office U.S. Navy.

Kanoglu, U. and Synolakis, C. E. (1998). Long wave runup on piecewise linear topographies. *J. Fluid Mech.*, 374:1–28.

Klaver, S. (2018). *Modelling the effects of excavation pits on fringing reefs*. PhD thesis, Delft University of technology.

Kuik, A., Vledder, G., and Holthuijsen, L. H. (1988). A method for the routine analysis of pitch-and-roll buoy wave data. *Journal of Physical Oceanography*, 18:1020–1034.

Lashley, C. H., Roelvink, D., van Dongeren, A., Buckley, M. L., and Lowe, R. J. (2018). Nonhydrostatic and surfbeat model predictions of extreme wave run-up in fringing reef environments. *Coastal Engineering*, 137(March):11–27.

Lippmann, T. C., Herbers, T. H. C., and Thornton, E. B. (1999). Gravity and Shear Wave Contributions to Nearshore Infragravity Motions. *Journal of Physical Oceanography*, 29(2):231–239.

List, J. H. (1991). Wave groupiness in the nearshore. 15:475–496.

Liu, P. L. F., Cho, Y.-S., Briggs, M. J., Kanoglu, U., and Synolakis, C. E. (1995). Runup of solitary waves on a circular Island. *Journal of Fluid Mechanics*, 302:259.

López-Ruiz, A., Solari, S., Ortega-Sánchez, M., and Losada, M. (2015). A simple approximation for wave refraction - Application to the assessment of the nearshore wave directionality. *Ocean Modelling*, 96:324–333.

Lowe, R. J. and Falter, J. L. (2015). Oceanic Forcing of Coral Reefs. *Annual Review of Marine Science*, 7(1):43–66.

Lowe, R. J., Falter, J. L., Monismith, S. G., and Atkinson, M. J. (2009). A numerical study of circulation in a coastal reef-lagoon system. *Journal of Geophysical Research: Oceans*, 114(6):1–18.

Merrifield, M. A., Becker, J. M., Ford, M., and Yao, Y. (2014). Observations and estimates of wave-driven water level extremes at the Marshall Islands. *Geophysical Research Letters*, 41(20):7245–7253.

Mitsuyasu, H., Tasai, F., Suhara, T., Mizuno, S., Ohkusu, M., Honda, T., and Rikiishi, K. (1975). Observations of the Directional Spectrum of Ocean WavesUsing a Cloverleaf Buoy.

Monismith, S. G. (2007). Hydrodynamics of Coral Reefs. *Annual Review of Fluid Mechanics*, 39(1):37–55.

Nwogu, O. and Demirbilek, Z. (2010). Infragravity Wave Motions and Runup over Shallow Fringing Reefs. *Journal of Waterway, Port, Coastal, and Ocean Engineering*, 136(6):295–305.

Pearson, S. G. (2016). Predicting Wave-Induced Flooding on Low-Lying Tropical Islands Using a Bayesian Network. Technical Report July, Delft University of Technology, Delft.

Pearson, S. G., Storlazzi, C. D., van Dongeren, A. R., Tissier, M. F., and Reniers, A. J. (2017). A Bayesian-Based System to Assess Wave-Driven Flooding Hazards on Coral Reef-Lined Coasts. *Journal of Geophysical Research: Oceans*, 122(12):10099–10117.

Péquignet, A. C. N., Becker, J. M., and Merrifield, M. A. (2014). Energy transfer between wind waves and low-frequency oscillations on a fringing reef, Ipan, Guam. *Journal of Geophysical Research: Oceans*, 119(10):6709–6724.

Péquignet, A. C. N., Becker, J. M., Merrifield, M. A., and Aucan, J. (2009). Forcing of resonant modes on a fringing reef during tropical storm Man-Yi. *Geophysical Research Letters*, 36(3):20–23.

Perry, C. T., Alvarez-Filip, L., Graham, N. A. J., Mumby, P. J., Wilson, S. K., Kench, P. S., Manzello, D. P., Morgan, K. M., Slangen, A. B. A., Thomson, D. P., Januchowski-Hartley, F., Smithers, S. G., Steneck, R. S., Carlton, R., Edinger, E. N., Enochs, I. C., Estrada-Saldívar, N., Haywood, M. D. E., Kolodziej, G., Murphy, G. N., Pérez-Cervantes, E., Suchley, A., Valentino, L., Boenish, R., Wilson, M., and Macdonald, C. (2018). Loss of coral reef growth capacity to track future increases in sea level. *Nature*, 558(7710):396–400.

Pierson, W. J. and Moskowitz, L. (1964). A proposed spectral form for fully developed wind seas based on the similarity theory of S. A. Kitaigorodskii. *Journal of Geophysical Research*, 69(24):5181–5190.

Pocinki, L. (1950). the Application of Conformal Transformations to ocean wave refraction problems. *American Geophysical Union*, 31(6):857–866.

Pomeroy, A., Lowe, R., Symonds, G., Van Dongeren, A., and Moore, C. (2012a). The dynamics of infragravity wave transformation over a fringing reef. *Journal of Geophysical Research: Oceans*, 117(11):1–17.

Pomeroy, A., van Dongeren, A. R., Lowe, R. J., van Thiel de Vries, J. S. M., and Roelvink, J. A. (2012b). Low-frequency wave resonance in fringing reef environments. *Coastal Engineering 2012*, pages 1–10.

Quataert, E., Storlazzi, C., Van Rooijen, A., Cheriton, O., and Van Dongeren, A. (2015). The influence of coral reefs and climate change on wave-driven flooding of tropical coastlines. *Geophysical Research Letters*, 42(15):6407–6415.

Raubenheimer, B., Guza, R. T., and Elgar, S. (1996). Wave transformation across the inner surf zone. *Journal of Geophysical Research C: Oceans*, 101(C11):25589–25597.

Rawlings, J. O., Pantula, S. G., and Dickey, D. A. (1998). *Applied Regression Analysis: A Research Tool.*

Roeber, V. and Bricker, J. D. (2015). Destructive tsunami-like wave generated by surf beat over a coral reef during Typhoon Haiyan. *Nature Communications*, 6:1–9.

Roelvink, D., van Dongeren, A., McCall, R., Hoonhout, B., van Rooijen, A., van Geer, P., de Vet, L., Nederhoff, K., and Quataert, E. (2015). XBeach Technical Reference : Kingsday Release. pages 1–141.

Semedo, A., Vettor, R., Breivik, Ø., Sterl, A., Reistad, M., Soares, C. G., and Lima, D. (2014). The wind sea and swell waves climate in the Nordic seas. *Ocean Dynamics*, 65(2):223–240.

Shimozono, T., Tajima, Y., Kennedy, A. B., Nobuoka, H., Sasaki, J., and Sato, S. (2015). Combined infragravity wave and sea-swell runup over fringing reefs by super typhoon Haiyan. *Journal of Geophysical Research: Oceans*, 120(6):4463–4486.

Smit, P., Stelling, G., Roelvink, D., van Thiel de Vries, J. S. M., McCall, R., Van Dongeren, A. R., Zwinkels, C., and Jacobs, R. (2010). XBeach : Non-hydrostatic model.

Smith, S. D., Anderson, R. J., Oost, W. A., Kraan, C., Maat, N., De Cosmo, J., Katsaros, K. B., Davidson, K. L., Bumke, K., Hasse, L., and Chadwick, H. M. (1992). Sea surface wind stress and drag coefficients: The hexos results. *Boundary-Layer Meteorology*, 60(1-2):109–142.

Stockdon, H. F., Holman, R. A., Howd, P. A., and Sallenger, A. H. (2006). Empirical parameterization of setup, swash, and runup. *Coastal Engineering*, 53(7):573–588.

Storlazzi, C. D., Elias, E. P., and Berkowitz, P. (2015). Many Atolls May be Uninhabitable Within Decades Due to Climate Change. *Scientific Reports*, 5:1–9.

Storlazzi, C. D., Gingerich, S. B., Van Dongeren, A., Cheriton, O. M., Swarzenski, P. W., Quataert, E., Voss, C. I., Field, D. W., Annamalai, H., Piniak, G. A., and McCall, R. (2018). Most atolls will be uninhabitable by the mid-21st century because of sea-level rise exacerbating wave-driven flooding. *Science Advances*, 4(4):1–10.

Su, S. F. and Ma, G. (2018). Modeling two-dimensional infragravity motions on a fringing reef. *Ocean Engineering*, 153(December 2017):256–267.

Svendsen, A. (2006). *Introduction to nearshore hydrodynamics.* World Scientific Publishing, Delaware.

Symonds, G., Black, K. P., and Young, I. R. (1995). Wave-driven flow over shallow reefs. *Journal of Geophysical Research*, 100(C2):2639–2648.

Symonds, G., Huntley, D. A., and Bowen, A. J. (1982). Long Wave Generation by a Time-Varying Breakpoint. *Journal of Geophysical Research*, 87(C1):492–498.

Tajima, Y., Gunasekara, K. H., Shimozono, T., and Cruz, E. C. (2016a). Study on Locally Varying Inundation Characteristics Induced by Super Typhoon Haiyan. Part 1: Dynamic Behavior of Storm Surge and Waves Around San Pedro Bay. *Coastal Engineering Journal*, 58(01):1640002.

Tajima, Y., Lapidez, J. P., Camelo, J., Saito, M., Matsuba, Y., Shimozono, T., Bautista, D., Turiano, M., and Cruz, E. (2017). Post-Disaster Survey of Storm Surge and Waves Along the Coast of Batanes, the Philippines, Caused by Super Typhoon Meranti/Ferdie. *Coastal Engineering Journal*, 59(01):1750009.

Tajima, Y., Shimozono, T., Gunasekara, K. H., and Cruz, E. C. (2016b). Study on Locally Varying Inundation Characteristics Induced by Super Typhoon Haiyan. Part 2: Deformation of Storm Waves on the Beach with Fringing Reef Along the East Coast of Eastern Samar. *Coastal Engineering Journal*, 58(1):1640003–1–1640003–24.

Terry, J. P. and Goff, J. (2013). One hundred and thirty years since Darwin: 'Reshaping' the theory of atoll formation. *Holocene*, 23(4):615–619.

Tissier, M. F. S., Bonneton, P., and Ruessink, B. G. (2017). Infragravity Waves and Bore Merging. *Coastal Dynamics 2017*, (117):1–15.

Toba, Y. (1972). Local balance in the air-sea boundary processes - I. on the growth process of wind waves. *Journal of the Oceanographical Society of Japan*, 28(3):109–120.

Van der Meer, J. (2002). Technical report wave run-up and wave overtopping at dikes. Technical report, Technical Advisory Committee on Flood Defence - The Netherlands (TAW), Delft.

van Dongeren, A., Battjes, J., Janssen, T., van Noorloos, J., Steenhauer, K., Steenbergen, G., and Reniers, A. (2007). Shoaling and shoreline dissipation of low-frequency waves. *Journal of Geophysical Research: Oceans*, 112(2):1–15.

Van Dongeren, A., Lowe, R., Pomeroy, A., Trang, D. M., Roelvink, D., Symonds, G., and Ranasinghe, R. (2013). Numerical modeling of low-frequency wave dynamics over a fringing coral reef. *Coastal Engineering*, 73:178–190.

Vetter, O., Becker, J. M., Merrifield, M. A., Pequignet, A. C., Aucan, J., Boc, S. J., and Pollock, C. E. (2010). Wave setup over a Pacific Island fringing reef. *Journal of Geophysical Research: Oceans*, 115(12):1–13.

Vieira Da Silva, G., Silva, P. G. D., Araujo, R. S., Klein, A. H. D. F., and Toldo, E. E. (2017). Wave run-up on embayed beaches. Study case: Itapocorói bay, Southern Brazil. *Brazilian Journal of Oceanography*, 65(2):187–200.

Vincent, C. L. and Briggs, M. J. (1989). Refraction - diffraction of irregular waves over a mound. *Journal of Waterway, Port, Coastal, and Ocean Engineering*, 115(2):269–284.

Woodroffe, C. D. (2008). Reef-island topography and the vulnerability of atolls to sea-level rise. *Global and Planetary Change*, 62(1-2):77–96.

WRI (2011). Reefs at Risk - Revisited. Technical report, World Resource Institute, Washington DC.

Zijlema, M., Stelling, G., and Smit, P. (2011). SWASH: An operational public domain code for simulating wave fields and rapidly varied flows in coastal waters. *Coastal Engineering*, 58(10):992–1012.

Zijlema, M. and Stelling, G. S. (2008). Efficient computation of surf zone waves using the nonlinear shallow water equations with non-hydrostatic pressure. *Coastal Engineering*, 55(10):780–790.

A

Directional spreading s-parameter

The directional spreading of a wave field can be expressed with a mean direction and a value that represents the spread of the directional distribution. Whereas the shape of the distribution could be unimodal (single mean direction), bimodal (two mean directions) or can be skewed. Assumed is that an offshore wave field has a theoretical shape and thus can be described by a JONSWAP frequency spectrum and an unimodal directional spectrum. Two typical directional distribution are (1) the Gaussian or Normal model and σ, and (2) the Mitsuyasu et al. (1975) model. Both are parametric models and use a θ_0 to describe the mean direction, however the first expression uses σ to describe the directional width and the latter a s parameter, see Equation A.1 & A.2 (Benoit et al., 1997).

$$D(\theta) = \frac{1}{\sqrt{2\pi}\sigma} \exp\left(-\frac{(\theta-\theta_0)^2}{2\sigma^2}\right) \tag{A.1}$$

Valid for $[-\pi \leq \theta \leq \pi]$ and where:

σ	Width of the directional distribution [rad]
θ	Wave direction [rad]
θ_0	Mean wave direction [rad]

$$D(\theta) = A(s)\cos^{2s}\left(\frac{\theta-\theta_0}{2}\right) \tag{A.2}$$

Valid for $[-\pi \leq \theta \leq \pi]$, where:

$A(s)$	$2^{2s-1}\frac{\Gamma^2(s+1)}{\Gamma(2s+1)}$, sets area below distribution to 1.0
θ	Wave direction [rad]
s	The directional width parameter [-]

The two parameters σ and s are related to each other via the following equation (Barstow et al., 2005):

$$\sigma = \sqrt{\frac{2}{s+1}} \tag{A.3}$$

A comparison of the two models is shown in Figure A.1, with a s-value of 10 using the Mitsuyasu et al. (1975) model, which corresponds with a σ of 24°(Equation A.3). Small deviations between the methods can be found, especially the height of the peaks differ. Plots with multiple s-values show that the difference between the two models will decrease with a lower directional width or larger s-values.

XBeach uses the Mitsuyasu et al. (1975) model to describe the directional distribution. This study will use several s-values during the model study, hence a parameter range has to be determined. The parameter space will visually be investigated by plotting multiple distributions, and in such a way that the whole range

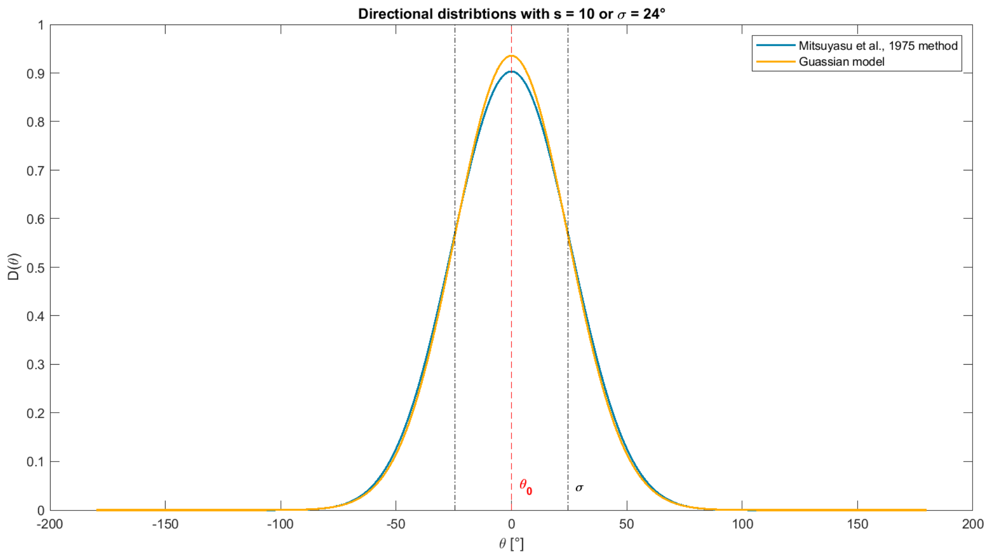

Figure A.1: A comparison of the Mitsuyasu et al. (1975) and Gaussian directional model

of distribution is covered by a limited number of s-values in order to minimize number of model runs. The directional distributions for different s-values is given in Figure A.2, with parameter range: s = [2 10 50 200 10000]. The distribution with the smallest directional width or largest s-value, can be seen as a wave field with a single direction or unidirectional waves, such a wave field only contains long crested waves.

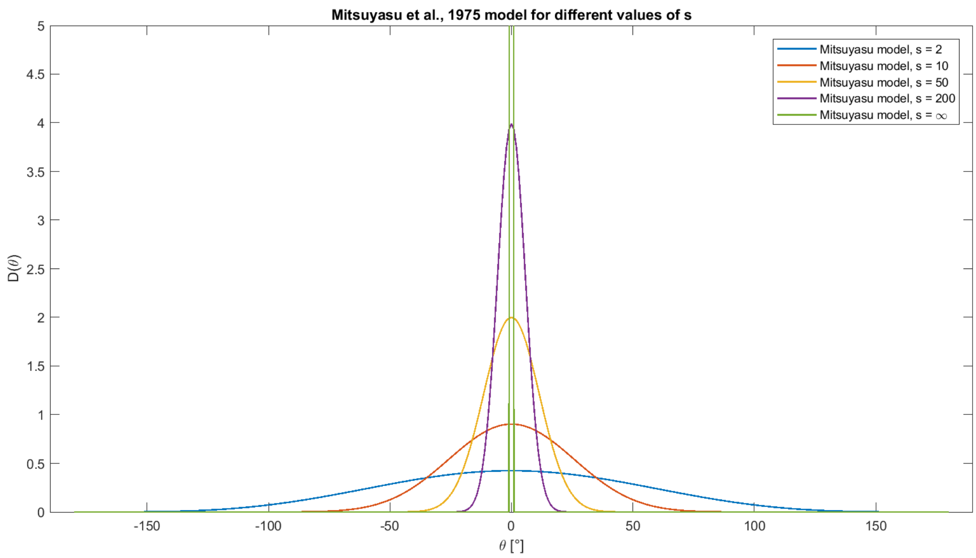

Figure A.2: A comparison of different s-values of the Mitsuyasu et al. (1975) model, Note that the distribution with the smallest directional width is extending beyond the graphs limit.

In Figure A.2 can be seen that a distribution with a large directional width has energy propagation with an angle larger than 90 degrees relative to the mean direction. Moreover, in this study the propagation of waves towards a coral reef coastline is considered. So waves with an angle, relative to the shore normal, larger than 90 degrees won't reach the shoreline. These waves have to be corrected in calculations with the directional distributions.

B

Sensitivity analysis grid

The goal of this appendix is to analyse the 'best' grid size. Various grid sizes are forced by a wind sea and a swell wave field. The grid size parameters are: points per wave length (ppwl) (i.e. controlling parameter for x grid discretization) and dy. Subsequently, key parameters are compared and the roughest grid size with reasonable results is used. It is expected that the grid of a wind sea wave field and swell wave field is different due to the wave field characteristics.

Key parameters
This study focuses on the wave runup in a coral reef environment. Next to that, the literature study has shown that the wave runup in a coral reef environment can be controlled by the LF wave motions (i.e. infragravity and very low frequency wave motions), for this reason an accurate representation of the LF motions is desired. Next to that, the evolution of wave energy (i.e. H_{rms}) in x-direction at the middle of the y-direction is compared. This gives insight in the effect of the grid on the total wave energy in a certain cross-section. To sumup, the following parameters are compared:

1. H_{rms} distribution in x-direction
2. H_{HF} at the beach toe
3. H_{LF} at the beach toe
4. Runup ($R2\%$) and setup (η_{setup}) at the beach

B.1. Wind sea wave field

The domain width (i.e. y-direction) of wind sea waves equals 500 m. The cross-shore domain length depends mainly on the depth of offshore boundary and the reef geometry, thus, is variable. At first, the influence of ppwl on the model results is investigated. The model setup is shown in Table B.1.

Reef geometry			
Reef flat width	W_{reef}	200	[m]
Fore reef slope	β_{fr}	1/10	[-]
Beach slope	β_b	1/10	[-]
Reef flat submergence	h_0	2	[m]
Bottom friction coefficient	c_f	0.02	[-]
Hydrodynamic conditions			
Wave height	H_{m0}	5.0	[m]
Wave steepness	s_0	0.05	[-]
Directional spread	s	10.0	[-]
Grid			
points per wave length	ppwl	20, 40, 60, 80	[-]
y grid size	dy	2,4,6,10	[m]

Table B.1: Model setup for sensitivity analysis of domain discretization, the reef geometry and hydrodynamic conditions are constant only the grid parameters are varied.

Results ppwl

Firstly, the influence of ppwl is investigated. The results of the model runs are shown in Figure B.1 and summed up in Table B.2. The following observations can be made:

1. A variation in the ppwl has little influence on the evolution of the H_{rms} in the cross shore direction.
2. In all simulation the H_{rms} drops when entering the domain, this could be due to the relatively high wave steepness s_0 chosen for the wind sea simulations. The large drop is not evident in the swell wave simulations.
3. Variations in the ppwl hardly affects H_{HF}, H_{LF} and η_{setup}, however it has some effect on the $R2\%$. This is evident when the model runs with a $ppwl = 20$ and $ppwl = 40$ are compared.

To conclude, the ppwl hardly influence the wave energy distribution across the model domain and key model output parameters. However, it has a little effect on the runup which is increased with 10 cm when modeling with a $ppwl = 40$ instead of 20. Additionally, adding ppwl will increase the model run time and using 40 ppwl will double the model time compared to a model run with 20 ppwl. So, considering the model output and model run time is are 20 ppwl used.

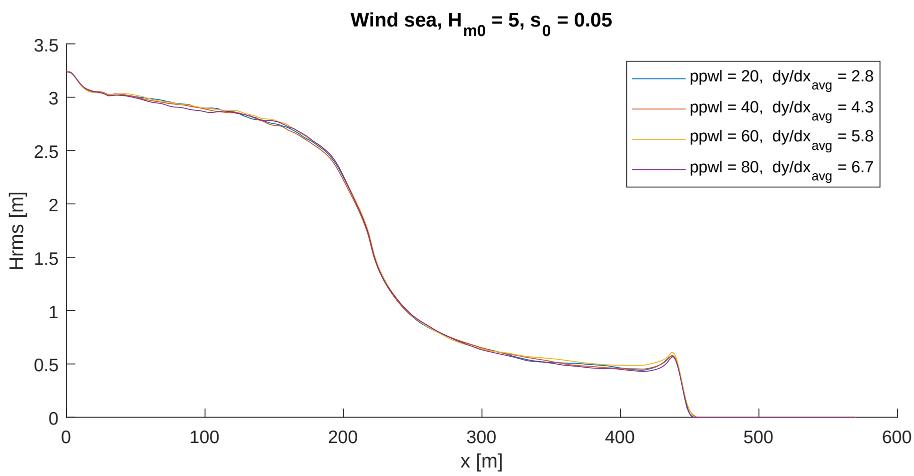

Figure B.1: Wave energy distribution in cross-shore direction for various $ppwl$. Cross section is placed at the center of the domain.

Model results wind sea							
$ppwl$ [-]	dy/dx_{avg} [-]	dy/dx_{min} [-]	dy/dx_{max} [-]	H_{HF} [m]	H_{LF} [m]	$R2\%$ [m]	η_{setup} [m]
20	2.8	8.0	2.35	0.52	0.35	3.06	0.47
40	4.3	8.0	2.35	0.50	0.36	3.16	0.49
60	5.8	8.0	2.67	0.48	0.41	3.19	0.49
80	6.7	8.0	3.63	0.47	0.37	3.17	0.48

Table B.2: Model output of the $ppwl$ sensitivity test. dx is variable in the cross shore direction and dy is constant in alongshore direction. Therefore, different dy/dx ratios can be calculated.

Discretization y-grid

Secondly, the discretization of the y-grid is investigated. The results of the model runs are shown in Figure B.2 and summed up in Table B.3. The following observations can be made:

1. The a small $dy = 2.0m$ results in a quick drop of the wave energy propagating towards shore. It is believed that the distribution with a $dy > 2.0$ give a more realistic representation of the actual wave energy distribution.
2. In all simulation the H_{rms} drops when entering the domain, this could be due to the relatively high wave steepness s_0 chosen for the wind sea simulations.
3. The parameters H_{HF}, H_{LF}, $R2\%$, η_{setup} are hardly influenced by the variations in the dy grid size.

To conclude, $dy = 2.0$ poorly repents the evolution of wave energy in the cross-shore direction. Furthermore, the key model output parameters are hardly influenced through the variations in dy. So the y grid size could reach from $dy = 4.0m$ until $dy = 10.0m$. However, a model produces erroneous results for large dy/dx ratios. Therefore, the y-grid is discretized with $dy = 4.0m$ when modeling wind sea wave fields. Note that this is a conservative value and chosen to ensure a dy/dx ratio below 10.

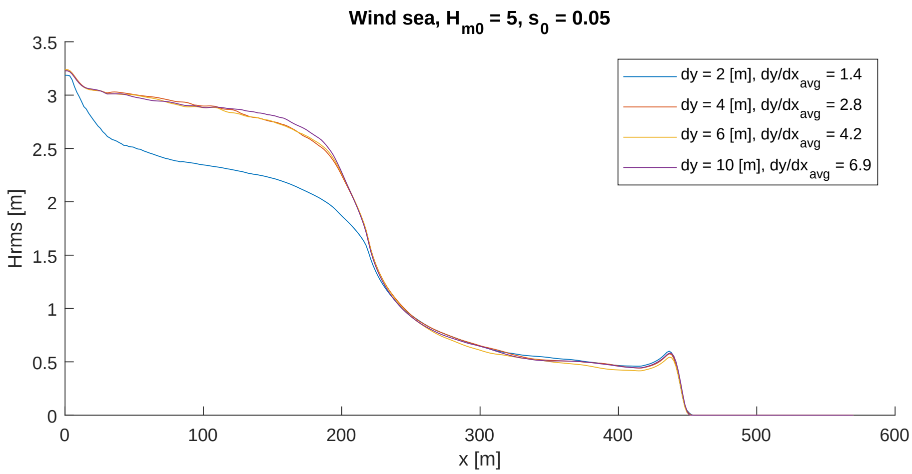

Figure B.2: Wave energy distribution in cross-shore direction for various dy. Cross section is placed at the center of the domain.

Model results wind sea							
dy [m]	dy/dx_{avg} [-]	dy/dx_{min} [-]	dy/dx_{max} [-]	H_{HF} [m]	H_{LF} [m]	$R2\%$ [m]	η_{setup} [m]
2.0	1.4	4.0	1.18	0.54	0.36	3.01	0.43
4.0	2.8	8.0	2.35	0.52	0.35	3.05	0.47
6.0	4.2	12.0	3.53	0.52	0.33	3.04	0.46
10.0	6.9	20.0	5.89	0.51	0.36	3.06	0.46

Table B.3: Model output of the dy sensitivity test. dx is variable in the cross shore direction and dy is constant in alongshore direction. Therefore, different dy/dx ratios can be calculated.

B.2. Swell wave field

The domain width (i.e. y-direction) of a model forced with swell waves is a little bit wider and equals 1000 m. The cross-shore domain length depends mainly on the depth of offshore boundary and the reef geometry, thus, is variable. The model setup is shown in Table B.4. The reef geometry of swell waves is the same as the geometry used for wind sea sensitivity analysis and is presented in Table B.1. At first, the influence of ppwl on the model results is investigated. Secondly, the influence of y grid discretization is investigated.

Hydrodynamic conditions			
Wave height	H_{m0}	5.0	[m]
Wave steepness	s_0	0.01	[-]
Directional spread	s	40.0	[-]
Grid			
points per wave length	ppwl	20, 40, 60, 80	[-]
y grid size	dy	4,6,8,10	[m]

Table B.4: Model setup for sensitivity analysis of domain discretization, the reef geometry and hydrodynamic conditions are constant only grid parameters are varied.

Results ppwl

Firstly, the influence of ppwl is investigated. The results of the model runs are shown in Figure B.3 and summed up in Table B.5. The following observations can be made:

1. A variation in the ppwl barely influences on the evolution of the H_{rms} in the cross shore direction.
2. The evolution of the wave energy of storm wave shows a sharp drop of the wave energy, whereas this drop is not present for swell waves.
3. Variations in the ppwl hardly affects H_{HF} and H_{LF}, however it has some effect on the $R2\%$ and η_{setup}. This is evident when the model runs with a $ppwl = 20$ and $ppwl = 40$ are compared.

Model results swell							
$ppwl$ [-]	dy/dx_{avg} [-]	dy/dx_{min} [-]	dy/dx_{max} [-]	H_{HF} [m]	H_{LF} [m]	$R2\%$ [m]	η_{setup} [m]
20	1.9	12.0	1.33	0.93	1.47	4.76	1.03
40	2.5	12.0	1.33	0.92	1.47	5.02	1.10
60	3.2	12.0	1.33	0.91	1.50	5.05	1.11
80	4.1	12.0	1.33	0.90	1.50	5.10	1.14

Table B.5: Model output of the $ppwl$ sensitivity test. dx is variable in the cross shore direction and dy is constant in alongshore direction. Therefore, different dy/dx ratios can be calculated.

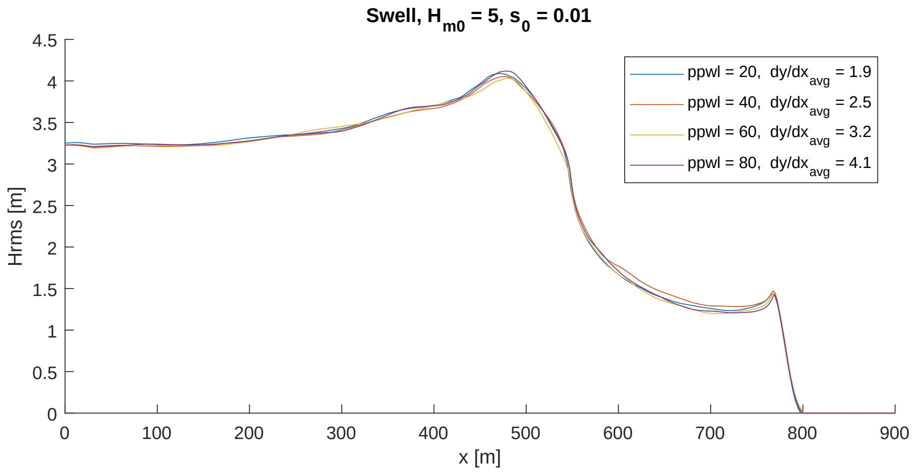

Figure B.3: Wave energy distribution in cross-shore direction for various $ppwl$. Cross section is placed at the center of the domain.

To conclude, the propagation and evolution of swell waves is hardly influenced by the ppwl. However, the runup ($R2\%$) and setup (η_{setup}) show a slight correlation with ppwl. In this case is chosen to model swell wave with 20 ppwl, since it seems to gives comparable results. More ppwl will increase the model runtime substantially, therefore 20 ppwl seems to be a good compromise between computational time and accuracy.

Discretization y-grid

Secondly, the discretization of the y-grid is investigated. The results of the model runs are shown in Figure B.4 and summed up in Table B.6. The following observations can be made:

1. Note that, a simulation with $dy = 2.0m$ became unstable, thus not output exists.
2. Any variations of dy leads to small variations in the wave energy evolution. Close to the coastline (at $x \approx 800m$) the wave energy distribution for model runs $dy = 4m$ and $dy = 6m$ are similar, but deviate for model runs with $dy = 8m$ and $dy = 10m$.
3. The parameters H_{HF}, H_{LF}, $R2\%$ and η_{setup} are hardly influenced by the variations in the dy grid size.

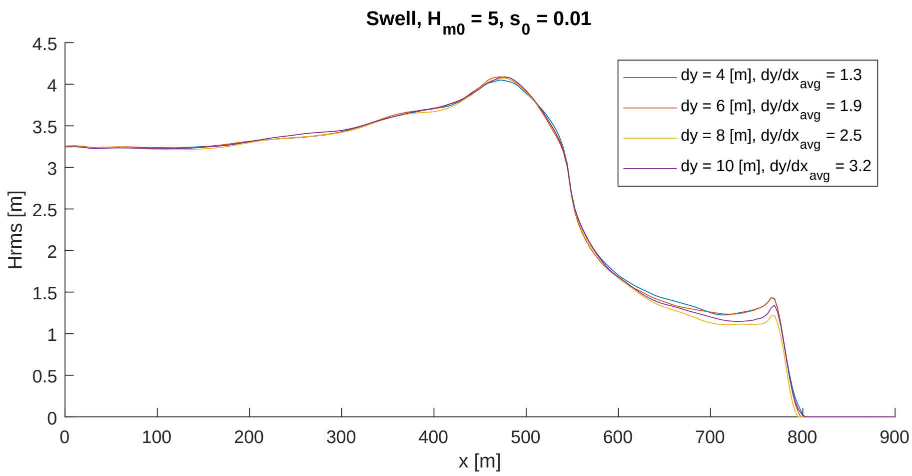

Figure B.4: Wave energy distribution in cross-shore direction for various dy. Cross section is placed at the center of the domain.

To conclude, the key model output parameters are hardly influenced through the variations in dy. So the y grid size could reach from $dy = 4.0m$ until $dy = 10.0m$. Therefore, the y-grid is discretized with $dy = 4.0m$ when modeling swell wave fields. note that this value is same as the value used for wind sea.

Model results swell							
dy [m]	dy/dx_{avg} [-]	dy/dx_{min} [-]	dy/dx_{max} [-]	H_{HF} [m]	H_{LF} [m]	$R2\%$ [m]	η_{setup} [m]
4.0	1.3	8.0	0.89	0.90	1.42	4.68	1.02
6.0	1.9	12.0	1.33	0.93	1.47	4.66	1.03
8.0	2.5	16.0	1.78	0.91	1.49	4.60	1.02
10.0	3.2	20.0	2.22	0.90	1.44	4.69	1.02

Table B.6: Model output of the dy sensitivity test. dx is variable in the cross shore direction and dy is constant in alongshore direction. Therefore, different dy/dx ratios can be calculated.

C

Vorticity analysis

In this Appendix the Vorticity in the XB NH model domain is analyzed. The vorticity around the z-axis (i.e. horizontal vorticity or eddies) can be calculated with the formulation presented here, see Equation C.1. To calculate the vorticity with this formulation global XB NH data is necessary. To limit the amount of data 4 time stamps of global data are obtained from XB NH. These 4 global data maps in time are used calculate the vorticity, by taking the absolute vorticity and average alongshore and over time. In this way cross-shore evolution of absolute vorticity averaged over time was obtained.

$$\omega_z = \frac{\delta v}{\delta x} - \frac{\delta u}{\delta y} \tag{C.1}$$

Where:

v, u	x,y velocities [m/s]
ω_z	Horizontal vorticity [1/s]

C.1. Influence Wave Directional Spread on Vorticity

The results in Figure C.1 indicate a decreased generation of vorticity for a more narrow directional spectrum. This is in line with the priori expectations. However, not with the directional broadening found in Section 4.1.3. Therefore, the size of the instantaneous vorticity fields is investigated, see C.2.

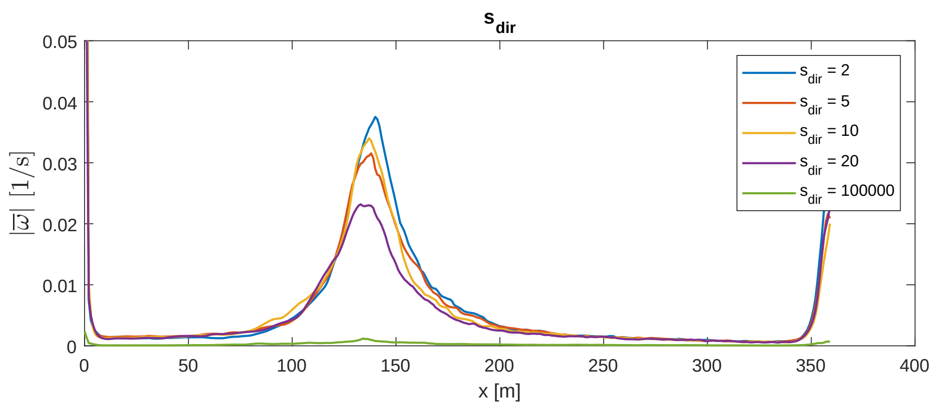

Figure C.1: The influence of directional spreading on vorticity for wind sea waves. The model setup; $W_{reef} = 200$ m, $\beta_f = 0.1$, $h_0 = 2.0$ m and $H_{m0,0} = 3.0$ m.

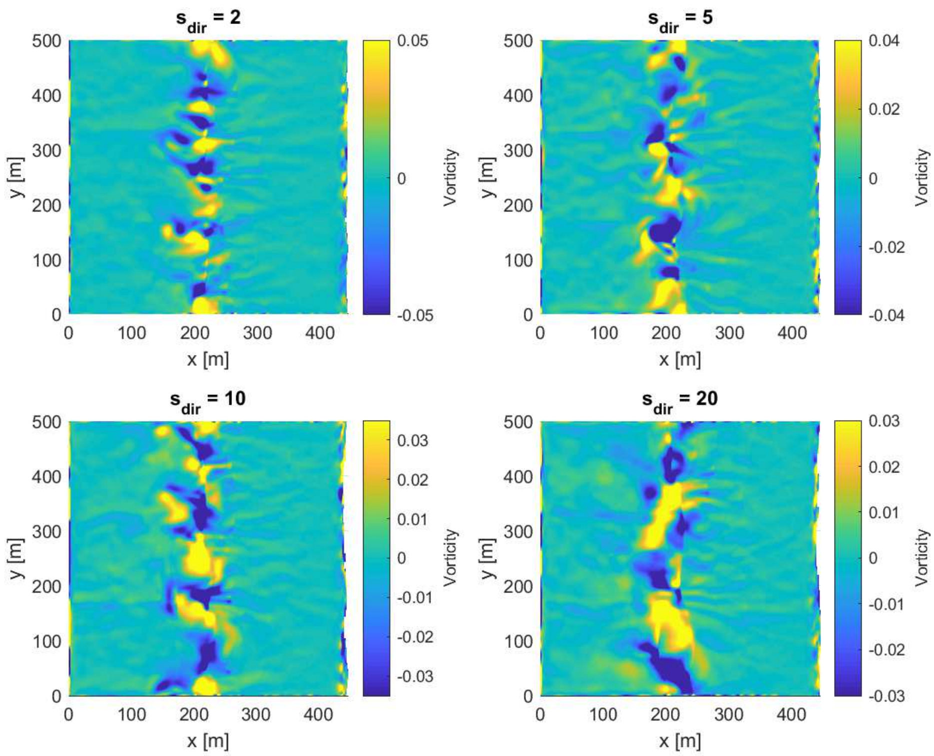

Figure C.2: The influence of directional spreading on the instantaneous 2DH vorticity fields for wind sea waves. The model setup; W_{reef} = 200 m, β_f = 0.1, h_0 = 2.0 m, s_{dir} = 20 and $H_{m0,0}$ = 3.0 m.

C.2. Influence Wave steepness on Vorticity

The influence of wave steepness on the generation of vorticity is shown Figure C.3. This shows that less vorticity is generated for swell waves than for storm waves. This is not in line with the directional broadening found for swell wave and for wind sea waves. Therefore, the 2DH vorticity fields are compared and it is found that the size of the vorticity fields is larger for swell waves than for wind sea waves, see Figure C.4.

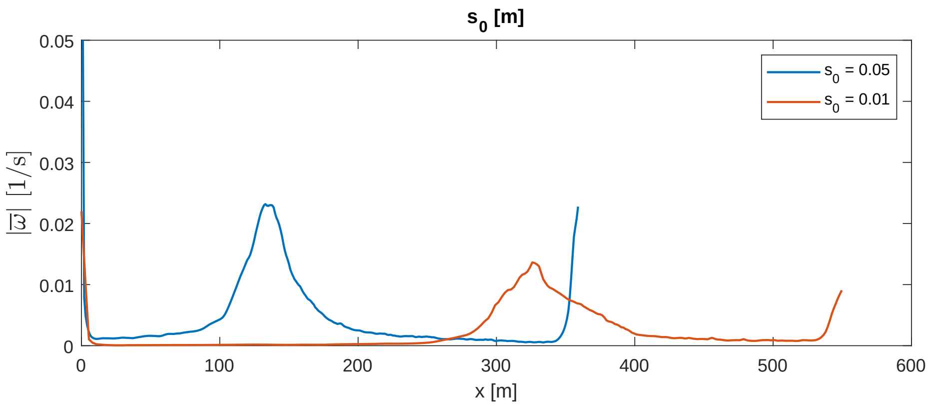

Figure C.3: The influence of directional spreading on vorticity for wind sea waves. The model setup; W_{reef} = 200 m, β_f = 0.1, h_0 = 2.0 m and $H_{m0,0}$ = 3.0 m.

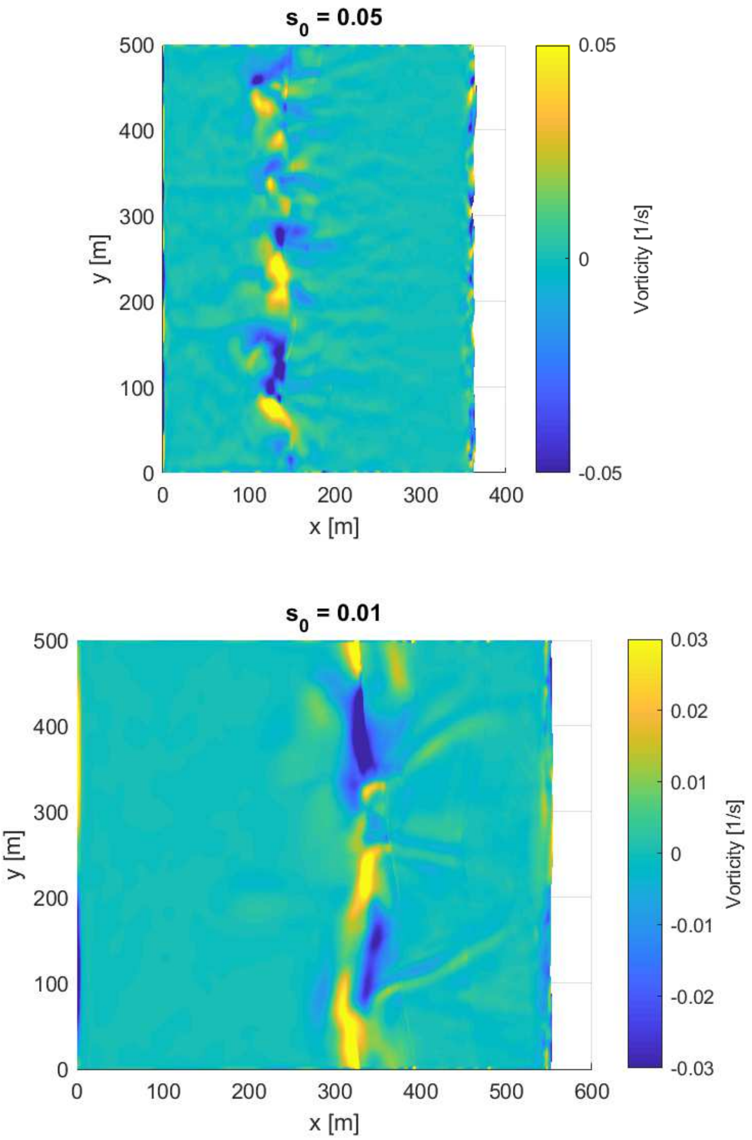

Figure C.4: The influence of wave steepness on the instantaneous 2DH vorticity fields. The model setup; W_{reef} = 200 m, β_f = 0.1, h_0 = 2.0 m, s_{dir} = 20 and $H_{m0,0}$ = 3.0 m.

C.3. Influence of Reef Geometry and Wave Forcing on Vorticity

Lastly, the influence of the reef geometry and wave forcing on the absolute average vorticity is calculated, see Figure C.5. The results are in line with the findings on directional broadening and suggest that more directional broadening will occur when the amount of vorticity increases. Given that the wave steepness and directional spreading do not change since these affect the size fo the vorticity fields.

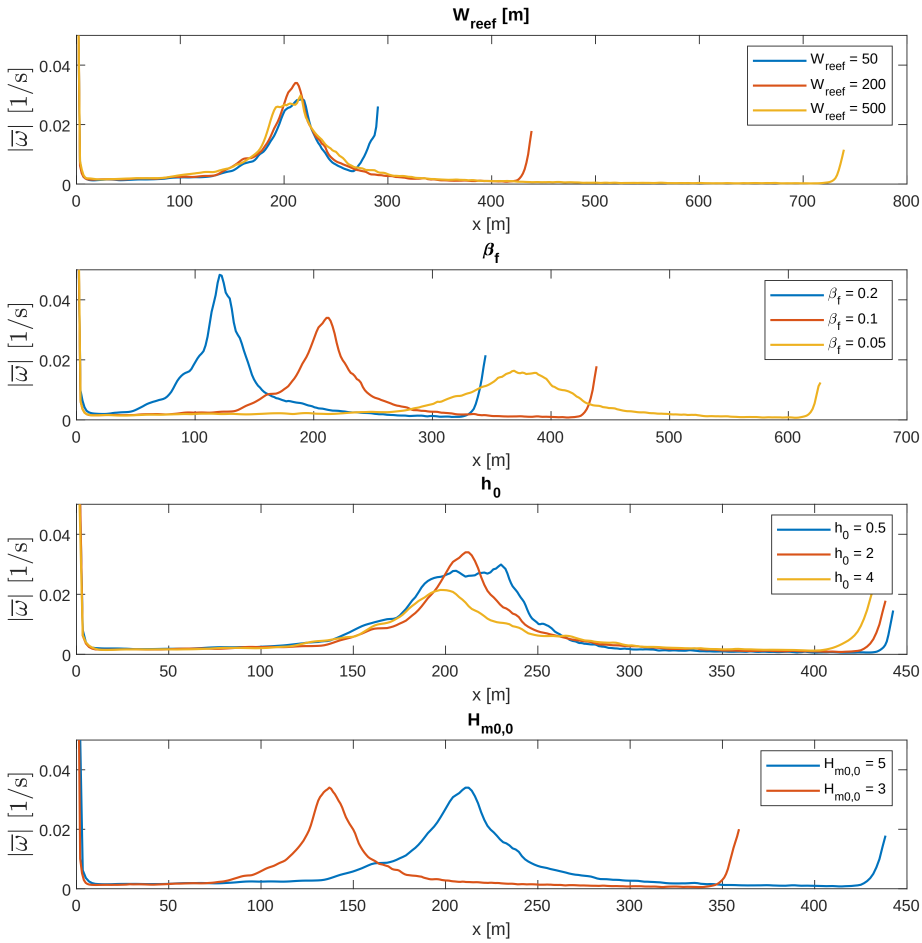

Figure C.5: The influence of directional spreading on vorticity for wind sea waves. The model setup; W_{reef} = 200 m, β_f = 0.1, h_0 = 2.0 m and $H_{m0,0}$ = 3.0 m.

D

Radiation stresses and wave setup

In this Appendix a radiation stress and setup analysis is performed in order to explain the influence s_{dir} on runup in different reef environments. A gradient in the radiation stresses is obtained when the wave energy or H_{rms} changes. However, this valid when it is assumed that the incident wave field has no directional spreading. The true radiation stresses can be calculated with the formulation presented in the background study (Feddersen, 2004), and is for convenience repeated here. The radiation stress formulation from Feddersen (2004) is called the true radiation stress or $S_{xx,tr}$.

$$S_{xx} = E_0 \left(\frac{c_g(\overline{f})}{c(\overline{f})} (1+S) - \frac{1}{2} \right) \tag{D.1}$$

Where:

S_{xx}	Radiation stresses $[kg/s^2]$
E_0	Wave energy $(1/8 \rho g H_{rms})$
S	Correction for directional spreading $(\cos^2(\overline{\theta})(1-\sigma^{*2}) + \sin^2(\overline{\theta})\sigma^{*2})$
σ^*	Is the directional spreading and is given in Kuik et al. (1988)
$\overline{\theta}$	Mean wave direction
$c_g(\overline{f})$	Energy weighted wave group velocity band passed to the HF band
$c(\overline{f})$	Energy weighted wave velocity band passed to the HF band

For normal incident waves reduces the reduction S to $S = (1-\sigma^{*2})$. This means that a directionally narrow banded wave field leads to the $S = 1$ and the S_{xx} becomes $S_{xx} = (2n - 1/2) * E_0$, this is equal to the narrow banded estimation of radiation stresses ($S_{xx,nb}$) and can be seen as the radiation stresses in a 1D model or 2DH model with $s_{dir} = \infty$.

With the radiation stress, radiation stress gradients can be calculated. With these gradients the wave setup can be determined with the following formulation. This it the cross-shore momentum balance where it is assumed that the wave forces are purely balanced by a water level difference.

$$\frac{dS_{xx}}{dx} = -\rho_w g h \frac{d\eta}{dx} \tag{D.2}$$

D.1. Directional spreading and radiation stresses

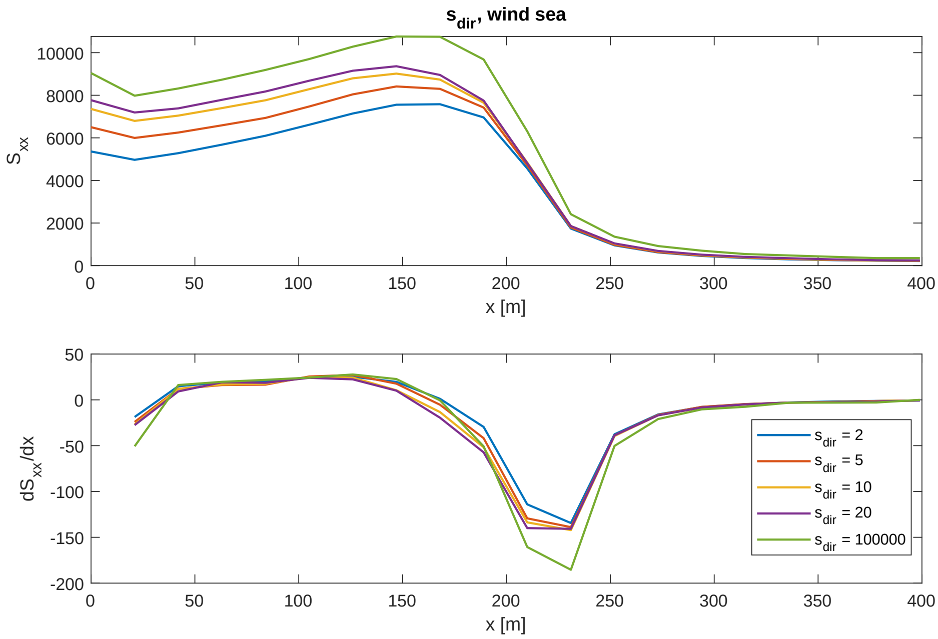

Figure D.1: The influence of directional spreading on the radiation stresses for wind sea waves. In the top figure the radiation stress evolution in x-direction is shown for different directional spreading. In the lower figure the radiation stress gradients are shown. The model setup; $W_{reef} = 200$ m, $\beta_f = 0.1$, $h_0 = 2.0$ m and $H_{m0,0} = 5$ m.

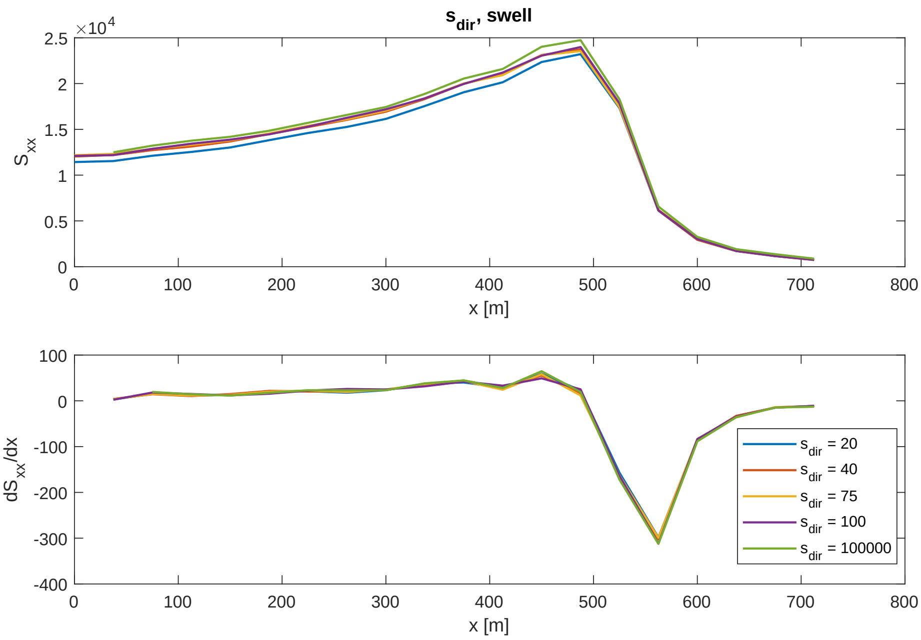

Figure D.2: The influence of directional spreading on the radiation stresses for swell waves. In the top figure the radiation stress evolution in x-direction is shown for different directional spreading. In the lower figure the radiation stress gradients are shown. The model setup; $W_{reef} = 200$ m, $\beta_f = 0.1$, $h_0 = 2.0$ m and $H_{m0,0} = 5$ m.

D.2. Radiation Stresses and Setup in Different Reef Environments

In this section the radiation stress and setup are calculated. The setup is compared with the setup in XB NH model. Furthermore, a comparison with narrow banded approximation of S_{xx} (i.e. 1D model) and true S_{xx} with directional spreading. In this way, the influence of directional spreading on setup is investigated.

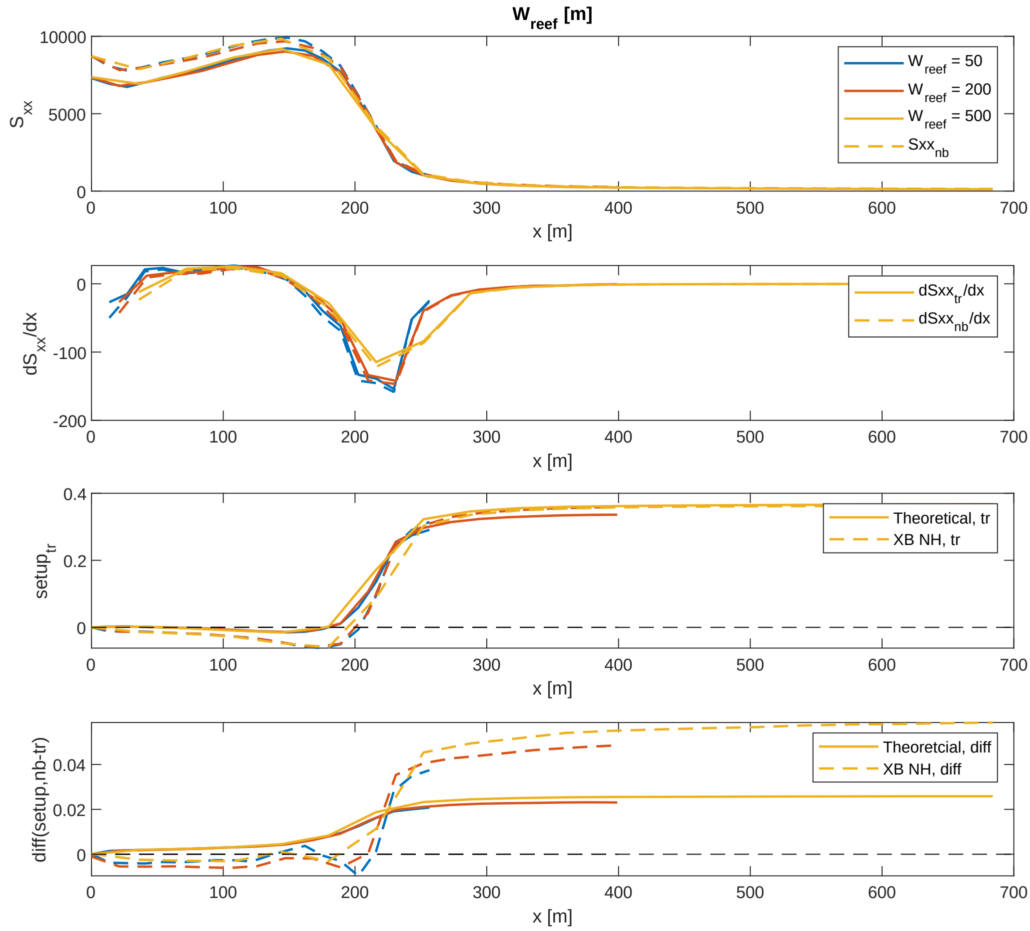

Figure D.3: The evolution of radiation stresses for wind sea waves and different W_{reef}. The radiation stress evolution, radiation stress gradient, setup (theoretical and XB NH), difference between theoretical true and narrow banded setup and XB NH true and narrow banded setup are shown. The model setup; $s_0 = 0.05$, $\beta_f = 0.1$, $h_0 = 2.0$ m and $H_{m0,0} = 5$ m.

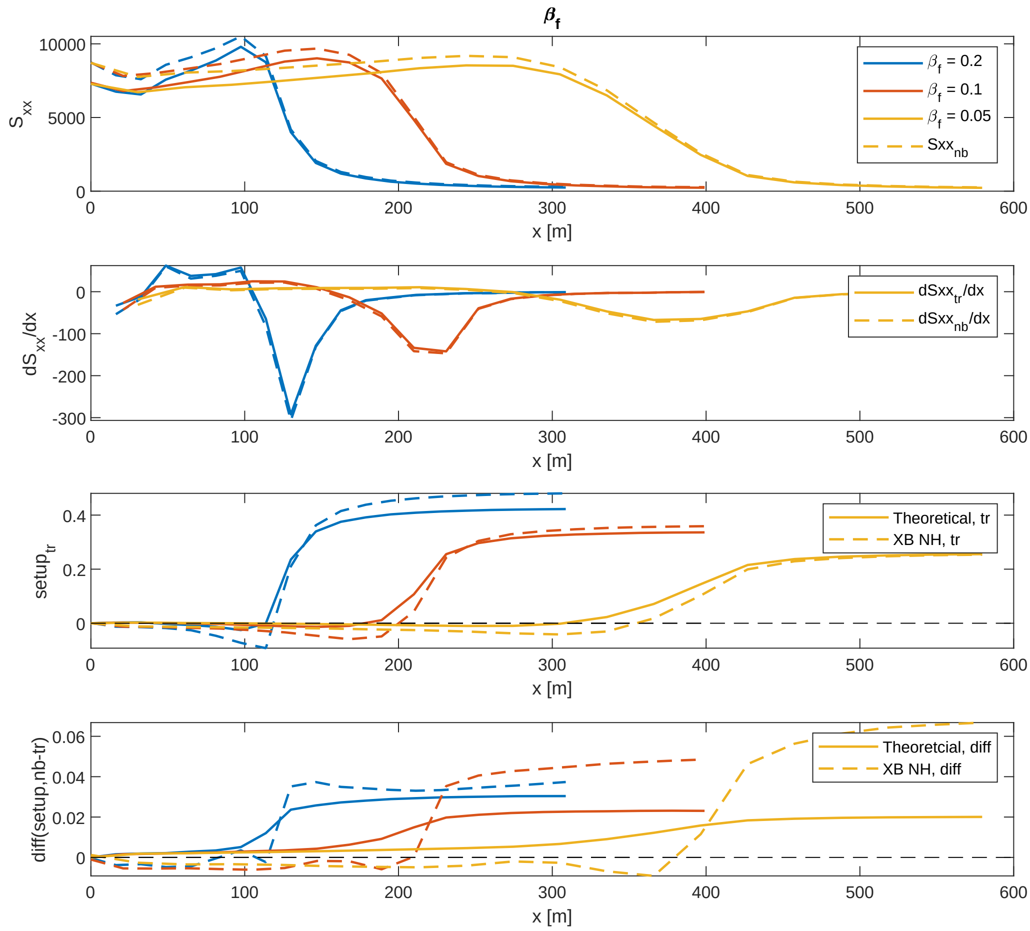

Figure D.4: The evolution of radiation stresses for wind sea waves and different β_f. The radiation stress evolution, radiation stress gradient, setup (theoretical and XB NH), difference between theoretical true and narrow banded setup and XB NH true and narrow banded setup are shown. The model setup; $s_0 = 0.05$, $W_{reef} = 200$ m, $h_0 = 2.0$ m and $H_{m0,0} = 5$ m.

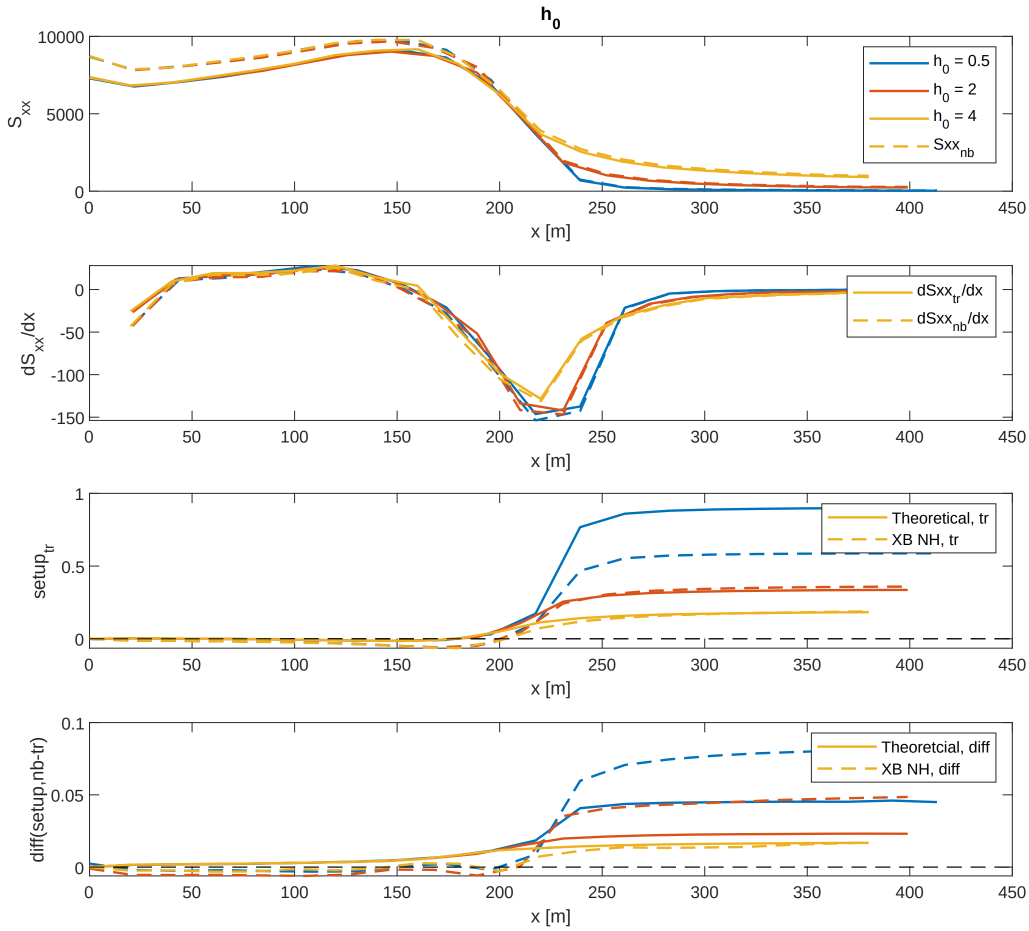

Figure D.5: The evolution of radiation stresses for wind sea waves and different h_0. The radiation stress evolution, radiation stress gradient, setup (theoretical and XB NH), difference between the theoretical true and narrow banded setup and XB NH true and narrow banded setup, are shown. The model setup; $s_0 = 0.05$, $\beta_f = 0.1$, $W_{reef} = 200$ m and $H_{m0,0} = 5$ m.

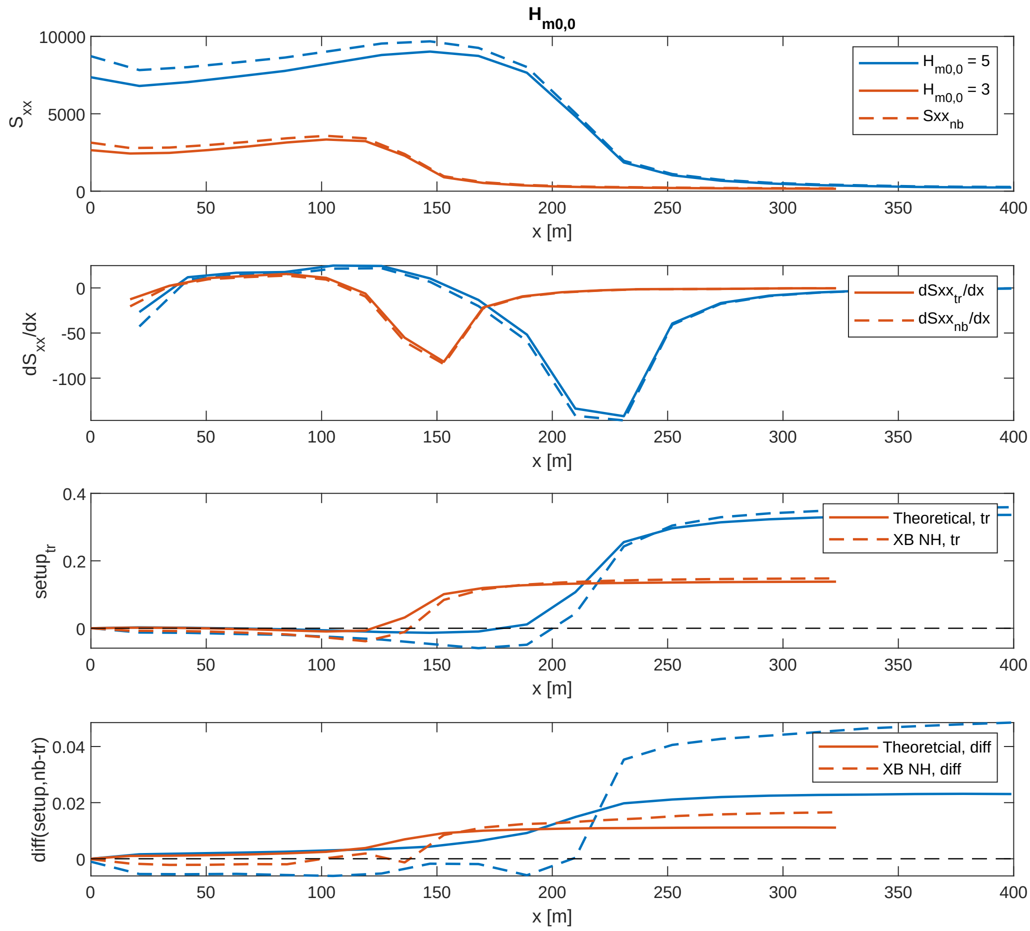

Figure D.6: The evolution of radiation stresses for wind sea waves and different H_{m0}. The radiation stress evolution, radiation stress gradient, setup (theoretical and XB NH), difference between theoretical true and narrow banded setup and XB NH true and narrow banded setup are shown. The model setup; $s_0 = 0.05$, $\beta_f = 0.1$, $W_{reef} = 200$ m and $h_0 = 2.0$ m.

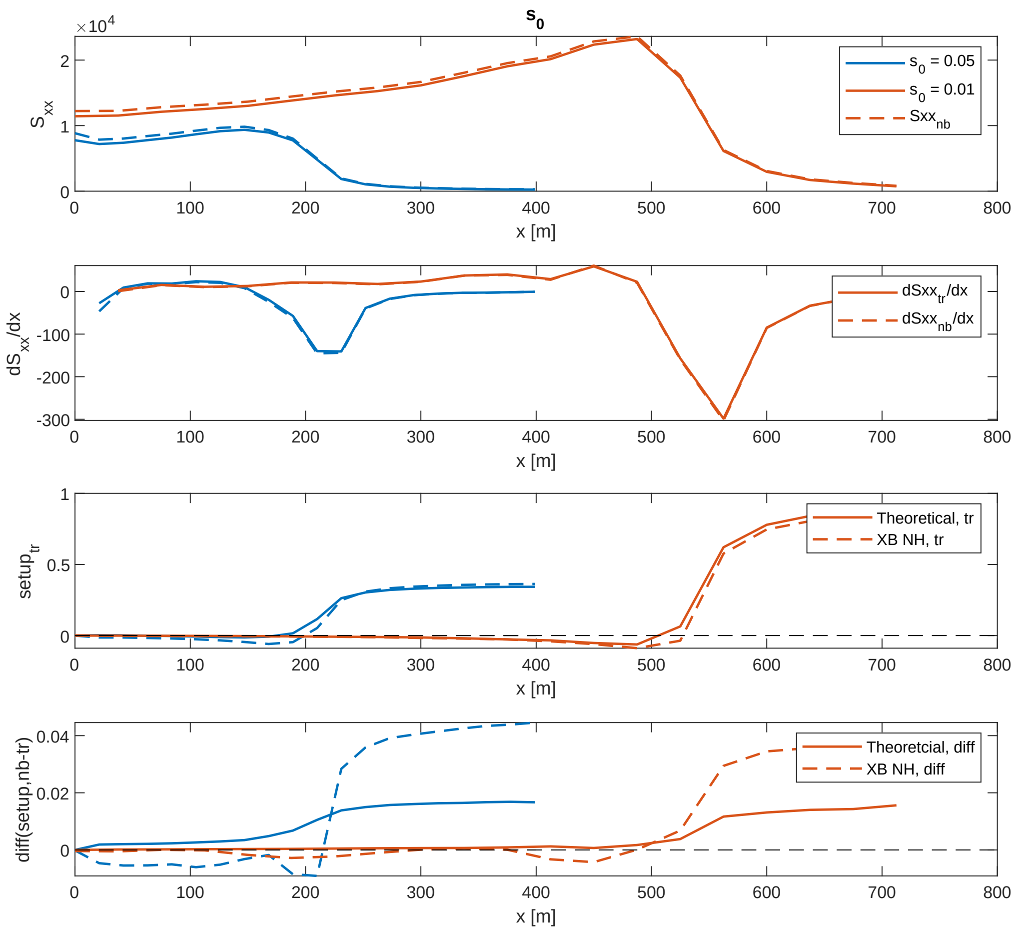

Figure D.7: The evolution of radiation stresses for wind sea waves and different s_0. The radiation stress evolution, radiation stress gradient, setup (theoretical and XB NH), difference between theoretical true and narrow banded setup and XB NH true and narrow banded setup are shown. The model setup; $H_{m0,0} = 5.0$ m, $\beta_f = 0.1$, $W_{reef} = 200$ m and $h_0 = 2.0$ m.

E

Regression models

In this Appendix regression models are shown, which are used as supporting for the regression analysis performed in Section 5.3. Firstly the swell regression models are shown, subsequently the single variate linear regression analysis is shown for wind sea and swell waves.

E.1. Regression models swell waves

Visualization of the regression models presented in Section 5.3.3. The models are based on the single variate linear regression analysis and given relations in Section 5.1.

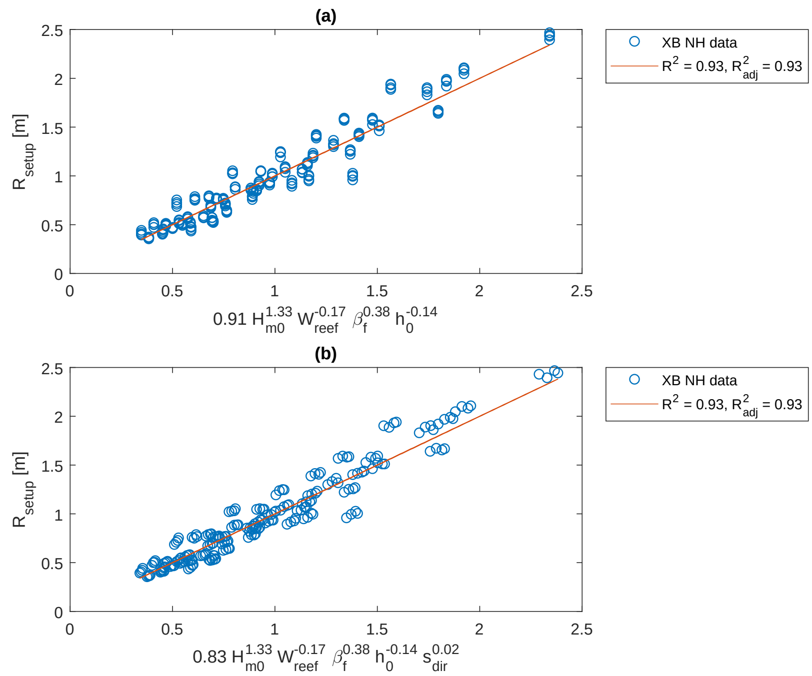

Figure E.1: The linear regression model with and without directional spreading. It shows that directional spreading has little effect on the explanatory power of the regression model, since the R^2_{adj} change is low.

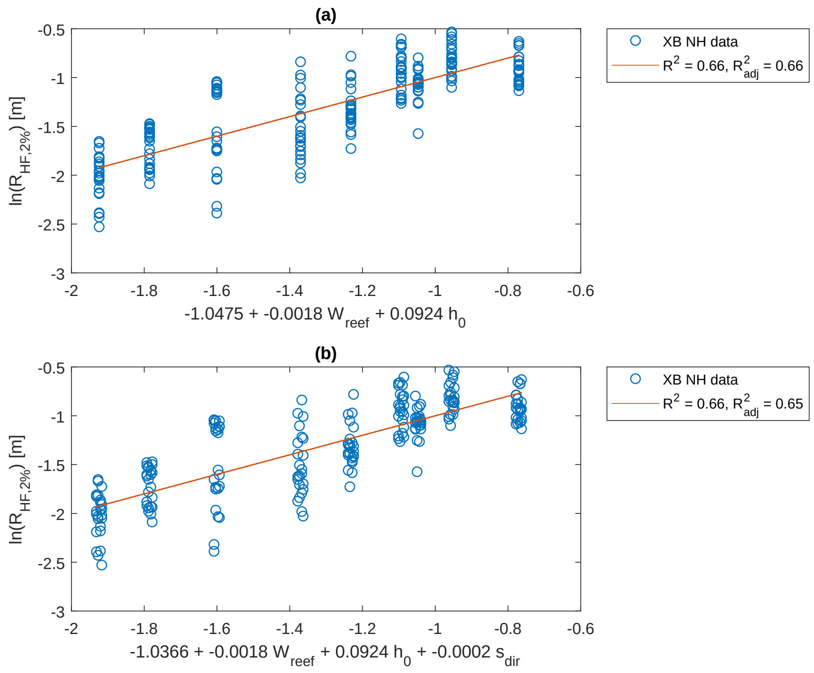

Figure E.2: The linear regression model with and without directional spreading. It shows that directional spreading has little effect on the explanatory power of the regression model, since the R^2_{adj} change is low.

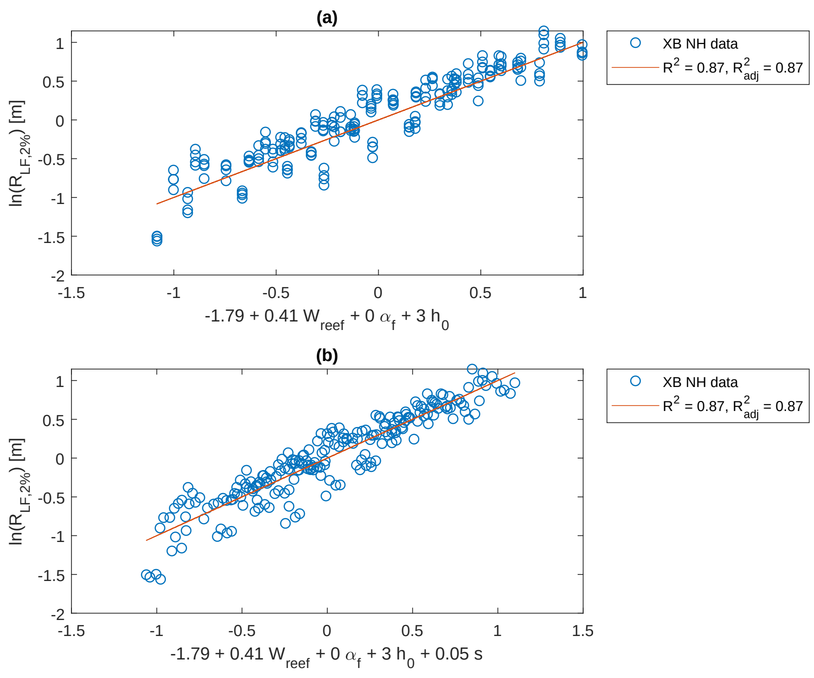

Figure E.3: The linear regression model with and without directional spreading. It shows that directional spreading has little effect on the explanatory power of the regression model, since the R^2_{adj} change is low.

E.2. Single variate linear regression analysis wind sea

In this Section the single variate linear regression analysis is shown. This analysis gave insight in the relations between the single variables and the runup components. The results are summed up below:

- **Setup: Figure E.4**
  - H_{m0} → $R^2 = 0.46$
  - β_f → $R^2 = 0.18$
  - W_{reef} → $R^2 = 0.04$
  - h_0 → $R^2 = 0.03$
  - s_{dir} → $R^2 = 0.01$
- **High frequency runup: Figure E.5**
  - h_0 → $R^2 = 0.75$
  - W_{reef} → $R^2 = 0.08$
  - s_{dir} → $R^2 = 0.004$
  - H_{m0} → $R^2 = 0.0$
  - β_f → $R^2 = 0.0$
- **Low frequency runup: Figure E.6**
  - H_{m0} → $R^2 = 0.40$
  - W_{reef} → $R^2 = 0.20$
  - h_0 → $R^2 = 0.06$
  - β_f → $R^2 = 0.06$
  - s_{dir} → $R^2 = 0.02$

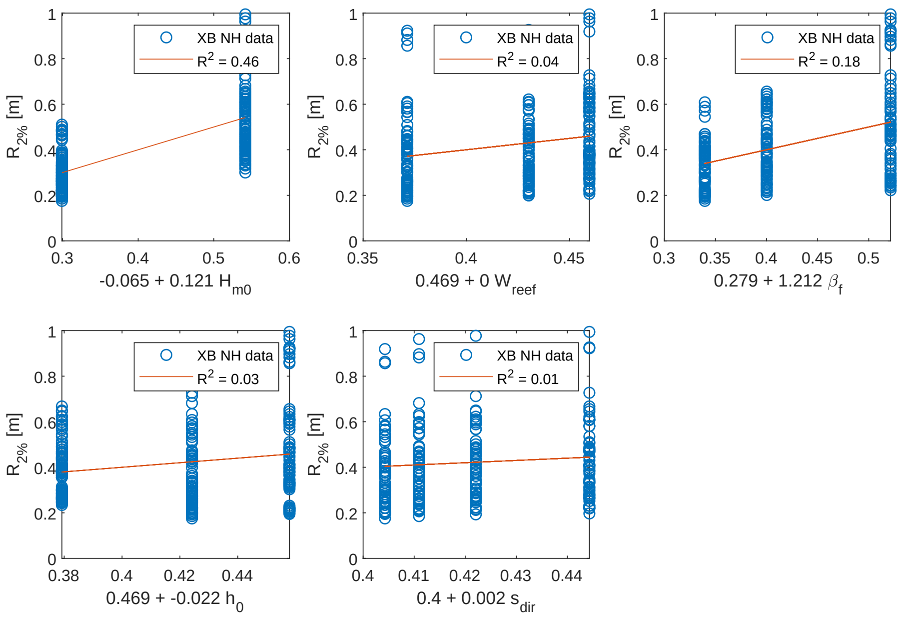

Figure E.4: Wind sea waves single variate linear regression models between setup (R_{setup}) and the model parameters. The method is described in Section 3.4. The figure indicates a strong relation between setup and h_0, W_{reef} and to a lesser extent with s_{dir}. No relation is found for H_{m0} and β_f.

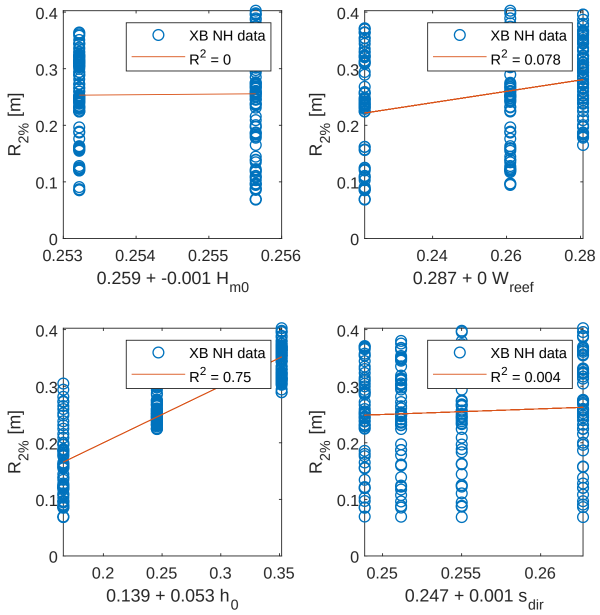

Figure E.5: Wind sea waves single variate linear regression models between HF runup (R_{HF}) and the model parameters. The method is described in Section 3.4. The figure indicates a strong relation between HF runup and H_{m0}, β_f and to a lesser extent with W_{reef}, h_0 and s_{dir}.

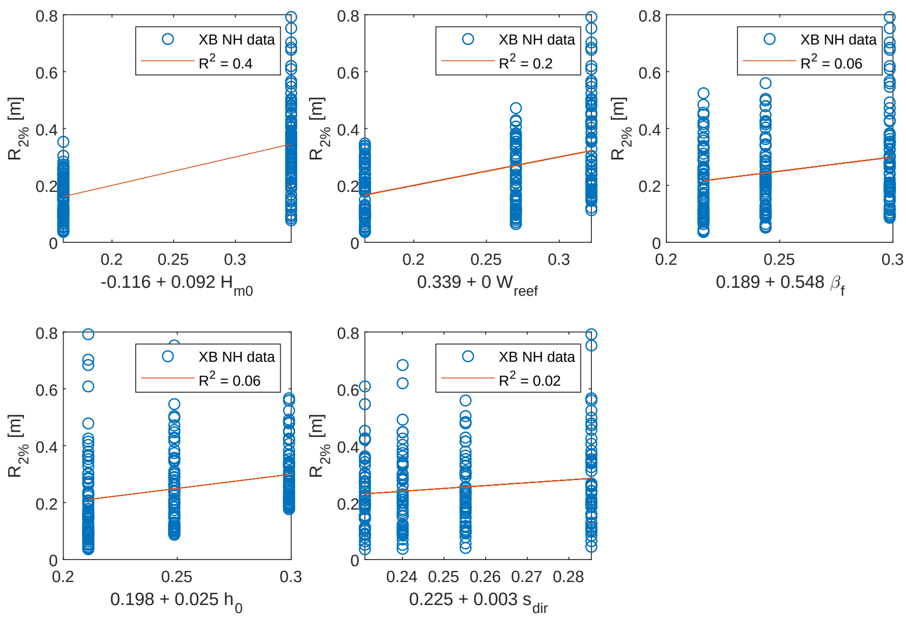

Figure E.6: Wind sea waves single variate linear regression models between LF runup (R_{LF}) and the model parameters. The method is described in Section 3.4.The figure indicates a strong relation between setup and H_{m0}, W_{reef} and to a lesser extent with β_f, h_0 and s_{dir}.

E.3. Single variate linear regression analysis swell

In this Section the single variate linear regression analysis is shown. This analysis gave insight in the relations between the single variables and the runup components under swell wave forcing. The results are summed up below:

- **Setup: Figure E.7**
  - H_{m0} → $R^2 = 0.45$
  - β_f → $R^2 = 0.21$
  - W_{reef} → $R^2 = 0.09$
  - h_0 → $R^2 = 0.06$
  - s_{dir} → $R^2 = 0.0$
- **High frequency runup: Figure E.8**
  - W_{reef} → $R^2 = 0.57$
  - h_0 → $R^2 = 0.06$
  - β_f → $R^2 = 0.05$
  - H_{m0} → $R^2 = 0.004$
  - s_{dir} → $R^2 = 0.0$
- **Low frequency runup: Figure E.9**
  - H_{m0} → $R^2 = 0.53$
  - W_{reef} → $R^2 = 0.19$
  - β_f → $R^2 = 0.12$
  - h_0 → $R^2 = 0.01$
  - s_{dir} → $R^2 = 0.0$

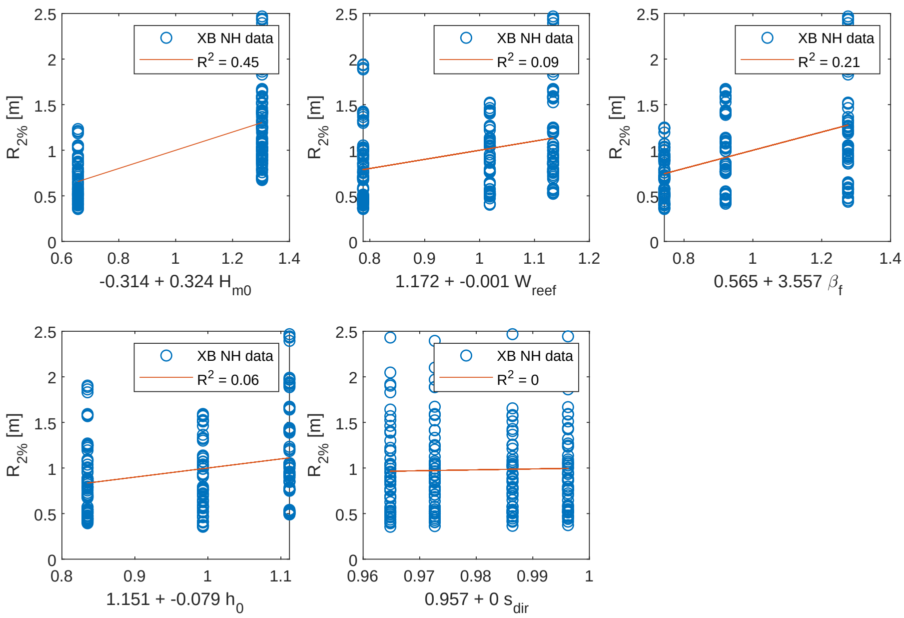

Figure E.7: Swell wave single variate linear regression models between setup (R_{setup}) and the model parameters. The method is described in Section 3.4. The figure indicates a strong relation between setup and h_0, W_{reef} and to a lesser extent with s_{dir}. No relation is found for H_{m0} and β_f.

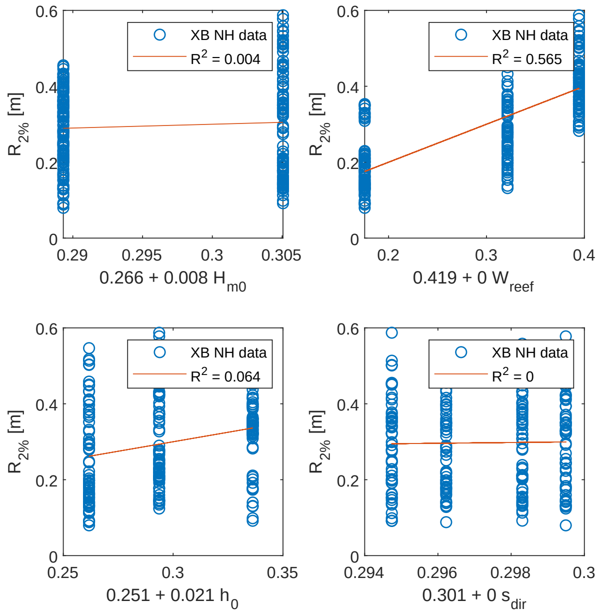

Figure E.8: Swell waves single variate linear regression models between HF runup (R_{HF}) and the model parameters. The method is described in Section 3.4. The figure indicates a strong relation between HF runup and H_{m0}, β_f and to a lesser extent with W_{reef}, h_0 and s_{dir}.

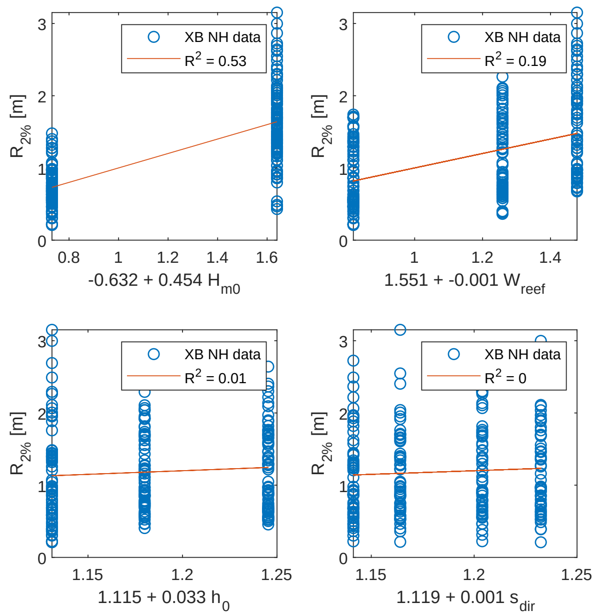

Figure E.9: Swell wave single variate linear regression models between LF runup (R_{LF}) and the model parameters. The method is described in Section 3.4.The figure indicates a strong relation between setup and H_{m0}, W_{reef} and to a lesser extent with β_f, h_0 and s_{dir}.